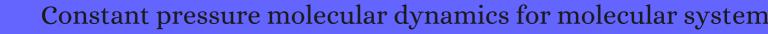
# CITATION REPORT List of articles citing



DOI: 10.1080/00268978300102851 Molecular Physics, 1983, 50, 1055-1076.

Source: https://exaly.com/paper-pdf/16160982/citation-report.pdf

Version: 2024-04-28

This report has been generated based on the citations recorded by exaly.com for the above article. For the latest version of this publication list, visit the link given above.

The third column is the impact factor (IF) of the journal, and the fourth column is the number of citations of the article.

| #    | Paper  | IF. | Citations |
|------|--|-----|-----------|
| 2284 | References. 557-586  |     |           |
| 2283 | Allosteric Modulation Mechanism of the mGluR5 Transmembrane Domain.  |     |           |
| 2282 | Restructuring a Deep Eutectic Solvent by Water: The Nanostructure of Hydrated Choline Chloride/Urea.   |     |           |
| 2281 | Revisiting Partition in Hydrated Bilayer Systems.  |     |           |
| 2280 | MiMiC: A Novel Framework for Multiscale Modeling in Computational Chemistry.   |     |           |
| 2279 | Self-Stabilized Giant Aggregates in Water from Room-Temperature Ionic Liquids with an Asymmetric PolarApolarPolar Architecture.                        |     |           |
| 2278 | Molecular Structure and Permeability at the Interface between Phase-Separated Membrane<br>Domains.   |     |           |
| 2277 | Tetrameric Charge-Zipper Assembly of the TisB Peptide in MembranesComputer Simulation and Experiment.  |     |           |
| 2276 | Lipid Rafts: Buffers of Cell Membrane Physical Properties.   |     |           |
| 2275 | Asymmetric Hybridization Orbitals at the Charged Interface Initiates New Surface Reactions: A Quantum Mechanics Exploration.                           |     |           |
| 2274 | Ultrafast Spectroscopy of LipidWater Interfaces: Transmembrane Crowding Drives HBond<br>Dynamics.  |     |           |
| 2273 | Preserved Transmembrane Segment Topology, Structure and Dynamics in Disparate Micellar Environments.   |     |           |
| 2272 | Site-Specific Hydrogen Exchange in a Membrane Environment Analyzed by Infrared Spectroscopy.   |     |           |
| 2271 | An Allosteric Pathway in Copper, Zinc Superoxide Dismutase Unravels the Molecular Mechanism of the G93A Amyotrophic Lateral Sclerosis-Linked Mutation. |     |           |
| 2270 | DNA Binding and Recognition of a CC Mismatch in a DNA Duplex by Water-Soluble Peptidocalix[4]arenes: Synthesis and Applications.                       |     |           |
| 2269 | Catalytic Roles of Histidine and Arginine in Pyruvate Class II Aldolase: A Perspective from QM/MM Metadynamics.  |     |           |
| 2268 | Plant Polypeptide Hormone Systemin Prefers Polyproline II Conformation in Solution.  |     |           |

| 2267 | Propensity for Proton Relay and Electrostatic Impact of Protein Reorganization in Slr1694 BLUF Photoreceptor.  |
|------|--|
| 2266 |  |
| 2265 | Molecular Architecture of the Blood Brain Barrier Tight Junction ProteinsA Synergistic Computational and In Vitro Approach.                                    |
| 2264 | Aromatic-Mediated Carbohydrate Recognition in Processive Serratia marcescens Chitinases.   |
| 2263 | Enzyme Catalysis that Paves the Way for SSulfhydration via Sulfur Atom Transfer.   |
| 2262 | Molecular Dynamics Simulations Predict the Pathways via Which Pristine Fullerenes Penetrate Bacterial Membranes.   |
| 2261 | Structure and Dynamics of Extracellular Loops in Human Aquaporin1 from Solid-State NMR and Molecular Dynamics.   |
| 2260 | Thermal, Mutual, and Self-Diffusivities of Binary Liquid Mixtures Consisting of Gases Dissolved in nAlkanes at Infinite Dilution.                              |
| 2259 | Structural Basis for Allosteric Regulation in the Major Antenna Trimer of Photosystem II.  |
| 2258 | Dynamical Model for the Counteracting Effects of Trimethylamine NOxide on Urea in Aqueous Solutions under Pressure.  |
| 2257 | Contrasting Modes of Self-Assembly and Hydrogen-Bonding Heterogeneity in Chlorosomes of Chlorobaculum tepidum.   |
| 2256 | Orientational Switch of the Lipase A Enzyme at the OilWater Interface: An Order of Magnitude Increase in Turnover Rate with a Single Surfactant Tag Explained. |
| 2255 | Refined Parameterization of Nonbonded Interactions Improves Conformational Sampling and Kinetics of Protein Folding Simulations.                               |
| 2254 | Molecular Determinants of A42 Adsorption to Amyloid Fibril Surfaces.   |
| 2253 | A Two-Metal-Ion-Mediated Conformational Switching Pathway for HDV Ribozyme Activation.   |
| 2252 | Molecular Docking Studies of Royleanone Diterpenoids from Plectranthus spp. as PGlycoprotein Inhibitors.   |
| 2251 | Nonadditive Ion Effects Drive Both Collapse and Swelling of Thermoresponsive Polymers in Water.  |
| 2250 | Reactive Center Loop Insertion in 1-Antitrypsin Captured by Accelerated Molecular Dynamics Simulation.   |

6

17

|      | CHARION  |       |
|------|--|-------|
| 2249 | Insights into the Mechanisms of Aquaporin3 Inhibition by Gold(III) Complexes: the Importance of Non-Coordinative Adduct Formation.   |       |
| 2248 | Osmolyte Induced Changes in Peptide Conformational Ensemble Correlate with Slower Amyloid Aggregation: A Coarse-Grained Simulation Study.  |       |
| 2247 | Revisiting Hydrogen Bond Thermodynamics in Molecular Simulations.  |       |
| 2246 | ResidueResidue Mutual Work Analysis of RetinalOpsin Interaction in Rhodopsin: Implications for ProteinLigand Binding.  |       |
| 2245 | Molecular-Dynamics Calculations for Ethylene Adsorbed on Graphite. <b>1984</b> , 53, 818-821   | 26    |
| 2244 | A unified formulation of the constant temperature molecular dynamics methods. <b>1984</b> , 81, 511-519  | 11345 |
| 2243 | A molecular dynamics method for simulations in the canonical ensemble. <i>Molecular Physics</i> , <b>1984</b> , 52, 255-268  | 6696  |
| 2242 | Molecular dynamics with coupling to an external bath. <b>1984</b> , 81, 3684-3690  | 21325 |
| 2241 | Monte Carlo simulation of the crystal to plastic crystal transition in carbon tetrachloride. <b>1985</b> , 119, 22-28  | 13    |
| 2240 | Constant pressure-constant temperature molecular dynamics for rigid and partially rigid molecular systems. <i>Molecular Physics</i> , <b>1985</b> , 54, 587-603                      | 116   |
| 2239 | Structure of solid t-butyl cyanide: Interpretation of experimental data by means of molecular dynamics simulation. <b>1985</b> , 83, 4726-4733                                       | 6     |
| 2238 | A Monte Carlo study of crystal structure transformations. <i>Molecular Physics</i> , <b>1985</b> , 54, 245-251 1.7   | 87    |
| 2237 | On the use of computer simulation to determine the excess free energy in fluid mixtures. <b>1986</b> , 26, 103-127   | 67    |
| 2236 | Molecular dynamics simulation of rigid molecules. <b>1986</b> , 4, 346-392   | 375   |
| 2235 | Constant-temperature-constant-pressure molecular-dynamics calculations for molecular solids: Application to solid nitrogen at high pressure. <b>1986</b> , 33, 339-342               | 25    |
| 2234 | Constant thermodynamic tension Monte Carlo studies of elastic properties of a two-dimensional system of hard cyclic hexamers. <i>Molecular Physics</i> , <b>1987</b> , 61, 1247-1258 | 299   |
|      |  |       |

Structure of solid t-butyl cyanide: A study by means of constant-temperature, constant-pressure, molecular-dynamics simulations. **1987**, 87, 4823-4828

2232 Structural transition on cooling of plastic adamantane: A molecular-dynamics study. **1987**, 59, 2574-2577

2233

## (1990-1987)

|                              | Molecular dynamics studies of the condensed phases of n-butane and their transitions. <i>Molecular Physics</i> , <b>1987</b> , 61, 669-692  | 1.7 | 35                      |
|------------------------------|---|-----|-------------------------|
| 2230                         | A computer simulation study of the melting and freezing properties of a system of Lennard-Jones particles. <i>Molecular Physics</i> , <b>1987</b> , 61, 597-615   | 1.7 | 25                      |
| 2229                         | Isothermal?isobaric molecular dynamics simulation of diatomic liquids and their mixtures. <b>1987</b> , 113, 43-52  |     | 32                      |
| 2228                         | Gas-surface potentials and the interpretation of experiments on the ethylene/graphite system using molecular dynamics calculations. <b>1987</b> , 25, 23-30   |     | 7                       |
| 2227                         | Computer simulation of transformations in solids. <b>1987</b> , 68, 193-213   |     | 3                       |
| 2226                         | Molecular dynamics study of MgSiO3 perovskite. <b>1988</b> , 16, 234  |     | 47                      |
| 2225                         | Elastic constants and statistical ensembles in molecular dynamics. <b>1988</b> , 8, 109-151   |     | 170                     |
| 2224                         | Theoretical studies of the structure and molecular dynamics of a peptide crystal. <b>1988</b> , 27, 5246-57   |     | 107                     |
| 2223                         | Study on liquid por interface of water. I. Simulational results of thermodynamic properties and orientational structure. <b>1988</b> , 88, 3233-3245  |     | 250                     |
|                              | Malagular durantica shudu afilipuid CGlassa and CGlussa Malagular Rhuitu 4000 C4 04 05  |     |                         |
| 2222                         | Molecular dynamics study of liquid CCl2F2 and CCIHF2. <i>Molecular Physics</i> , <b>1988</b> , 64, 91-95  | 1.7 | 19                      |
| 2222                         | Is the Isotropic Atom Atom Model Potential Adequate?. 1988, 1, 135-156  | 1.7 | 31                      |
| 2221                         |   | 1.7 | <u> </u>                |
| 2221                         | Is the Isotropic AtomAtom Model Potential Adequate?. 1988, 1, 135-156   | 1.7 | <u> </u>                |
| 2221                         | Is the Isotropic AtomAtom Model Potential Adequate?. 1988, 1, 135-156  Ferroelastic phase transition and phonons in a diatomic-molecular monolayer. 1989, 39, 677-688  Internal stress tensor in constant-pressure molecular dynamics of anisotropic molecular solids. 1989, 39, 11928-11931  | 1.7 | 31                      |
| 2221<br>2220<br>2219         | Is the Isotropic AtomAtom Model Potential Adequate?. 1988, 1, 135-156  Ferroelastic phase transition and phonons in a diatomic-molecular monolayer. 1989, 39, 677-688  Internal stress tensor in constant-pressure molecular dynamics of anisotropic molecular solids. 1989, 39, 11928-11931  | 1.7 | 31<br>2<br>1            |
| 2221<br>2220<br>2219<br>2218 | Is the Isotropic AtomAtom Model Potential Adequate?. 1988, 1, 135-156  Ferroelastic phase transition and phonons in a diatomic-molecular monolayer. 1989, 39, 677-688  Internal stress tensor in constant-pressure molecular dynamics of anisotropic molecular solids. 1989, 39, 11928-11931  A molecular dynamics study of the crystalline and liquid phases of pyridine. 1989, 130, 15-22  Structure and dynamics of the fluorperovskite, RbCaF3. 1989, 90, 5005-5010 | 1.7 | 31<br>2<br>1<br>24      |
| 2221<br>2220<br>2219<br>2218 | Is the Isotropic AtomAtom Model Potential Adequate?. 1988, 1, 135-156  Ferroelastic phase transition and phonons in a diatomic-molecular monolayer. 1989, 39, 677-688  Internal stress tensor in constant-pressure molecular dynamics of anisotropic molecular solids. 1989, 39, 11928-11931  A molecular dynamics study of the crystalline and liquid phases of pyridine. 1989, 130, 15-22  Structure and dynamics of the fluorperovskite, RbCaF3. 1989, 90, 5005-5010 | 1.7 | 31<br>2<br>1<br>24<br>9 |

| 2213         | Molekldynamik-Computersimulationen; Methodik, Anwendungen und Perspektiven in der Chemie. <b>1990</b> , 102, 1020-1055   | 83  |
|--------------|--|-----|
| 2212         | Location of melting point at 300 K of nitrogen by Monte Carlo simulation. <b>1990</b> , 92, 7570-7575  | 68  |
| 2211         | Deterministic Methods. <b>1990</b> , 13-50   |     |
| 2210         | Isobaric and Isothermal Molecular Dynamics Simulations of Diatomic Systems. <b>1990</b> , 4, 371-398   | 3   |
| 2209         | Vapour liquid equilibrium of a pure fluid from test particle method in combination with NpT molecular dynamics simulations. <i>Molecular Physics</i> , <b>1990</b> , 69, 463-473 | 123 |
| 2208         | Invariant molecular-dynamics approach to structural phase transitions. <b>1991</b> , 44, 2358-2361   | 261 |
| 2207         | An Introduction to Molecular Dynamics, with Applications to the Glass Transition. <b>1991</b> , 3-20   | 1   |
| 2206         | The structure and dynamics of silica polymorphs using a two-body effective potential model. <b>1991</b> , 95, 9176-9185  | 82  |
| 2205         | Molecular Dynamics Simulations at Constant Temperature and Pressure. 1991, 21-41   | 20  |
| 2204         | Phase Transition in Superionic Conductor Ag2Se:A Molecular Dynamics Study. <b>1991</b> , 60, 3745-3753   | 18  |
| 2203         | The condensed phases of pyrazine: A test of the Williams-Weller intermolecular potential. <b>1991</b> , 158, 59-64   |     |
| 2202         | Molecular dynamics of rigid polyatomic molecules on transputer arrays. <b>1991</b> , 62, 169-178   | 7   |
| 2201         | Correlations in the plastic crystal phase of n-butane. <b>1991</b> , 62, 279-288   | 1   |
| <b>22</b> 00 | Competing interactions and orientational ordering in (NaCN)1-x(KCN)x quadrupolar glasses. <b>1991</b> , 66, 624-627  | 7   |
| 2199         | Mechanical instability of alpha -quartz: A molecular dynamics study. <b>1991</b> , 67, 3559-3562   | 192 |
| 2198         | MODELING OF MONOLAYERS. <b>1991</b> , 305-338  | 3   |
| 2197         | Solid C70: A molecular-dynamics study of the structure and orientational ordering. <b>1992</b> , 46, 4958-4962   | 32  |
| 2196         | Constant-pressure molecular-dynamics simulations of the crystal-smectic transition in systems of soft parallel spherocylinders. <b>1992</b> , 46, 6541-6549                      | 46  |

| 2195 | Mechanical instability in ice Ih. A mechanism for pressure-induced amorphization. <b>1992</b> , 96, 5482-5487                               |        | 138 |
|------|---|--------|-----|
| 2194 | Dynamic simulations of water at constant chemical potential. <b>1992</b> , 96, 1333-1342  |        | 62  |
| 2193 | Monte Carlo simulations in the isoenthalpic-isotension-isobaric ensemble. <b>1992</b> , 46, 4645-4649                                       |        | 31  |
| 2192 | Novel molecular dynamics simulations at constant pressure. <i>Molecular Physics</i> , <b>1992</b> , 75, 669-688                             | ,      | 24  |
| 2191 | Ergodicity and Convergence of Fluctuations in Parrinello-Rahman Molecular Dynamics. <b>1992</b> , 291, 285                                  |        | 4   |
| 2190 | Nonlinear Molecular Dynamics and Monte Carlo Simulations Of Crystals at Constant Temperature and Tensorial Pressure. <b>1992</b> , 291, 597 |        |     |
| 2189 | Thermodynamic and Elastic Properties of Polyethylene at Elevated Temperatures. <b>1992</b> , 278, 61  |        | 9   |
| 2188 | Molecular-dynamics investigation of orientational freezing in solid C60. <b>1992</b> , 45, 1889-1895  |        | 106 |
| 2187 | Fluctuations and thermodynamic response functions in a Lennard-Jones solid. <b>1992</b> , 46, 5237-5241                                     |        | 37  |
| 2186 | Structural Memory in Pressure-Amorphized AlPO4. <b>1992</b> , 255, 1559-61  |        | 88  |
| 2185 | Mechanism of pressure-induced polymorphic transition in NaCl. <b>1992</b> , 46, 10547-10553   |        | 15  |
| 2184 | A first approach to a simple intermolecular potential model for the condensed phases of C60. <b>1992</b> , 97, 553-558                      |        | 25  |
| 2183 | High-pressure densification of amorphous silica. <b>1992</b> , 46, 5933-5938  |        | 127 |
| 2182 | Intermolecular interactions and the nature of orientational ordering in the solid fullerenes C 60 and C 70. <b>1992</b> , 341, 327-336      |        | 4   |
| 2181 | Exploration of the phase space of molecular systems: Assessment of established and new methods. <b>1992</b> , 43, 221-238                   |        | 17  |
| 2180 | A replicated data molecular dynamics strategy for the parallel Ewald sum. <b>1992</b> , 67, 392-406   |        | 83  |
| 2179 | Hoover NPT dynamics for systems varying in shape and size. <i>Molecular Physics</i> , <b>1993</b> , 78, 533-544                             | ,      | 871 |
| 2178 | Simulation of site-site soft-core liquid crystal models. <i>Molecular Physics</i> , <b>1993</b> , 80, 297-312                               | ,<br>, | 32  |

| 2177 | Thermodynamic Constraints. <b>1993</b> , 153-171  | 6  |
|------|---|----|
| 2176 | The structure and dynamics of solid benzene. II. Molecular dynamics studies. <b>1993</b> , 98, 8244-8255  | 18 |
| 2175 | Constant pressure molecular dynamics: Instantaneous external stress tensor in systems with periodic boundary conditions. <b>1993</b> , 65, 11-17                |    |
| 2174 | Molecular dynamics study of pressure-induced transition in MgF2. <b>1993</b> , 98, 3240-3245  | 19 |
| 2173 | Molecular-dynamics simulation of crystalline trans-polyacetylene. <b>1993</b> , 48, 12566-12574   | 6  |
| 2172 | References. <b>1993</b> , 240-253   |    |
| 2171 | Monte Carlo calculations on the orientational behaviour of solid nitrogen. 1994,  |    |
| 2170 | Phase transitions of water at constant excess chemical potential An application of grand molecular dynamics. <i>Molecular Physics</i> , <b>1994</b> , 82, 67-83 | 15 |
| 2169 | Ideal chemical potential contribution in molecular dynamics simulations of the grand canonical ensemble. <i>Molecular Physics</i> , <b>1994</b> , 82, 897-912   | 39 |
| 2168 | Multiple time scale methods for constant pressure molecular dynamics simulations of molecular systems. <i>Molecular Physics</i> , <b>1994</b> , 83, 255-272     | 42 |
| 2167 | Molecular dynamics simulation of crystalline poly(ethylene oxide). <b>1994</b> , 101, 10064-10073   | 97 |
| 2166 | Atomistic simulations incorporating nonlinear elasticity: Slow-stress relaxation and symmetry breaking. <b>1994</b> , 49, 11619-11633                           | 12 |
| 2165 | Low-temperature phase transition in C60-n-pentane. <b>1994</b> , 49, 9186-9189  | 14 |
| 2164 | Dislocation-mediated healing of ideal and adsorbed monolayers with vacancy damage. <b>1994</b> , 50, 8763-8772  | 6  |
| 2163 | A special-purpose computer for molecular dynamics: GRAPE-2A. <b>1994</b> , 20, 139-48   | 11 |
| 2162 | The integration of molecular dynamics simulations with imposed temperature and stress. <b>1994</b> , 79, 219-248  | 2  |
| 2161 | Dynamic origin of the orthorhombic symmetry of C60-n-pentane. <b>1994</b> , 89, 417-419   | 12 |
| 2160 | The role of non-deformable units in pressure-induced reversible amorphization of clathrasils. <b>1994</b> , 369, 724-727  | 74 |

| 2159 | Constant pressure molecular dynamics algorithms. <b>1994</b> , 101, 4177-4189  | 3338  |
|------|--|-------|
| 2158 | Pressure tensor of partial-charge and point-dipole lattices with bulk and surface geometries. <b>1994</b> , 49, 755-764  | 227   |
| 2157 | The effect of molecular shape anisotropy on surface melting. <b>1994</b> , 302, L331-L335  | 1     |
| 2156 | Pressure Calculation in Molecular Dynamics Simulations of Molecular Crystals. <b>1994</b> , 13, 221-230  | 5     |
| 2155 | Molecular Dynamics Simulation of Structure and Thermodynamic Properties of Tricalcium Phosphate. <b>1994</b> , 329-332   |       |
| 2154 | Molecular dynamics simulation of the dipalmitoylphosphatidylcholine (DPPC) lipid bilayer in the fluid phase using the NosEParrinello-Rahman NPT ensemble. <b>1995</b> , 232, 308-312 | 34    |
| 2153 | Bismuth valence and lattice dynamics studies in BaBiO3 by molecular dynamics. <b>1995</b> , 243, 262-272   |       |
| 2152 | Constant pressure molecular dynamics simulation: The Langevin piston method. <b>1995</b> , 103, 4613-4621  | 3093  |
| 2151 | Crystal stability limits at positive and negative pressures, and crystal-to-glass transitions. <b>1995</b> , 52, 6484-6491   | 51    |
| 2150 | A general pressure tensor calculation for molecular dynamics simulations. <i>Molecular Physics</i> , <b>1995</b> , 84, 577-595   | 82    |
| 2149 | Test of a simple model of the intermolecular potential of C60 on the series of KnC60, 0. <b>1995</b> , 102, 8132-8137  | 1     |
| 2148 | Reversible amorphization and structural memory effect in clathrasil dodecasil-3c. <b>1995</b> , 6, 165-170   | 4     |
| 2147 | A smooth particle mesh Ewald method. <b>1995</b> , 103, 8577-8593  | 14532 |
| 2146 | Molecular dynamics simulation of the orthobaric densities and surface tension of water. <b>1995</b> , 102, 4574-4583   | 557   |
| 2145 | Computer simulation of liquid/liquid interfaces. II. Surface tension-area dependence of a bilayer and monolayer. <b>1995</b> , 103, 10267-10276                                      | 174   |
| 2144 | Computer simulation of liquid/liquid interfaces. I. Theory and application to octane/water. <b>1995</b> , 103, 10252-10266   | 293   |
| 2143 | Stokesian Dynamics Simulations of Colloids Under Shear. <b>1995</b> , 15, 361-380  | 3     |
| 2142 | Molecular dynamics investigation of the structure of a fully hydrated gel-phase dipalmitoylphosphatidylcholine bilayer. <b>1996</b> , 70, 595-608                                    | 153   |

| 2141 | Constant-Pressure Molecular Dynamics Techniques Applied to Complex Molecular Systems and Solvated Proteins. <b>1996</b> , 100, 4314-4322                  | 28            |
|------|---|---------------|
| 2140 | Shear viscosity of polar fluids: Molecular dynamics calculations of water. <b>1996</b> , 105, 11190-11195   | 63            |
| 2139 | The importance of the anisotropic energy term for the structure of the solid phases of nitrogen. <b>1996</b> , 105, 3235-3244                             | 27            |
| 2138 | Explicit reversible integrators for extended systems dynamics. <i>Molecular Physics</i> , <b>1996</b> , 87, 1117-1157 1.7                                 | 1296          |
| 2137 | Pressure induced amorphization of materials. <b>1996</b> , 40, 1-77   | 286           |
| 2136 | Prediction of thermodynamic properties for fluid nitrogen with molecular dynamics simulations. <b>1996</b> , 17, 1349-1363                                | 11            |
| 2135 | Derivation of conventional crystallographic descriptions of new phases from results of ab initio inorganic structure modelling. <b>1996</b> , 29, 503-508 | 11            |
| 2134 | Application of the Nos⊞oover Chain Algorithm to the Study of Protein Dynamics. <b>1996</b> , 100, 1927-1937   | 111           |
| 2133 | The Pressure and Pressure Tensor for Macromolecular Systems. <b>1996</b> , 100, 905-908   | 4             |
| 2132 | The condensed phases of carboranes. <b>1996</b> , 105, 2436-2440  | 18            |
| 2131 | A molecular dynamics model of the amorphous regions of polyethylene oxide. <b>1996</b> , 105, 1668-1681   | 45            |
| 2130 | Lennard-Jones potential model for the condensed phases of C70. <b>1996</b> , 53, 2159-2162  | 7             |
| 2129 | Structural Transformations of Ice at High Pressures Via Molecular Dynamics Simulations. <b>1996</b> , 18, 115-132   | 2             |
| 2128 | A molecular-dynamics simulation of the orientational melting of potassium perchlorate. <b>1996</b> , 33, 365-370  | 5             |
| 2127 | Molecular modelling of a polyarylethersulfone under bulk conditions. <b>1996</b> , 4, 151-159   | 17            |
| 2126 | A molecular dynamics study of the CO2/NaCl(001) system. <b>1997</b> , 106, 5693-5705  | 6             |
| 2125 | Mechanisms of membrane rupture: From cracks to pores. <b>1997</b> , 56, 2997-3009   | 16            |
| 2124 | Rotational ordering in solid deuterium and hydrogen: A path integral Monte Carlo study. <b>1997</b> , 55, 12253-122                                       | 16 <b>6</b> 4 |

| 2123 | Molecular dynamics study of a lipid bilayer: Convergence, structure, and long-time dynamics. <b>1997</b> , 106, 5731-5743  | 58   |
|------|--|------|
| 2122 | Non-equilibrium molecular dynamics simulation of the shear viscosity of liquid methanol: adaptation of the Ewald sum to Lees-Edwards boundary conditions. <i>Molecular Physics</i> , <b>1997</b> , 92, 55-62 | 55   |
| 2121 | Structural Transformations of Ice at High Pressures via Molecular Dynamics Simulations II. <b>1997</b> , 18, 395-406   | 2    |
| 2120 | Some Aspects of Phase Diagrams of Homonuclear Diatomic Assemblies, Including Melting and Critical Point Properties. <b>1997</b> , 35, 131-151  | 2    |
| 2119 | Large Scale Atomistic Simulations using the Tight Binding Approach. <b>1997</b> , 491, 481   |      |
| 2118 | Structure and Dynamics of Zeolites Investigated by Molecular Dynamics. <b>1997</b> , 97, 2845-2878   | 237  |
| 2117 | Modern Computational Methodology Applied to the Simulation of Blocked Trialanine Peptide in Vacuo, Water Clusters, and Bulk Water. <b>1997</b> , 101, 7592-7603  | 21   |
| 2116 | Intermolecular Potential for the Hexahydro-1,3,5-trinitro-1,3,5-s-triazine Crystal (RDX): A Crystal Packing, Monte Carlo, and Molecular Dynamics Study. <b>1997</b> , 101, 798-808                           | 107  |
| 2115 | High-pressure four-coordinated structure of SiO2. <b>1997</b> , 56, 10878-10881  | 18   |
| 2114 | Crystal Packing and Molecular Dynamics Studies of the 5-Nitro-2,4-dihydro-3H-1,2,4-triazol-3-one Crystal. <b>1997</b> , 101, 3605-3613   | 31   |
| 2113 | Calculation of vibrational properties of selenium. <b>1997</b> , 9, 1049-1066  | 12   |
| 2112 | Atomic stress isobaric scaling for systems subjected to holonomic constraints. <b>1997</b> , 106, 195-199  | 31   |
| 2111 | Metric tensor as the dynamical variable for variable-cell-shape molecular dynamics. <b>1997</b> , 55, 8733-8742  | 128  |
| 2110 | Single particle orientational potential for the N2 molecules in the cubic phase of nitrogen. <b>1997</b> , 100, 417-421  | 7    |
| 2109 | ORAC: A Molecular dynamics program to simulate complex molecular systems with realistic electrostatic interactions. <b>1997</b> , 18, 1848-1862  | 152  |
| 2108 | Relaxation of Crystals with the Quasi-Newton Method. <b>1997</b> , 131, 233-240  | 1913 |
| 2107 | Pressure dependence and activation volume for the water exchange mechanism in NaCl(aq) from MD simulations. <b>1997</b> , 276, 114-121   | 22   |
| 2106 | Molecular Dynamics Study of Proton Binding to Silica Surfaces. <b>1998</b> , 198, 119-129  | 39   |

| 2105 | Estimation of infinite dilution activity coefficients in aqueous mixtures via molecular simulation. <b>1998</b> , 153, 45-61  | 11 |
|------|---|----|
| 2104 | Rotational dynamics in orientationally disordered KClO4. <b>1998</b> , 10, 57-62  |    |
| 2103 | Self-locking of a modulated single overlayer in a nanotribology simulation. <b>1998</b> , 419, 29-37  | 14 |
| 2102 | The ordered, orientationally disordered and glassy phases of P4S3. <i>Molecular Physics</i> , <b>1998</b> , 94, 815-820 <sub>1.7</sub>  |    |
| 2101 | Water Exchange around Li+ and Na+ in LiCl(aq) and NaCl(aq) from MD Simulations. 1998, 102, 6089-6097  | 51 |
| 2100 | Molecular Dynamics of Atactic Polypropylene Melts. <b>1998</b> , 31, 7944-7952  | 53 |
| 2099 | Molecular Dynamics Study on Electrostatic Properties of a Lipid Bilayer: Polarization, Electrostatic Potential, and the Effects on Structure and Dynamics of Water near the Interface. <b>1998</b> , 102, 6647-6654 | 49 |
| 2098 | Molecular Packing and NPT-Molecular Dynamics Investigation of the Transferability of the RDX Intermolecular Potential to 2,4,6,8,10,12-Hexanitrohexaazaisowurtzitane. <b>1998</b> , 102, 948-952                    | 61 |
| 2097 | A Voronoi analysis of lipid area fluctuation in a bilayer. <b>1998</b> , 109, 1517-1521   | 77 |
| 2096 | Parallel tight-binding molecular dynamics code based on integration of HPF and optimized parallel libraries. <b>1998</b> , 104-111  |    |
| 2095 | Two dimensional umbrella sampling techniques for the computer simulation study of helical peptides at thermal equilibrium: The 3K(I) peptide in vacuo and solution. <b>1998</b> , 109, 11061-11073                  | 29 |
| 2094 | Pressure calculation in polar and charged systems using Ewald summation: Results for the extended simple point charge model of water. <b>1998</b> , 109, 2791-2797  | 59 |
| 2093 | Coordinates scaling and multiple time step algorithms for simulation of solvated proteins in the NPT ensemble. <b>1998</b> , 109, 5194-5202   | 88 |
| 2092 | Efficient stress relaxation in molecular dynamics simulations of semiflexible n-alkanes. <b>1998</b> , 58, 6766-6780  | 13 |
| 2091 | A Phase Diagram for the Ice VIIVIIIVIII Transitions. 1998, 12, 271-279  | 7  |
| 2090 | Large-scale molecular-dynamics simulations of martensitic nucleation and shape-memory effects in transition metal alloys. <b>1998</b> , 65, 79-108  | 11 |
| 2089 | Molecular dynamics studies of the hexagonal mesophase of sodium dodecylsulphate in aqueous solution. <i>Molecular Physics</i> , <b>1998</b> , 95, 377-384   | 19 |
| 2088 | Rotational dynamics and velocity segregation in plastic KClO4 : a molecular dynamics simulation.  Molecular Physics, 1998, 93, 703-711  |    |

| <sup>2087</sup> 60, 292-298  | 39                     |
|--|------------------------|
| Assessing the driving force of a structural distortion by the simulated evolution of the local density of states. <b>1999</b> , 59, 3480-3488  | 13                     |
| Molecular Dynamics Machine: Special-Purpose Computer for Molecular Dynamics Simulations. <b>1999</b> , 21, 401-415   | 65                     |
| 2084 Molecular dynamics algorithms for path integrals at constant pressure. <b>1999</b> , 110, 3275-3290   | 165                    |
| 2083 Molecular Dynamics Studies of Amorphous Poly(Tetrafluoroethylene). <b>1999</b> , 21, 325-342  | 8                      |
| Potential energy landscape of a model glass former: thermodynamics, anharmonicities, and finite size effects. <b>1999</b> , 60, 6507-18  | 169                    |
| 2081 MD-simulation study of the hydrophobic hydration of nonionic surfactants. <b>1999</b> , 156, 489-500  | 8                      |
| 2080 Regularities at phase transitions in molecular assemblies. <b>1999</b> , 265, 24-30   | 6                      |
| 2079 Parallel molecular dynamics simulation: Implementation of PVM for a lipid membrane. <b>1999</b> , 116, 295-310  | 9                      |
| An high performance Fortran implementation of a Tight-Binding Molecular Dynamics simulation. $^{2078}$ <b>1999</b> , 120, 255-268  | 3                      |
|  |                        |
| 2077 Simulation of thermal conductivity and heat transport in solids. <b>1999</b> , 59, 4125-4133  | 114                    |
| 2077 Simulation of thermal conductivity and heat transport in solids. <b>1999</b> , 59, 4125-4133  2076 Molecular dynamics simulation of polar chains under an external electric field. <b>1999</b> , 6, 59-66   |                        |
|  |                        |
| 2076 Molecular dynamics simulation of polar chains under an external electric field. <b>1999</b> , 6, 59-66  A modified version of the Cornell et al. force field with improved sugar pucker phases and helical  | 114                    |
| 2076 Molecular dynamics simulation of polar chains under an external electric field. <b>1999</b> , 6, 59-66  A modified version of the Cornell et al. force field with improved sugar pucker phases and helical repeat. <b>1999</b> , 16, 845-62   | 114<br>810             |
| 2076 Molecular dynamics simulation of polar chains under an external electric field. <b>1999</b> , 6, 59-66  2075 A modified version of the Cornell et al. force field with improved sugar pucker phases and helical repeat. <b>1999</b> , 16, 845-62  2074 Voids and clusters in expanded water. <b>1999</b> , 110, 2109-2115   | 114<br>810<br>60       |
| 2076 Molecular dynamics simulation of polar chains under an external electric field. 1999, 6, 59-66  2075 A modified version of the Cornell et al. force field with improved sugar pucker phases and helical repeat. 1999, 16, 845-62  2074 Voids and clusters in expanded water. 1999, 110, 2109-2115  2073 Chain formation in homogeneous gasIlquid nucleation of polar fluids. 1999, 111, 4762-4773  Molecular Packing and Molecular Dynamics Study of the Transferability of a Generalized Nitramine | 114<br>810<br>60<br>45 |

| 2069 Reversible integrators for basic extended system molecular dynamics. <i>Molecular Physics</i> , <b>1999</b> , 97,   | , 825-8 <u>3</u> . <del>2</del> ⁄ | 14  |
|--|-----------------------------------|-----|
| Computer Simulation Studies of Finite Temperature Conformational Equilibrium in Alanine-Based Peptides. <b>1999</b> , 103, 1752-1766   |                                   | 35  |
| Treatment of electrostatic interactions in computer simulations and calculation of thermodynamic properties such as free energies and pressures. <b>1999</b> ,                 | С                                 | 8   |
| 2066 HPF parallelization of a Molecular Dynamics code: Strategies and performances. <b>1999</b> , 535-542  |                                   |     |
| PARALLELIZATION OF A TIGHT-BINDING MOLECULAR DYNAMICS CODE BY USING THE HPF ENVIRONMENT. <b>2000</b> , 211-219   |                                   |     |
| 2064 Test of a simple and flexible S8 model molecule in ∃-S8 crystals. <b>2000</b> , 319, 20-26  |                                   | 6   |
| 2063 Study of sulfur \(\text{H}\)-S8 crystals with an anisotropic inter-molecular potential model. <b>2000</b> , 261, 317-33   | 21                                | 1   |
| 2062 Thermodynamics of supercooled liquids in the inherent-structure formalism: a case study. <b>2000</b> , 12   | 2, 6525-653                       | 460 |
| Test of a simple and flexible molecule model for $\oplus$ -, $\oplus$ and $\oplus$ S8 crystals. <b>2000</b> , 112, 282-286   |                                   | 7   |
| Constant pressure path integral molecular dynamics studies of quantum effects in the liquid state properties of n-alkanes. <b>2000</b> , 112, 870-880                          |                                   | 19  |
| The ordered and orientationally disordered crystalline phases of the flexible C4F8 molecule. <b>2000</b> , 112, 3787-3791  | 1                                 | 3   |
| Search for precursor of pressure-induced amorphization of molecular crystal SnI4: Thermodynamic stability of low-pressure crystalline phase. <b>2000</b> , 112, 10379-10390    | c                                 | 19  |
| 2057 Simulations of the nucleation of AgBr from solution. <b>2000</b> , 113, 6276-6284   |                                   | 56  |
| Structural and thermoelastic properties of crystalline and amorphous TiSi2 phases by tight-binding molecular dynamics. <b>2000</b> , 61, 14405-14413                           | g<br>                             | 15  |
| Structure and predicted near edge x-ray absorption fine structure spectra for the surface of liquid formamide from molecular-dynamics simulation. <b>2000</b> , 113, 3374-3380 |                                   | 6   |
| Generalized Gaussian moment thermostatting: A new continuous dynamical approach to the canonical ensemble. <b>2000</b> , 112, 1685-1700  |                                   | 107 |
| Spatial and energetic-entropic decomposition of surface tension in lipid bilayers from molecular dynamics simulations. <b>2000</b> , 113, 3882-3893                            |                                   | 226 |
| Shear viscosity and dielectric constant in aqueous isopropanol and aqueous acetonitrile. <i>Moleculai</i> 2052 <i>Physics</i> , <b>2000</b> , 98, 287-293                      | r<br>1.7                          | 16  |

#### (2001-2000)

2051 Efficient particle-mesh Ewald based approach to fixed and induced dipolar interactions. **2000**, 113, 10913-1092**3**29

| 2050 Understanding Modern Molecular Dynamics: Techniques and Applications. <b>2000</b> , 104, 159-178  | 259      |
|--|----------|
| Non-Hamiltonian molecular dynamics: Generalizing Hamiltonian phase space principles to non-Hamiltonian systems. <b>2001</b> , 115, 1678-1702   | 244      |
| Promotion of Crystal Phase Transitions by Mass-of-cell Control in Molecular Dynamics Simulations:  Phase Transitions in Benzene Crystals. <b>2001</b> , 26, 273-285                              | 4        |
| The ice/water interface: Molecular dynamics simulations of the basal, prism, {202 1}, and {21 1 0} interfaces of ice Ih. <b>2001</b> , 114, 3713-3726  | 84       |
| 2046 Lithium Ion Motion in LiZr2(PO4)3. <b>2001</b> , 105, 6785-6791   | 22       |
| 2045 Lipid Bilayers. <b>2001</b> ,   | 49       |
| 2044 Self-diffusion of silicon in TiSi2 competing phases by tight-binding molecular dynamics. <b>2001</b> , 20, 39   | 94-400 3 |
| 2043 SIMULATION STUDIES OF CRYSTAL-SMECTIC TRANSITION. <b>2001</b> , 366, 117-124  | 7        |
| 2042 Constrained Isothermalßobaric Molecular Dynamics with Full Atomic Virial 2001, 105, 6710-6715   | 13       |
| 2041 Insights into Protein Compressibility from Molecular Dynamics Simulations. <b>2001</b> , 105, 715-724   | 56       |
| 2040 Equation of State for Liquid Tin Tetraiodide under Hydrostatic Pressure. <b>2001</b> , 70, 1321-1326  | 4        |
| 2039 GROMACS 3.0: a package for molecular simulation and trajectory analysis. <b>2001</b> , 7, 306-317   | 5502     |
| Molecular dynamics study of the dipalmitoyl phosphatidylcholine bilayer in the liquid crystal phase: an effect of the potential force fields on the membrane structure. <b>2001</b> , 90, 95-103 | 4        |
| A simulation study on the absorption of molybdenum species in the channels of HZSM-5 zeolite. <b>2037 2001</b> , 168, 225-232  | 21       |
| Validation of nitroxyl spin-label force-field parameters through molecular dynamics simulations. <b>203</b> 6 <b>2001</b> , 22, 1113-1123  | 1        |
| 2035 Constant pressure molecular dynamics on a hypercylinder. <b>2001</b> , 64, 026112   | 4        |
| Molecular dynamics simulation of the liquid por interface of dipolar fluids under different electrostatic boundary conditions. <b>2001</b> , 114, 5842-5852                                      | 35       |

| 2033 | Ground-state structure of ₹3N4 by first-principles calculations. 2001, 64,   | 3   |
|------|--|-----|
| 2032 | Toward an anisotropic atom। tom model for the crystalline phases of the molecular S8 compound. <b>2001</b> , 115, 9421-9426  | 8   |
| 2031 | Ab initio simulation of first-order amorphous-to-amorphous phase transition of silicon. <b>2001</b> , 64,  | 73  |
| 2030 | Fluctuations and thermodynamics properties of the constant shear strain ensemble. <b>2001</b> , 114, 8769-8774   | 13  |
| 2029 | Monte Carlo simulations of Wyoming sodium montmorillonite hydrates. <b>2001</b> , 114, 1405-1413   | 146 |
| 2028 | Rapid calculation of the Coulomb component of the stress tensor for three-dimensional systems with two-dimensional periodicity. <b>2001</b> , 115, 4457-4462       | 26  |
| 2027 | Computer simulation of polar bent-core molecules. <b>2002</b> , 66, 061702   | 16  |
| 2026 | Amorphous silica between confining walls and under shear: A computer simulation study. <b>2002</b> , 117, 10796-10804  | 3   |
| 2025 | Calculation of the group-based pressure in molecular simulations. II. Numerical tests and application to liquid water. <b>2002</b> , 116, 6898-6909                | 10  |
| 2024 | Pressure-induced structural phase transition of paracrystalline silicon. <b>2002</b> , 66,   | 8   |
| 2023 | Computationally efficient method to calculate the Coulomb interactions in three-dimensional systems with two-dimensional periodicity. <b>2002</b> , 116, 3430-3448 | 32  |
| 2022 | Virial pressure of periodic systems with long range forces. <b>2002</b> , 117, 2449-2450   | 13  |
| 2021 | Computational Approaches to Biochemical Reactivity. 2002,  | 10  |
| 2020 | Orientational phase transition between hexagonal solids in planar systems of hard cyclic pentamers and heptamers. <b>2002</b> , 14, 1261-1273                      | 11  |
| 2019 | Ion Mobility and Levitation Effect: Anomalous Diffusion in Nasicon-Type Structure. <b>2002</b> , 106, 3443-3448  | 14  |
| 2018 | Transport Coefficients of Xylene Isomers. <b>2002</b> , 106, 13010-13017   | 10  |
| 2017 | Reduction of the glass transition temperature in polymer films: a molecular-dynamics study. <b>2002</b> , 65, 021507   | 183 |
| 2016 | Simulation of pressure-driven phase transitions from tetrahedral crystal structures. <b>2002</b> , 65,   | 32  |

2015 THEORETICAL STUDIES. **2002**, 185-201

| 2014 | Development of transferable interaction models for water. III. Reparametrization of an all-atom polarizable rigid model (TTM2R) from first principles. <b>2002</b> , 116, 1500-1510        | 160  |
|------|--|------|
| 2013 | Free Energy Calculations. The Long and Winding Gilded Road. <b>2002</b> , 28, 1-12   | 79   |
| 2012 | A molecular dynamics method for simulations in the canonical ensemble. <i>Molecular Physics</i> , <b>2002</b> , 100, 191-198   | 193  |
| 2011 | Calculation of the group-based pressure in molecular simulations. I. A general formulation including Ewald and particle-particleparticle-mesh electrostatics. <b>2002</b> , 116, 6880-6897 | 39   |
| 2010 | Energy control of a molecular dynamics cell for the promotion of crystal phase transitions.  Molecular Physics, <b>2002</b> , 100, 3915-3919   | 3    |
| 2009 | Molecular Dynamics Study on the Density Fluctuation of Supercritical Water 2002, 1, 83-88  | 4    |
| 2008 | High pressure simulations of biomolecules. <b>2002</b> , 1595, 185-200   | 51   |
| 2007 | Rigid-body dynamics in the isothermal-isobaric ensemble: a test on the accuracy and computational efficiency. <b>2003</b> , 24, 920-30   | 78   |
| 2006 | Quantum chemical contributions on the reactivity of solids. <b>2003</b> , 176, 575-586   | 1    |
| 2005 | Influence of temperature, pressure and internal degrees of freedom on hydrogen bonding and diffusion in liquid ethanol. <b>2003</b> , 286, 303-314   | 17   |
| 2004 | Synthesis and self-organization of rodflendron and dendronflodflendron molecules. <b>2003</b> , 41, 3501-3518  | 39   |
| 2003 | Structure of gramicidin a in a lipid bilayer environment determined using molecular dynamics simulations and solid-state NMR data. <b>2003</b> , 125, 9868-77                              | 115  |
| 2002 | Polarizable Atomic Multipole Water Model for Molecular Mechanics Simulation. <b>2003</b> , 107, 5933-5947  | 1148 |
| 2001 | Molecular Simulation of Disjoining-Pressure Isotherms for Free Aqueous Thin Films. <b>2003</b> , 107, 13076-13083  | 26   |
| 2000 | Dynamic properties of screw dislocations in Cu: A molecular dynamics study. <b>2003</b> , 67,  | 37   |
| 1999 | Configurational entropy and cooperativity between ligand binding and dimerization in glycopeptide antibiotics. <b>2003</b> , 125, 3988-94  | 47   |
| 1998 | Predicting crystal structures: the Parrinello-Rahman method revisited. <b>2003</b> , 90, 075503  | 482  |

| 1997 | Advances in biomolecular simulations: methodology and recent applications. 2003, 36, 257-306   | 116 |
|------|--|-----|
| 1996 | Membrane protein dynamics versus environment: simulations of OmpA in a micelle and in a bilayer. <b>2003</b> , 329, 1035-53  | 125 |
| 1995 | The implementation of slab geometry for membrane-channel molecular dynamics simulations. <b>2003</b> , 85, 97-107  | 64  |
| 1994 | Mixed bilayer containing dipalmitoylphosphatidylcholine and dipalmitoylphosphatidylserine: lipid complexation, ion binding, and electrostatics. <b>2003</b> , 85, 3120-31  | 140 |
| 1993 | Molecular dynamics simulation of a dipalmitoylphosphatidylcholine bilayer with NaCl. 2003, 84, 3743-50   | 205 |
| 1992 | Constant pressure-constant temperature molecular dynamics: a correct constrained NPT ensemble using the molecular virial. <i>Molecular Physics</i> , <b>2003</b> , 101, 765-778  | 56  |
| 1991 | An algorithm to describe molecular scale rugged surfaces and its application to the study of a water/lipid bilayer interface. <b>2003</b> , 119, 2199-2205   | 85  |
| 1990 | Extended methods of molecular dynamic simulations under hydrostatic pressure and/or isostress. <b>2003</b> , 118, 9926-9936  | 10  |
| 1989 | Ewald summation of electrostatic multipole interactions up to the quadrupolar level. 2003, 119, 7471-7483  | 101 |
| 1988 | Elastic properties of dense solid phases of hard cyclic pentamers and heptamers in two dimensions. <b>2003</b> , 67, 036121  | 84  |
| 1987 | Conductivity of molten sodium chloride and its supercritical vapor in strong dc electric fields. <b>2003</b> , 118, 7477   | 30  |
| 1986 | Simulation by Molecular Dynamics. 2003,  |     |
| 1985 | High density amorphous form and polyamorphic transformations of silicon. <b>2004</b> , 93, 055503  | 75  |
| 1984 | Heat capacity effects associated with the hydrophobic hydration and interaction of simple solutes: a detailed structural and energetical analysis based on molecular dynamics simulations. <b>2004</b> , 120, 10605-17 | 69  |
| 1983 | Interpretation of x-ray and neutron diffraction patterns for liquid and amorphous yttrium and lanthanum aluminum oxides from computer simulation. <b>2004</b> , 69,  | 26  |
| 1982 | Stochastic Liouville equation simulation of multidimensional vibrational line shapes of trialanine. <b>2004</b> , 121, 10577-98  | 71  |
| 1981 | Temperature dependence of the hydrophobic hydration and interaction of simple solutes: an examination of five popular water models. <b>2004</b> , 120, 6674-90   | 241 |
| 1980 | Dynamic simulation of pressure-driven phase transformations in crystalline Al2O3. <b>2004</b> , 69,  | 16  |

| 1979 | Combined Monte Carlo and molecular dynamics simulation of hydrated 18:0 sphingomyelin-cholesterol lipid bilayers. <b>2004</b> , 120, 9841-7   | 68  |
|------|---|-----|
| 1978 | Study of the Nature and Mechanism of the Rhombohedral-to-Cubic Phase Transition in ⊞-AlF3with Molecular Dynamics Simulations. <b>2004</b> , 108, 3437-3445  | 25  |
| 1977 | Raman investigation of the $n(2)$ - $o(2)$ binary system as a function of pressure and temperature. <b>2004</b> , 108, 6429-40  | 4   |
| 1976 | Effect of octupoleBctupole interactions on the thermodynamic stability of the low-pressure crystalline state of SnI4 molecular crystals. <b>2004</b> , 132, 305-308   | 6   |
| 1975 | Nonequilibrium Molecular Dynamics Simulations of Molten Sodium Chloride. <b>2004</b> , 25, 1375-1393  | 7   |
| 1974 | A simple topological representation of protein structure: implications for new, fast, and robust structural classification. <b>2004</b> , 56, 487-501   | 22  |
| 1973 | Molecular dynamics simulation of the liquidNapor interface: I. The orientational profile of 2-center LennardDones and of Stockmayer fluid molecules. <b>2004</b> , 115, 29-39   | 12  |
| 1972 | Molecular dynamics simulations of the elastic moduli of polymerBarbon nanotube composites. <b>2004</b> , 193, 1773-1788   | 276 |
| 1971 | Molecular dynamic simulation methods for anisotropic liquids. <b>2004</b> , 120, 5576-84  | 13  |
| 1970 | Molecular Dynamics Simulation of the Shear Viscosity of Molten Alkali Halides. <b>2004</b> , 108, 3658-3662   | 41  |
| 1969 | Molecular Dynamics Simulations of Surface Tensions of Aqueous Electrolytic Solutions. <b>2004</b> , 108, 9077-9084  | 49  |
| 1968 | Molecular Dynamics Simulations of Intercalated Poly(¡Caprolactone)-Montmorillonite Clay Nanocomposites. <b>2004</b> , 108, 10678-10686  | 44  |
| 1967 | Dissociation of Hydrogen Chloride and Proton Transfer in Liquid Glycerol: An Ab Initio Molecular Dynamics Study <b>2004</b> , 108, 19647-19656  | 15  |
| 1966 | Molecular Dynamics Simulation of Structure and Thermodynamic Properties of Poly(dimethylsilamethylene) and Hydrocarbon Solubility Therein: Toward the Development of Novel Membrane Materials for Hydrocarbon Separation. <b>2004</b> , 37, 1102-1112 | 44  |
| 1965 | Insights into the phosphoryl-transfer mechanism of cAMP-dependent protein kinase from quantum chemical calculations and molecular dynamics simulations. <b>2004</b> , 126, 529-42   | 64  |
| 1964 | Size dependent ion hydration, its asymmetry, and convergence to macroscopic behavior. <b>2004</b> , 120, 4457-66  | 133 |
| 1963 | Exterior site occupancy infers chloride-induced proton gating in a prokaryotic homolog of the ClC chloride channel. <b>2004</b> , 87, 1686-96   | 51  |
| 1962 | Simulation of the early stages of nano-domain formation in mixed bilayers of sphingomyelin, cholesterol, and dioleylphosphatidylcholine. <b>2004</b> , 87, 3312-22  | 154 |

| 1961 | Towards an accurate representation of electrostatics in classical force fields: efficient implementation of multipolar interactions in biomolecular simulations. <b>2004</b> , 120, 73-87 | 178   |
|------|---|-------|
| 1960 | Thermal conductivity of molten alkali halides from equilibrium molecular dynamics simulations. <b>2004</b> , 120, 8676-82   | 69    |
| 1959 | Gibbs Free Energy Perturbation Calculations: An Application to the Binding of Alkylammonium Cations by a Water-Soluble Calixarene. <b>2004</b> , 108, 11744-11752                         | 32    |
| 1958 | Structure and dynamics of sphingomyelin bilayer: insight gained through systematic comparison to phosphatidylcholine. <b>2004</b> , 87, 2976-89   | 126   |
| 1957 | Complexation of phosphatidylcholine lipids with cholesterol. <b>2004</b> , 86, 1345-56  | 130   |
| 1956 | Molecular Dynamics Simulation on Anelasticity under Tensile and Shearing Stresses in Single Component Amorphous Metal. <b>2005</b> , 46, 2875-2879  | 2     |
| 1955 | Structure and dynamics of water at the interface with phospholipid bilayers. <b>2005</b> , 123, 224702  | 110   |
| 1954 | How pH opens a H+ channel: the gating mechanism of influenza A M2. <b>2005</b> , 13, 1789-98  | 56    |
| 1953 | GROMACS: fast, flexible, and free. <b>2005</b> , 26, 1701-18  | 10273 |
| 1952 | The GROMOS software for biomolecular simulation: GROMOS05. <b>2005</b> , 26, 1719-51  | 514   |
| 1951 | Correlated dynamics determining x-ray diffuse scattering from a crystalline protein revealed by molecular dynamics simulation. <b>2005</b> , 95, 218103                                   | 24    |
| 1950 | Geometry optimization of periodic systems using internal coordinates. <b>2005</b> , 122, 124508   | 106   |
| 1949 | Self-consistent mean-field model based on molecular dynamics: application to lipid-cholesterol bilayers. <b>2005</b> , 123, 34910   | 35    |
| 1948 | Shear viscosity of molten alkali halides from equilibrium and nonequilibrium molecular-dynamics simulations. <b>2005</b> , 122, 224501  | 39    |
| 1947 | Dynamics on a torus. <b>2005</b> , 71, 016111   | 3     |
| 1946 | Time reversible and symplectic integrators for molecular dynamics simulations of rigid molecules. <b>2005</b> , 122, 224114   | 123   |
| 1945 | Pressure-dependent transition in protein dynamics at about revealed by molecular dynamics simulation. <b>2005</b> , 72, 061908  | 18    |
| 1944 | Molecular dynamics simulation approaches to K channels: conformational flexibility and physiological function. <b>2005</b> , 4, 112-20  | 18    |

| 1943 | Dynamics of water trapped between hydrophobic solutes. <b>2005</b> , 109, 6422-9   | 150 |
|------|--|-----|
| 1942 | Evolutionarily conserved functional mechanics across pepsin-like and retroviral aspartic proteases. <b>2005</b> , 127, 3734-42                               | 71  |
| 1941 | Molecular dynamics simulations of nanocomposites based on poly(epsilon-caprolactone) grafted on montmorillonite clay. <b>2005</b> , 109, 12287-96            | 42  |
| 1940 | Local density profiles are coupled to solute size and attractive potential for nanoscopic hydrophobic solutes. <b>2005</b> , 31, 457-463                     | 35  |
| 1939 | Structure of Normal and Supercooled Liquid Aluminum Oxide. <b>2005</b> , 17, 2662-2666   | 25  |
| 1938 | Solubility of methane in water: the significance of the methane-water interaction potential. <b>2005</b> , 109, 23596-604                                    | 26  |
| 1937 | On the mechanism of hydrophobic association of nanoscopic solutes. <b>2005</b> , 127, 3556-67  | 268 |
| 1936 | The effect of the rigidity of perfluoropolyether surfactant on its behavior at the water/supercritical carbon dioxide interface. <b>2005</b> , 109, 21725-31 | 14  |
| 1935 | Thermostat Algorithms for Molecular Dynamics Simulations. <b>2005</b> , 105-149  | 321 |
| 1934 | What contributions to protein side-chain dynamics are probed by NMR experiments? A molecular dynamics simulation analysis. <b>2005</b> , 349, 185-203        | 88  |
| 1933 | Nucleotide binding to the homodimeric MJ0796 protein: a computational study of a prokaryotic ABC transporter NBD dimer. <b>2005</b> , 579, 4193-9            | 32  |
| 1932 | Simulation of structural phase transitions by metadynamics. <b>2005</b> , 220,   | 80  |
| 1931 | Fluctuations and correlations in crystalline protein dynamics: a simulation analysis of staphylococcal nuclease. <b>2005</b> , 88, 2554-63                   | 61  |
| 1930 | A molecular dynamics study of the response of lipid bilayers and monolayers to trehalose. <b>2005</b> , 89, 4111-21  | 92  |
| 1929 | Methodological problems in pressure profile calculations for lipid bilayers. <b>2005</b> , 122, 124903   | 106 |
| 1928 | Pressure-induced ordering in adamantane: a Monte Carlo simulation study. <b>2005</b> , 109, 2014-20  | 11  |
| 1927 | Thermal conductivity of ethanol. <b>2005</b> , 123, 174503   | 33  |
| 1926 | Mechanical properties of Au nanowires under uniaxial tension with high strain-rate by molecular dynamics. <b>2005</b> , 16, 2972-2981                        | 40  |

| 1925 | Low-temperature and high-pressure induced swelling of a hydrophobic polymer-chain in aqueous solution. <b>2005</b> , 7, 2780-6   | 38  |
|------|--|-----|
| 1924 | Hydrogen bonding in ethanol under shear. <b>2005</b> , 122, 234509   | 19  |
| 1923 | The formation of low-dimensional inorganic nanotube crystallites in carbon nanotubes. <b>2006</b> , 124, 124706  | 19  |
| 1922 | Deprotonation of solvated formic acid: Car-Parrinello and metadynamics simulations. <b>2006</b> , 110, 2325-31   | 49  |
| 1921 | Constant surface tension molecular dynamics simulations of lipid bilayers with trehalose. <b>2006</b> , 32, 849-855  | 17  |
| 1920 | Pressure and thermal effects on elastic properties of single crystal from Monte-Carlo simulation. <b>2006</b> , 32, 465-470  |     |
| 1919 | Rotational Dynamics of Trimethylammonium Chloride Studied by MD Simulation and NMR. <b>2006</b> , 338, 205-209   | 2   |
| 1918 | The melting point of ice Ih for common water models calculated from direct coexistence of the solid-liquid interface. <b>2006</b> , 124, 144506  | 320 |
| 1917 | Numerical Stochastic Integration for Quasi-Symplectic Flows. <b>2006</b> , 27, 2121-2139   | 13  |
| 1916 | Influence of chain length and unsaturation on sphingomyelin bilayers. <b>2006</b> , 90, 851-63   | 100 |
| 1915 | Atomistic simulation studies of cholesteryl oleates: model for the core of lipoprotein particles. <b>2006</b> , 90, 2247-57  | 21  |
| 1914 | cAMP Modulation of the cytoplasmic domain in the HCN2 channel investigated by molecular simulations. <b>2006</b> , 90, 3428-33   | 16  |
| 1913 | The intrinsic flexibility of the Kv voltage sensor and its implications for channel gating. <b>2006</b> , 90, 1598-606   | 28  |
| 1912 | Molecular simulation of the binding of nerve growth factor peptide mimics to the receptor tyrosine kinase A. <b>2006</b> , 91, 2063-71   | 13  |
| 1911 | Molecular-dynamics simulation of a ceramide bilayer. <b>2006</b> , 124, 14708  | 45  |
| 1910 | Low-temperature protein dynamics: a simulation analysis of interprotein vibrations and the boson peak at 150 k. <b>2006</b> , 128, 2356-64   | 38  |
| 1909 | Absence of superheating for ice Ih with a free surface: a new method of determining the melting point of different water models. <i>Molecular Physics</i> , <b>2006</b> , 104, 3583-3592 | 56  |
| 1908 | Confusing cause and effect: energy-entropy compensation in the preferential solvation of a nonpolar solute in dimethyl sulfoxide/water mixtures. <b>2006</b> , 110, 12104-12             | 24  |

#### (2006-2006)

| 1907   | Transmembrane helix-helix interactions: comparative simulations of the glycophorin a dimer. <b>2006</b> , 45, 14298-310  | 62                       |
|--|--|--------------------------|
| 1906   | Inverse temperature transition of a biomimetic elastin model: reactive flux analysis of folding/unfolding and its coupling to solvent dielectric relaxation. <b>2006</b> , 110, 3576-87  | 26                       |
| 1905   | Molecular dynamics simulation of structure, thermodynamic, and dynamic properties of poly(dimethylsilamethylene), poly(dimethylsilatrimethylene) and their alternating copolymer. <b>2006</b> , 110, 16047-58  | 18                       |
| 1904   | Enthalpy-entropy contributions to the potential of mean force of nanoscopic hydrophobic solutes. <b>2006</b> , 110, 8459-63  | 115                      |
| 1903   | Assessment of isobaric-isothermal (NPT) simulations for finite systems. <b>2006</b> , 37, 526-536  | 15                       |
| 1902   | Protein-protein interactions in actin-myosin binding and structural effects of R405Q mutation: a molecular dynamics study. <b>2006</b> , 64, 156-66  | 26                       |
| 1901   | Protein dynamics from X-ray crystallography: anisotropic, global motion in diffuse scattering patterns. <b>2007</b> , 66, 941-53   | 31                       |
| 1900   | Constant pressureEemperature molecular dynamics on a torus. <b>2006</b> , 359, 61-65   | 2                        |
| 1899   | Elastic constants of diamond from molecular dynamics simulations. <b>2006</b> , 18, S1737-50   | 37                       |
|  |  |                          |
| 1898   | A comparative theoretical study of dipeptide solvation in water. <b>2006</b> , 27, 672-84  | 35                       |
| 1898<br>1897                                 | A comparative theoretical study of dipeptide solvation in water. <b>2006</b> , 27, 672-84  Constant surface-tension molecular-dynamics simulation methods for anisotropic systems. <b>2006</b> , 124, 64705  | 35<br>8                  |
|  | Constant surface-tension molecular-dynamics simulation methods for anisotropic systems. <b>2006</b> , 124, 64705   |                          |
| 1897   | Constant surface-tension molecular-dynamics simulation methods for anisotropic systems. <b>2006</b> , 124, 64705  A molecular dynamics simulation study of buckyballs in water: atomistic versus coarse-grained  | 8                        |
| 1897<br>1896                                 | Constant surface-tension molecular-dynamics simulation methods for anisotropic systems. 2006, 124, 64705  A molecular dynamics simulation study of buckyballs in water: atomistic versus coarse-grained models of C60. 2006, 125, 34502  The behavior of reorientational correlation functions of water at the water-lipid bilayer interface. 2006, 125, 094713  The Jarzynski identity derived from general Hamiltonian or non-Hamiltonian dynamics reproducing   | 8                        |
| 1897<br>1896<br>1895                         | Constant surface-tension molecular-dynamics simulation methods for anisotropic systems. 2006, 124, 64705  A molecular dynamics simulation study of buckyballs in water: atomistic versus coarse-grained models of C60. 2006, 125, 34502  The behavior of reorientational correlation functions of water at the water-lipid bilayer interface. 2006, 125, 094713  The Jarzynski identity derived from general Hamiltonian or non-Hamiltonian dynamics reproducing   | 8<br>35<br>36            |
| 1897<br>1896<br>1895                         | Constant surface-tension molecular-dynamics simulation methods for anisotropic systems. 2006, 124, 64705  A molecular dynamics simulation study of buckyballs in water: atomistic versus coarse-grained models of C60. 2006, 125, 34502  The behavior of reorientational correlation functions of water at the water-lipid bilayer interface. 2006, 125, 094713  The Jarzynski identity derived from general Hamiltonian or non-Hamiltonian dynamics reproducing NVT or NPT ensembles. 2006, 125, 144109   | 8<br>35<br>36<br>34      |
| 1897<br>1896<br>1895<br>1894                 | Constant surface-tension molecular-dynamics simulation methods for anisotropic systems. 2006, 124, 64705  A molecular dynamics simulation study of buckyballs in water: atomistic versus coarse-grained models of C60. 2006, 125, 34502  The behavior of reorientational correlation functions of water at the water-lipid bilayer interface. 2006, 125, 094713  The Jarzynski identity derived from general Hamiltonian or non-Hamiltonian dynamics reproducing NVT or NPT ensembles. 2006, 125, 144109  A multiscale approach for quantitative simulations of diffusion induced segregation. 2006, 14, 389-408  Adding salt to an aqueous solution of t-butanol: is hydrophobic association enhanced or reduced?.  | 8<br>35<br>36<br>34      |
| 1897<br>1896<br>1895<br>1894<br>1893<br>1892 | Constant surface-tension molecular-dynamics simulation methods for anisotropic systems. 2006, 124, 64705  A molecular dynamics simulation study of buckyballs in water: atomistic versus coarse-grained models of C60. 2006, 125, 34502  The behavior of reorientational correlation functions of water at the water-lipid bilayer interface. 2006, 125, 094713  The Jarzynski identity derived from general Hamiltonian or non-Hamiltonian dynamics reproducing NVT or NPT ensembles. 2006, 125, 144109  A multiscale approach for quantitative simulations of diffusion induced segregation. 2006, 14, 389-408  Adding salt to an aqueous solution of t-butanol: is hydrophobic association enhanced or reduced?. 2006, 124, 154508  Electronic density response of liquid water using time-dependent density functional theory. 2006, | 8<br>35<br>36<br>34<br>1 |

| 1889 | Solubility of gases and solvents in silicon polymers: molecular simulation and equation of state modeling. <b>2007</b> , 33, 851-860   | 14  |
|------|--|-----|
| 1888 | Conformational analysis of lipid molecules by self-organizing maps. <b>2007</b> , 126, 054707  | 16  |
| 1887 | Explicit symplectic integrators of molecular dynamics algorithms for rigid-body molecules in the canonical, isobaric-isothermal, and related ensembles. <b>2007</b> , 126, 084103  | 74  |
| 1886 | Molecular dynamics simulations of local field factors. <b>2007</b> , 127, 014501   | 4   |
| 1885 | Deprotonation by dehydration: the origin of ammonium sensing in the AmtB channel. 2007, 3, e22   | 38  |
| 1884 | Anisotropic pressure molecular dynamics for atomic fluid systems. <b>2007</b> , 40, 8585-8598  | 1   |
| 1883 | Molecular simulation with variable protonation states at constant pH. <b>2007</b> , 126, 164112  | 75  |
| 1882 | Molecular Dynamics Simulations of Tribology. <b>2007</b> , 79-102  | 7   |
| 1881 | Nonequilibrium Molecular Dynamics. <b>2007</b> , 291-397   | 15  |
| 1880 | Energy Profiles for Organic Reactions in Solution. <b>2007</b> , 469-488   | 25  |
| 1879 | Phase diagrams and surface properties of modified water models. <i>Molecular Physics</i> , <b>2007</b> , 105, 3029-3033  | 27  |
| 1878 | Atomistic Simulation of Poly(dimethylsiloxane): Force Field Development, Structure, and Thermodynamic Properties of Polymer Melt and Solubility of n-Alkanes, n-Perfluoroalkanes, and Noble and Light Gases. <b>2007</b> , 40, 1720-1729 | 30  |
| 1877 | Molecular dynamics simulations of boron-nitride nanotubes embedded in amorphous Si-B-N. <b>2007</b> , 39, 502-517  | 21  |
| 1876 | Polyamorphic transformation of silicon in first-principles molecular-dynamics simulation. <b>2007</b> , 353, 3463-346  | 661 |
| 1875 | Structure and dynamics in liquid alumina: Simulations with an ab initio interaction potential. <b>2007</b> , 353, 3500-3504  | 30  |
| 1874 | Coarse-grained molecular dynamics simulations of membrane proteins and peptides. <b>2007</b> , 157, 593-605  | 275 |
| 1873 | Heterogeneity even at the speed limit of folding: large-scale molecular dynamics study of a fast-folding variant of the villin headpiece. <b>2007</b> , 374, 806-16  | 154 |
| 1872 | Picosecond fluctuating protein energy landscape mapped by pressure temperature molecular dynamics simulation. <b>2007</b> , 104, 17261-5   | 63  |

| 1871 | Polyunsaturation in lipid membranes: dynamic properties and lateral pressure profiles. <b>2007</b> , 111, 3139-50  | 163 |
|------|--|-----|
| 1870 | Numerical Simulation in Molecular Dynamics. 2007,  | 2   |
| 1869 | Biological Membrane Ion Channels. <b>2007</b> ,  | 36  |
| 1868 | New effective method for quantitative analysis of diffusion jumps, applied in molecular dynamics simulations of small molecules dispersed in short chain systems. <b>2007</b> , 111, 13683-93        | 18  |
| 1867 | Molecular dynamics simulations of three protegrin-type antimicrobial peptides: interplay between charges at the termini,   | 13  |
| 1866 | Phase diagrams of alkali halides using two interaction models: a molecular dynamics and free energy study. <b>2007</b> , 126, 024503   | 20  |
| 1865 | Dynamic arrangement of ion pairs and individual contributions to the thermal stability of the cofactor-binding domain of glutamate dehydrogenase from Thermotoga maritima. <b>2007</b> , 46, 8537-49 | 24  |
| 1864 | Hydrophobic Solvation: Aqueous Methane Solutions. <b>2007</b> , 84, 864  | 5   |
| 1863 | Catabolite activator protein in aqueous solution: a molecular simulation study. <b>2007</b> , 111, 1496-501  | 14  |
| 1862 | Molecular Thermodynamics of Methane Solvation in tert-Butanol-Water Mixtures. <b>2007</b> , 3, 194-200   | 18  |
| 1861 | Insight into the putative specific interactions between cholesterol, sphingomyelin, and palmitoyl-oleoyl phosphatidylcholine. <b>2007</b> , 92, 1125-37  | 115 |
| 1860 | Cholesterol surrogates: a comparison of cholesterol and 16:0 ceramide in POPC bilayers. <b>2007</b> , 92, 920-7  | 68  |
| 1859 | Molecular dynamics simulations of SOPS and sphingomyelin bilayers containing cholesterol. <b>2007</b> , 92, 1284-95  | 38  |
| 1858 | Methods in Membrane Lipids. 2007,  | 16  |
| 1857 | Comparative MD analysis of the stability of transthyretin providing insight into the fibrillation mechanism. <b>2007</b> , 86, 73-82   | 19  |
| 1856 | Pressure and salt effects in simulated water: two sides of the same coin?. <b>2007</b> , 46, 8907-11   | 76  |
| 1855 | Druck- und Salzeffekte in simuliertem Wasser: zwei Seiten einer Medaille?. <b>2007</b> , 119, 9065-9069  | 10  |
| 1854 | Molecular dynamic simulations of ionic liquids: a reliable description of structure, thermodynamics and dynamics. <b>2007</b> , 8, 2464-70   | 316 |

| 1853 | Exploration of the conformational space of myosin recovery stroke via molecular dynamics. <b>2007</b> , 125, 127-37  | 16    |
|------|--|-------|
| 1852 | Simulation of the liquidNapor interface of molten LiBeF3. <b>2007</b> , 10, 1131-1136  | 17    |
| 1851 | A Molecular Dynamic Study of Cementitious Calcium Silicate Hydrate (CBH) Gels. 2007, 90, 070915225431002   | -?13) |
| 1850 | The signaling pathway of rhodopsin. <b>2007</b> , 15, 611-23   | 49    |
| 1849 | On the calculation of velocity-dependent properties in molecular dynamics simulations using the leapfrog integration algorithm. <b>2007</b> , 127, 184102  | 68    |
| 1848 | A molecular dynamics study of the aluminosilicate chains structure in Al-rich calcium silicate hydrated (CBH) gels. <b>2008</b> , 205, 1324-1329   | 53    |
| 1847 | Ionic liquids: dissecting the enthalpies of vaporization. <b>2008</b> , 9, 549-55  | 117   |
| 1846 | On the validity of Stokes-Einstein and Stokes-Einstein-Debye relations in ionic liquids and ionic-liquid mixtures. <b>2008</b> , 9, 1851-8   | 127   |
| 1845 | The solvent-dependent shift of the amide I band of a fully solvated peptide as a local probe for the solvent composition in the peptide/solvent interface. <b>2008</b> , 9, 2742-50  | 11    |
| 1844 | Temperature and concentration effects on the solvophobic solvation of methane in aqueous salt solutions. <b>2008</b> , 9, 2722-30  | 12    |
| 1843 | Salt effects on the structure of water probed by attenuated total reflection infrared spectroscopy and molecular dynamics simulations. <b>2008</b> , 9, 2731-6   | 23    |
| 1842 | Phosphodiester bond rupture in 5? and 3? cytosine monophosphate in aqueous environment and the effect of low-energy electron attachment: A Car <b>B</b> arrinello QM/MM molecular dynamics study. <b>2008</b> , 462, 289-294 | 14    |
| 1841 | Continuum interpretation of virial stress in molecular simulations. <b>2008</b> , 45, 4340-4346  | 281   |
| 1840 | A comparative study of two classical force fields on statics and dynamics of [EMIM][BF4] investigated via molecular dynamics simulations. <b>2008</b> , 129, 224501  | 81    |
| 1839 | Coarse-grained molecular dynamics simulations of the energetics of helix insertion into a lipid bilayer. <b>2008</b> , 47, 11321-31  | 85    |
| 1838 | Protein-protein interaction investigated by steered molecular dynamics: the TCR-pMHC complex. <b>2008</b> , 95, 3575-90  | 88    |
| 1837 | Elastic constants of silicon materials calculated as a function of temperature using a parametrization of the second-generation reactive empirical bond-order potential. <b>2008</b> , 77,                                   | 48    |
| 1836 | Cholesterol packing around lipids with saturated and unsaturated chains: a simulation study. <b>2008</b> , 24, 6858-65   | 88    |

## (2008-2008)

| 1835 | Nonequilibrium molecular dynamics calculation of the thermal conductivity based on an improved relaxation scheme. <b>2008</b> , 129, 074106  | 16  |
|------|--|-----|
| 1834 | Formation of ice-like water structure on the surface of an antifreeze protein. <b>2008</b> , 112, 6193-202   | 77  |
| 1833 | Modeling and molecular dynamics simulation of the human gonadotropin-releasing hormone receptor in a lipid bilayer. <b>2008</b> , 112, 10704-13  | 31  |
| 1832 | Role of the active-site solvent in the thermodynamics of factor Xa ligand binding. 2008, 130, 2817-31  | 500 |
| 1831 | The effect of the water/methane interface on methane hydrate cages: the potential of mean force and cage lifetimes. <b>2008</b> , 129, 034701  | 38  |
| 1830 | Effects of familial Alzheimer's disease mutations on the folding nucleation of the amyloid beta-protein. <b>2008</b> , 381, 221-8  | 88  |
| 1829 | Mg2SiO4 liquid under high pressure from molecular dynamics. <b>2008</b> , 256, 185-192   | 45  |
| 1828 | Methyl group dynamics and the onset of anharmonicity in myoglobin. <b>2008</b> , 112, 5522-33  | 46  |
| 1827 | Unfolding and melting of DNA (RNA) hairpins: the concept of structure-specific 2D dynamic landscapes. <b>2008</b> , 10, 4227-39  | 28  |
| 1826 | Modeling of aqueous poly(oxyethylene) solutions: 1. Atomistic simulations. <b>2008</b> , 112, 2388-98  | 75  |
| 1825 | Role of Mg2+ in hammerhead ribozyme catalysis from molecular simulation. <b>2008</b> , 130, 3053-64  | 93  |
| 1824 | Atomistic Simulation of Poly(dimethylsiloxane) Permeability Properties to Gases and n-Alkanes. <b>2008</b> , 41, 5899-5907   | 17  |
| 1823 | Notes on "Ewald summation of electrostatic multipole interactions up to quadrupolar level" [J. Chem. Phys. 119, 7471 (2003)]. <b>2008</b> , 129, 074102                                | 42  |
| 1822 | Computing the stability diagram of the Trp-cage miniprotein. <b>2008</b> , 105, 17754-9  | 133 |
| 1821 | New concept of solute distribution around a diffusive crystal-solution interface of a binary Lennard-Jones mixture from the viewpoint of molecular dynamics. <b>2008</b> , 128, 044716 | 6   |
| 1820 | Effect of flexibility on surface tension and coexisting densities of water. <b>2008</b> , 128, 174703  | 47  |
| 1819 | The evolution of intermediate-range order in molten network-forming materials. 2008, 128, 214507   | 12  |
| 1818 | Polyamorphism and the evolution of intermediate-range order in molten ZnCl2. <b>2008</b> , 20, 244123  | 13  |

| 1817 | Molecular transport across fluid interfaces: coupling between solute dynamics and interface fluctuations. <b>2008</b> , 78, 041605  | 11  |
|------|---|-----|
| 1816 | Solvophobic solvation and interaction of small apolar particles in imidazolium-based ionic liquids. <b>2008</b> , 100, 115901   | 18  |
| 1815 | The thickness of a liquid layer on the free surface of ice as obtained from computer simulation. <b>2008</b> , 129, 014702  | 116 |
| 1814 | Bibliography. 419-549   |     |
| 1813 | Molecular Dynamics Computations for Proteins: A Case Study in Membrane Ion Permeation. 2009,  |     |
| 1812 | Kinase-activity-independent functions of atypical protein kinase C in Drosophila. <b>2009</b> , 122, 3759-71  | 58  |
| 1811 | Molecular dynamics simulation of structural and dynamic properties of selenium structures with different degrees of amorphization. <b>2009</b> , 21, 405402   | 3   |
| 1810 | Dynamic allostery in the methionine repressor revealed by force distribution analysis. <b>2009</b> , 5, e1000574  | 48  |
| 1809 | Calculations of the thermal conductivities of ionic materials by simulation with polarizable interaction potentials. <b>2009</b> , 130, 104507  | 64  |
| 1808 | Progress and challenges in the automated construction of Markov state models for full protein systems. <b>2009</b> , 131, 124101  | 303 |
| 1807 | Mechanisms of constitutive activation of Janus kinase 2-V617F revealed at the atomic level through molecular dynamics simulations. <b>2009</b> , 115, 1692-700  | 27  |
| 1806 | Mechanistic studies of displacer-protein binding in chemically selective displacement systems using NMR and MD simulations. <b>2009</b> , 102, 1428-37  | 10  |
| 1805 | Structure and dynamics of the influenza A M2 channel: a comparison of three structures. <b>2009</b> , 15, 1317-28   | 11  |
| 1804 | CarParrinello and path integral molecular dynamics study of the intramolecular hydrogen bond in the novel class of anionic H-chelates: 6-Nitro-2,3-dipyrrol-2-ylquinoxaline anion. <b>2009</b> , 480, 173-177 | 6   |
| 1803 | The neighbor list algorithm for a parallelepiped box in molecular dynamics simulations. <b>2009</b> , 54, 1463-1469   | 6   |
| 1802 | Signaling pathways of PDZ2 domain: a molecular dynamics interaction correlation analysis. <b>2009</b> , 74, 145-54  | 128 |
| 1801 | Structural effects of clinically observed mutations in JAK2 exons 13-15: comparison with V617F and exon 12 mutations. <b>2009</b> , 9, 58   | 25  |
| 1800 | Prediction of partition coefficients and infinite dilution activity coefficients of 1-ethylpropylamine and 3-methyl-1-pentanol using force field methods. <b>2009</b> , 285, 19-23                            | 13  |

#### (2009-2009)

| 1799 | assessment of the structure and density of water at near-ambient conditions. <b>2009</b> , 113, 11959-64  |     | 302 |
|------|---|-----|-----|
| 1798 | An elemental mercury diffusion coefficient for natural waters determined by molecular dynamics simulation. <b>2009</b> , 43, 3183-6   |     | 50  |
| 1797 | Reordering hydrogen bonds using hamiltonian replica exchange enhances sampling of conformational changes in biomolecular systems. <b>2009</b> , 113, 6484-94  |     | 12  |
| 1796 | Systematic coarse-graining of a multicomponent lipid bilayer. <b>2009</b> , 113, 1501-10  |     | 92  |
| 1795 | Molecular dynamics studies of the interactions of water and amino acid analogues with quartz surfaces. <b>2009</b> , 25, 1638-44  |     | 69  |
| 1794 | Exploring molecular mechanisms of ligand recognition by opioid receptors with metadynamics. <b>2009</b> , 48, 10020-9   |     | 71  |
| 1793 | Morphology and interfacial action of nanocomposites formed from ethylene-vinyl acetate copolymers and organoclays. <b>2009</b> , 113, 11898-905   |     | 12  |
| 1792 | Molecular dynamics studies of the transmembrane domain of gp41 from HIV-1. <b>2009</b> , 1788, 1804-12  |     | 29  |
| 1791 | Lithium speciation in aqueous fluids at high P and T studied by ab initio molecular dynamics and consequences for Li-isotope fractionation between minerals and fluids. <b>2009</b> , 73, 5428-5434                       |     | 42  |
| 1790 | Threshold occupancy and specific cation binding modes in the hammerhead ribozyme active site are required for active conformation. <b>2009</b> , 388, 195-206   |     | 38  |
| 1789 | Dynamic structure factors from lipid membrane molecular dynamics simulations. <b>2009</b> , 96, 1828-38   |     | 20  |
| 1788 | Undulation contributions to the area compressibility in lipid bilayer simulations. <b>2009</b> , 97, 2754-60  |     | 68  |
| 1787 | Temperature dependence of the solubility of carbon dioxide in imidazolium-based ionic liquids. <b>2009</b> , 113, 12727-35  |     | 92  |
| 1786 | Optimized molecular dynamics force fields applied to the helix-coil transition of polypeptides. <b>2009</b> , 113, 9004-15  |     | 595 |
| 1785 | Anomalies in water as obtained from computer simulations of the TIP4P/2005 model: density maxima, and density, isothermal compressibility and heat capacity minima. <i>Molecular Physics</i> , <b>2009</b> , 107, 365-374 | 1.7 | 131 |
| 1784 | Plastic crystal phases of simple water models. <b>2009</b> , 130, 244504  |     | 55  |
| 1783 | The phase diagram of water at high pressures as obtained by computer simulations of the TIP4P/2005 model: the appearance of a plastic crystal phase. <b>2009</b> , 11, 543-55   |     | 63  |
| 1782 | Docking Ligands on Protein Surfaces: The Case Study of Prion Protein. <b>2009</b> , 5, 2565-73  |     | 30  |

| 1781                         | Paramagnetic perturbation of the 19F NMR chemical shift in fluorinated cysteine by O2: a theoretical study. <b>2009</b> , 113, 10916-22  | 4                |
|------------------------------|--|------------------|
| 1780                         | Atomistic Structural Modelling of Ionomer Membrane Morphology. <b>2009</b> , 413-436   | 3                |
| 1779                         | Molecular dynamics study of biomembrane/local anesthetics interactions. <i>Molecular Physics</i> , <b>2009</b> , 107, 1437-1443  | 17               |
| 1778                         | Pressure-induced structural phase transitions in CdSe: a metadynamics study. <b>2009</b> , 130, 124712   | 25               |
| 1777                         | Encapsulation of myoglobin in a cetyl trimethylammonium bromide micelle in vacuo: a simulation study. <b>2009</b> , 48, 1006-15  | 32               |
| 1776                         | Structural ultrafast dynamics of macromolecules: diffraction of free DNA and effect of hydration. <b>2009</b> , 11, 10619-32   | 10               |
| 1775                         | Water permeation through stratum corneum lipid bilayers from atomistic simulations. <b>2009</b> , 5, 4549  | 52               |
| 1774                         | Umbrella sampling simulations of biotin carboxylase: is a structure with an open ATP grasp domain stable in solution?. <b>2009</b> , 113, 10097-103  | 6                |
| 1773                         | Molecular Simulation of Cross-Linked Epoxy and EpoxyPOSS Nanocomposite. 2009, 42, 4319-4327  | 147              |
|                              |  |                  |
| 1772                         | Molecular dynamics simulations of methane hydrate decomposition. <b>2009</b> , 113, 1913-21  | 109              |
|                              | Molecular dynamics simulations of methane hydrate decomposition. 2009, 113, 1913-21  How Does Solute-Polarization Affect the Hydrophobic Hydration of Methane?. 2009, 223, 1091-1104   | 109              |
|                              |  |                  |
| 1771                         | How Does Solute-Polarization Affect the Hydrophobic Hydration of Methane?. <b>2009</b> , 223, 1091-1104  Correlation of Static and Dynamic Heterogeneities in Supercooled Water by Means of Molecular  | 8                |
| 1771<br>1770                 | How Does Solute-Polarization Affect the Hydrophobic Hydration of Methane?. 2009, 223, 1091-1104  Correlation of Static and Dynamic Heterogeneities in Supercooled Water by Means of Molecular Dynamics Simulations. 2009, 223, 1001-1010  Basis for resistance to imatinib in 16 BCR-ABL mutants as determined using molecular dynamics.   | 8<br>5           |
| 1771<br>1770<br>1769         | How Does Solute-Polarization Affect the Hydrophobic Hydration of Methane?. <b>2009</b> , 223, 1091-1104  Correlation of Static and Dynamic Heterogeneities in Supercooled Water by Means of Molecular Dynamics Simulations. <b>2009</b> , 223, 1001-1010  Basis for resistance to imatinib in 16 BCR-ABL mutants as determined using molecular dynamics. <b>2009</b> , 4, 164-73  Simulated tempering distributed replica sampling: A practical guide to enhanced conformational   | 8<br>5<br>7      |
| 1771<br>1770<br>1769<br>1768 | How Does Solute-Polarization Affect the Hydrophobic Hydration of Methane?. 2009, 223, 1091-1104  Correlation of Static and Dynamic Heterogeneities in Supercooled Water by Means of Molecular Dynamics Simulations. 2009, 223, 1001-1010  Basis for resistance to imatinib in 16 BCR-ABL mutants as determined using molecular dynamics. 2009, 4, 164-73  Simulated tempering distributed replica sampling: A practical guide to enhanced conformational sampling. 2010, 256, 012011   | 8<br>5<br>7<br>2 |
| 1771<br>1770<br>1769<br>1768 | How Does Solute-Polarization Affect the Hydrophobic Hydration of Methane?. 2009, 223, 1091-1104  Correlation of Static and Dynamic Heterogeneities in Supercooled Water by Means of Molecular Dynamics Simulations. 2009, 223, 1001-1010  Basis for resistance to imatinib in 16 BCR-ABL mutants as determined using molecular dynamics. 2009, 4, 164-73  Simulated tempering distributed replica sampling: A practical guide to enhanced conformational sampling. 2010, 256, 012011  Computer Simulation of n-Butylamine-Intercalated B-Zirconium Phosphate. 2010, 57, 1015-1021  Molecular Dynamics Simulation for the Impact of N-Decanol Surfactants on the Liquid-Vapor | 8<br>5<br>7<br>2 |

## (2010-2010)

| 1763 Practical considerations for building GROMOS-compatible small-molecule topologies. <b>2010</b> , 50, 2221-35  | 154 |
|--|-----|
| 1762 pH-driven helix rotations in the influenza M2 H+ channel: a potential gating mechanism. <b>2010</b> , 39, 1043-9  | 5   |
| CarParrinello and path integral molecular dynamics study of the hydrogen bonds in 2-acetyl-1,8-dihydroxy-3,6-dimethylnaphthalene. <b>2010</b> , 499, 56-61               | 4   |
| 1760 Thrombin allosteric modulation revisited: a molecular dynamics study. <b>2010</b> , 16, 725-35  | 14  |
| Isoform-specific determinants in the HP1 binding to histone 3: insights from molecular simulations. <b>2010</b> , 38, 1571-81  | 8   |
| Tyrosine aminotransferase: biochemical and structural properties and molecular dynamics simulations. <b>2010</b> , 1, 1023-32  | 27  |
| New Bending Algorithm for Field-Driven Molecular Dynamics. <b>2009</b> , 5, 315-22   | 2   |
| Glass transition and structural properties of glycidyloxypropyl-heptaphenyl polyhedral oligomeric silsesquioxane-epoxy nanocomposites. <b>2010</b> , 102, 461-467        | 21  |
| 1755 Theoretical study on a new kind of thienyl-functionalized polysilane. <b>2010</b> , 21, 1263-1271   | 8   |
| The wurtzite to rock salt transition in CdSe: A comparison between molecular dynamics and metadynamics simulations. <b>2010</b> , 12, 157-162                            | 13  |
| Atomistic insight into chondroitin-6-sulfate glycosaminoglycan chain through quantum mechanics calculations and molecular dynamics simulation. <b>2010</b> , 31, 1670-80 | 9   |
| Sugar treatment of human lipoprotein particles and their separation by capillary electrophoresis. <b>2010</b> , 33, 2528-35  | 5   |
| Ab initio simulations of peptide-mineral interactions. <b>2010</b> , 4, 51-60  | 9   |
| Integral modeling approach to study the phase behavior of complex solids: application to phase transitions in MgSiO3 pyroxenes. <b>2010</b> , 66, 535-41                 | 5   |
| Molecular dynamics study of interaction and substrate channeling between neuron-specific enolase and B-type phosphoglycerate mutase. <b>2010</b> , 78, 1691-704          | 8   |
| Structural facets of disease-linked human prion protein mutants: a molecular dynamic study. <b>2010</b> , 78, 3270-80  | 41  |
| 1747 An aqueous H+ permeation pathway in the voltage-gated proton channel Hv1. <b>2010</b> , 17, 869-875   | 131 |
| 1746 Extensions of the Ewald method for Coulomb interactions in crystals. <b>2010</b> , 458-481  | 5   |

| 1745 | MOLECULAR DYNAMICS SIMULATION OF ADSORPTION OF ANILINE BY ⊞-ZIRCONIUM PHOSPHATE. <b>2010</b> , 09, 861-873   |     | 1   |
|------|--|-----|-----|
| 1744 | Electrolytes in a nanometer slab-confinement: ion-specific structure and solvation forces. <b>2010</b> , 133, 164511   |     | 34  |
| 1743 | Computational investigation of lipid hydration water of L⊞ 1-palmitoyl-2-oleoyl-sn-glycero-3-phosphocholine at three hydration levels. <i>Molecular Physics</i> , <b>2010</b> , 108, 2027-2036             | 1.7 | 17  |
| 1742 | Computer simulations of aqua metal ions for accurate reproduction of hydration free energies and structures. <b>2010</b> , 132, 104505   |     | 12  |
| 1741 | Spatial averaging for small molecule diffusion in condensed phase environments. <b>2010</b> , 133, 044506  |     | 6   |
| 1740 | Stretched exponential dynamics in lipid bilayer simulations. <b>2010</b> , 133, 115101   |     | 22  |
| 1739 | Application of the Generalized Ewald Method to a Molecular System. <b>2010</b> , 79, 024004  |     | 4   |
| 1738 | Structure and dynamics of the protic ionic liquid monomethylammonium nitrate ([CH3NH3][NO3]) from ab initio molecular dynamics simulations. <b>2010</b> , 132, 124506                                      |     | 106 |
| 1737 | Modeling the relationship between the p53 C-terminal domain and its binding partners using molecular dynamics. <b>2010</b> , 114, 13201-13   |     | 17  |
| 1736 | Diffusivities and Viscosities of Poly(ethylene oxide) Oligomers 2010, 55, 4273-4280  |     | 15  |
| 1735 | Putative active states of a prototypic g-protein-coupled receptor from biased molecular dynamics. <b>2010</b> , 98, 2347-55  |     | 52  |
| 1734 | Residue-specific side-chain packing determines the backbone dynamics of transmembrane model helices. <b>2010</b> , 99, 2541-9  |     | 25  |
| 1733 | Local Chain Dynamics and Dynamic Heterogeneity in Cross-Linked Epoxy in the Vicinity of Glass Transition. <b>2010</b> , 43, 6505-6510  |     | 33  |
| 1732 | Development of molecular simulation methods to accurately represent protein-surface interactions: The effect of pressure and its determination for a system with constrained atoms. <b>2010</b> , 5, 85-95 |     | 22  |
| 1731 | Practically Efficient QM/MM Alchemical Free Energy Simulations: The Orthogonal Space Random Walk Strategy. <b>2010</b> , 6, 2253-66  |     | 29  |
| 1730 | Computational mutagenesis studies of hammerhead ribozyme catalysis. <b>2010</b> , 132, 13505-18  |     | 17  |
| 1729 | Assessment of the transferability of a protein force field for the simulation of peptide-surface interactions. <b>2010</b> , 26, 7396-404  |     | 60  |
| 1728 | In silico calculation of acidity constants of carbonic acid conformers. <b>2010</b> , 114, 12914-7   |     | 14  |

| 1727 | Another Coarse Grain Model for Aqueous Solvation: WAT FOUR?. <b>2010</b> , 6, 3793-3807   | 90  |
|------|---|-----|
| 1726 | Dynamic correlation between pressure-induced protein structural transition and water penetration. <b>2010</b> , 114, 2281-6   | 60  |
| 1725 | Conformational and solvent entropy contributions to the thermal response of nucleic acid-based nanothermometers. <b>2010</b> , 114, 2076-82   | 10  |
| 1724 | Rearrangement of Dewar benzene derivatives studied by DFT. <b>2010</b> , 75, 576-81   | 13  |
| 1723 | Bovine chymosin: a computational study of recognition and binding of bovine kappa-casein. <b>2010</b> , 49, 2563-73   | 21  |
| 1722 | Solution study of engineered quartz binding peptides using replica exchange molecular dynamics. <b>2010</b> , 11, 3266-74   | 26  |
| 1721 | Automated force field optimisation of small molecules using a gradient-based workflow package. <b>2010</b> , 36, 1182-1196  | 20  |
| 1720 | On the molecular origins of biomass recalcitrance: the interaction network and solvation structures of cellulose microfibrils. <b>2010</b> , 114, 13333-41                                      | 112 |
| 1719 | Exploring the changes in the structure of $\oplus$ -helical peptides adsorbed onto a single walled carbon nanotube using classical molecular dynamics simulation. <b>2010</b> , 114, 14048-58   | 52  |
| 1718 | Membrane simulations mimicking acidic pH reveal increased thickness and negative curvature in a bilayer consisting of lysophosphatidylcholines and free fatty acids. <b>2010</b> , 1798, 938-46 | 40  |
| 1717 | Assessing the stability of Alzheimer's amyloid protofibrils using molecular dynamics. <b>2010</b> , 114, 1652-60  | 299 |
| 1716 | On the self-assembly of a highly selective benzothiazole-based TIM inhibitor in aqueous solution. <b>2010</b> , 26, 16681-9   | 7   |
| 1715 | Determining the three-phase coexistence line in methane hydrates using computer simulations. <b>2010</b> , 133, 064507  | 162 |
| 1714 | Speciation in aqueous MgSO(4) fluids at high pressures and high temperatures from ab initio molecular dynamics and Raman spectroscopy. <b>2010</b> , 114, 15565-72                              | 39  |
| 1713 | Melting point and phase diagram of methanol as obtained from computer simulations of the OPLS model. <b>2010</b> , 132, 094505  | 19  |
| 1712 | Atomistic evidence of how force dynamically regulates thiol/disulfide exchange. <b>2010</b> , 132, 16790-5  | 55  |
| 1711 | Cholesterol orientation and tilt modulus in DMPC bilayers. <b>2010</b> , 114, 7524-34   | 73  |
| 1710 | Sequence-dependent interaction of 即eptides with membranes. <b>2010</b> , 114, 13585-92  | 27  |

| Predicting water uptake in poly(perfluorosulfonic acids) using force field simulation methods. <b>2010</b> , 12, 14543-52  Volumetric properties of human islet amyloid polypeptide in liquid water. <b>2010</b> , 12, 4233-8  | 9   |
|--|---|
| Volumetric properties of human islet amyloid polypeptide in liquid water. <b>2010</b> , 12, 4233-8   |   |
|  | 15  |
| Charybdotoxin unbinding from the mKv1.3 potassium channel: a combined computational and experimental study. <b>2011</b> , 115, 11490-500   | 24  |
| Study of structural and dynamic properties of liquid phenyltrimethoxysilane. <b>2011</b> , 13, 11864-71  | 5   |
| Conditional reversible work method for molecular coarse graining applications. <b>2011</b> , 13, 10468-74  | 70  |
| Limiting diffusion coefficients of ionic liquids in water and methanol: a combined experimental and molecular dynamics study. <b>2011</b> , 13, 3268-73  | 29  |
| From NMR relaxation to fractional Brownian dynamics in proteins: results from a virtual experiment. <b>2011</b> , 115, 12370-9   | 12  |
| Molecular Dynamics Study of Water Interacting with Siloxane Surface Modified by Poly(ethylene oxide) Chains. <b>2011</b> , 115, 18740-18751  | 8   |
| Hofmeister ion interactions with model amide compounds. <b>2011</b> , 115, 13781-7   | 88  |
| Non-adiabatic dynamics of interfacial systems: a case study of a nanoparticle penetration into a   |   |
| lipid bilayer. <b>2011</b> , 37, 525-536   | 5   |
|  | 53  |
|  |   |
| Effect of Curvature on the $\oplus$ -Helix Breaking Tendency of Carbon Based Nanomaterials. <b>2011</b> , 115, 8886-8892  A molecular dynamics approach for the association of apolipoproteinB-100 and chondroitin-6-sulfate. <b>2011</b> , 115, 4818-25   | 53  |
| Effect of Curvature on the $\oplus$ -Helix Breaking Tendency of Carbon Based Nanomaterials. <b>2011</b> , 115, 8886-8892  A molecular dynamics approach for the association of apolipoproteinB-100 and chondroitin-6-sulfate. <b>2011</b> , 115, 4818-25   | 53<br>5   |
| Effect of Curvature on the $\oplus$ -Helix Breaking Tendency of Carbon Based Nanomaterials. <b>2011</b> , 115, 8886-8892  A molecular dynamics approach for the association of apolipoproteinB-100 and chondroitin-6-sulfate. <b>2011</b> , 115, 4818-25  Effect of galactosylceramide on the dynamics of cholesterol-rich lipid membranes. <b>2011</b> , 115, 14424-34  Characterization of interactions between PilA from Pseudomonas aeruginosa strain K and a model  | 53<br>5   |
| Effect of Curvature on the H-Helix Breaking Tendency of Carbon Based Nanomaterials. 2011, 115, 8886-8892  A molecular dynamics approach for the association of apolipoproteinB-100 and chondroitin-6-sulfate. 2011, 115, 4818-25  Effect of galactosylceramide on the dynamics of cholesterol-rich lipid membranes. 2011, 115, 14424-34  Characterization of interactions between PilA from Pseudomonas aeruginosa strain K and a model membrane. 2011, 115, 8004-8  Molecular dynamics simulations of pregelification mixtures for the production of imprinted xerogels. 2011, 27, 5062-70  Molecular transport through surfactant-covered oil-water interfaces: role of physical properties of | 53<br>5<br>14<br>18   |
| C Ln Fe  | conditional reversible work method for molecular coarse graining applications. 2011, 13, 10468-74  imiting diffusion coefficients of ionic liquids in water and methanol: a combined experimental and nolecular dynamics study. 2011, 13, 3268-73  rom NMR relaxation to fractional Brownian dynamics in proteins: results from a virtual xperiment. 2011, 115, 12370-9  Molecular Dynamics Study of Water Interacting with Siloxane Surface Modified by Poly(ethylene xide) Chains. 2011, 115, 18740-18751  Iofmeister ion interactions with model amide compounds. 2011, 115, 13781-7 |

## (2011-2011)

| 1691 | Optimizing Nucleus Size Metrics for Liquid-Solid Nucleation from Transition Paths of Near-Nanosecond Duration. <b>2011</b> , 2, 1133-8  | 48  |
|------|---|-----|
| 1690 | Gramicidin A backbone and side chain dynamics evaluated by molecular dynamics simulations and nuclear magnetic resonance experiments. I: molecular dynamics simulations. <b>2011</b> , 115, 7417-26 | 31  |
| 1689 | Atomic scale view on partially molten rocks: Molecular dynamics simulations of melt-wetted olivine grain boundaries. <b>2011</b> , 116,   | 11  |
| 1688 | Interpretation of fluctuation spectra in lipid bilayer simulations. <b>2011</b> , 100, 2104-11  | 98  |
| 1687 | Toward a predictive understanding of slow methyl group dynamics in proteins. <b>2011</b> , 101, 910-5   | 35  |
| 1686 | Molecular insight into conformational transition of amyloid 即eptide 42 inhibited by (-)-epigallocatechin-3-gallate probed by molecular simulations. <b>2011</b> , 115, 11879-87                     | 108 |
| 1685 | In vitro polymerization of microtubules with a fullerene derivative. <b>2011</b> , 5, 6306-14   | 45  |
| 1684 | Short range hydrogen diffusion in Na3AlH6. <b>2011</b> , 13, 10546-55   | 6   |
| 1683 | Molecular simulation of diffusion of hydrogen, carbon monoxide, and water in heavy n-alkanes. <b>2011</b> , 115, 1429-39  | 57  |
| 1682 | Electroporation of the E. coli and S. Aureus membranes: molecular dynamics simulations of complex bacterial membranes. <b>2011</b> , 115, 13381-8   | 158 |
| 1681 | Molecular Dynamics Study of Hydrated Poly(ethylene oxide) Chains Grafted on Siloxane Surface. <b>2011</b> , 44, 3639-3648   | 19  |
| 1680 | Adsorption of collagen onto single walled carbon nanotubes: a molecular dynamics investigation. <b>2011</b> , 13, 13046-57  | 19  |
| 1679 | Examination of the $\oplus$ -chitin structure and decrystallization thermodynamics at the nanoscale. <b>2011</b> , 115, 4516-22   | 61  |
| 1678 | NANOINDENTATION SIMULATION ON MECHANICAL BEHAVIOR OF NANOCRYSTALLINE Ni. <b>2011</b> , 25, 1689-1700  | 3   |
| 1677 | Initial stage of cheese production: a molecular modeling study of bovine and camel chymosin complexed with peptides from the chymosin-sensitive region of Easein. <b>2011</b> , 59, 5636-47         | 22  |
| 1676 | Molecular dynamics simulation of liquid methanol. I. Molecular modeling including C-H vibration and Fermi resonance. <b>2011</b> , 134, 024509  | 45  |
| 1675 | Surface Hydroxyl Identity and Reactivity in Akagan[te. <b>2011</b> , 115, 17036-17045   | 28  |
| 1674 | Molecular Dynamics Simulation Study of Chlorophyll a in Different Organic Solvents. <b>2011</b> , 7, 1131-40  | 30  |

| 1673 | Steered molecular dynamics simulations reveal important mechanisms in reversible monoamine oxidase B inhibition. <b>2011</b> , 50, 6441-54                                 | 19  |
|------|--|-----|
| 1672 | Prediction of equilibrium Li isotope fractionation between minerals and aqueous solutions at high P and T: An efficient ab initio approach. <b>2011</b> , 75, 6112-6123    | 55  |
| 1671 | Transport properties of Mg2SiO4 liquid at high pressure: Physical state of a magma ocean. <b>2011</b> , 312, 463-470   | 35  |
| 1670 | Exploring the conformational dynamics and membrane interactions of PorB from C. glutamicum: a multi-scale molecular dynamics simulation study. <b>2011</b> , 1808, 1746-52 | 6   |
| 1669 | Molecular dynamics simulations reveal insights into key structural elements of adenosine receptors. <b>2011</b> , 50, 4194-208   | 60  |
| 1668 | Common structural traits across pathogenic mutants of the human prion protein and their implications for familial prion diseases. <b>2011</b> , 411, 700-12                | 54  |
| 1667 | Dynamical behaviour of the human <b>#</b> -adrenoceptor under agonist binding. <b>2011</b> , 37, 907-913   | 7   |
| 1666 | Size and sequence and the volume change of protein folding. <b>2011</b> , 133, 6020-7  | 93  |
| 1665 | Bilayer structure and lipid dynamics in a model stratum corneum with oleic acid. <b>2011</b> , 115, 3164-71  | 53  |
| 1664 | Keep It Flexible: Driving Macromolecular Rotary Motions in Atomistic Simulations with GROMACS. <b>2011</b> , 7, 1381-1393  | 33  |
| 1663 | A Comparative Study for Molecular Dynamics Simulations of Liquid Benzene. <b>2011</b> , 7, 2240-52   | 53  |
| 1662 | How do aminoadamantanes block the influenza M2 channel, and how does resistance develop?. <b>2011</b> , 133, 9903-11   | 64  |
| 1661 | Effects of Carbon Nanotubes on Structure and Elasticity of Lipid Bilayers. <b>2011</b> , 7, 674-689  | 3   |
| 1660 | Insight into the phosphodiesterase mechanism from combined QM/MM free energy simulations. <b>2011</b> , 278, 2579-95   | 19  |
| 1659 | Biophysical and computational studies of membrane penetration by the GRP1 pleckstrin homology domain. <b>2011</b> , 19, 1338-46  | 50  |
| 1658 | The MOLDY short-range molecular dynamics package. <b>2011</b> , 182, 2587-2604   | 31  |
| 1657 | The adsorption of xyloglucan on cellulose: effects of explicit water and side chain variation. <b>2011</b> , 346, 2595-602   | 44  |
| 1656 | Reversible Hydrogen Storage by Controlled Buckling of Graphene Layers. <b>2011</b> , 115, 25523-25528  | 133 |

| 1655 | Alcohol Adsorption onto Silicalite from Aqueous Solution. <b>2011</b> , 115, 18659-18669   | 32  |
|------|--|-----|
| 1654 | Atomistic simulations of pressure-induced structural transformations in solids. <b>2011</b> , 79, 241-252  | 20  |
| 1653 | A molecular dynamics study of the thermal response of crystalline cellulose I#2011, 18, 207-221  | 31  |
| 1652 | A systematic study of fundamentals in ⊞-helical coiled coil mimicry by alternating sequences of<br>and □amino acids. <b>2011</b> , 41, 733-42  | 10  |
| 1651 | Structural properties of hydroxyl-substituted alkyl benzenesulfonates at the water/vapor and water/decane interfaces. <b>2011</b> , 54, 1078-1085                                    | 10  |
| 1650 | How T cell receptors interact with peptide-MHCs: a multiple steered molecular dynamics study. <b>2011</b> , 79, 3007-24  | 36  |
| 1649 | Competitive absorption of epoxy monomers on carbon nanotube: A molecular simulation study. <b>2011</b> , 49, 1123-1130   | 13  |
| 1648 | Lipid composition influences the release of Alzheimer's amyloid 即eptide from membranes. <b>2011</b> , 20, 1530-45  | 72  |
| 1647 | Insights into the structural stability of Bax from molecular dynamics simulations at high temperatures. <b>2011</b> , 20, 2035-46  | 6   |
| 1646 | Combination of the CHARMM27 force field with united-atom lipid force fields. <b>2011</b> , 32, 1400-10   | 57  |
| 1645 | Comparing the structural properties of human and rat islet amyloid polypeptide by MD computer simulations. <b>2011</b> , 156, 43-50  | 41  |
| 1644 | Structural characteristics of hydration sites in lysozyme. <b>2011</b> , 156, 31-42  | 11  |
| 1643 | Molecular dynamics simulation of interfaces and surfaces in structures derived from and ZSM-5 crystallites. <b>2011</b> , 406, 2931-2947   | 6   |
| 1642 | Self-consistent mean-field model for palmitoyloleoylphosphatidylcholine-palmitoyl sphingomyelin-cholesterol lipid bilayers. <b>2011</b> , 83, 031925                                 | 6   |
| 1641 | Li-isotope fractionation between silicates and fluids: Pressure dependence and influence of the bonding environment. <b>2011</b> , 23, 333-342                                       | 45  |
| 1640 | A novel current pathway parallel to the central pore in a mutant voltage-gated potassium channel. <b>2011</b> , 286, 20031-42  | 5   |
| 1639 | Interaction of actin with carcinoembryonic antigen-related cell adhesion molecule 1 (CEACAM1) receptor in liposomes is Ca2+- and phospholipid-dependent. <b>2011</b> , 286, 27528-36 | 8   |
| 1638 | Mutant alcohol dehydrogenase leads to improved ethanol tolerance in Clostridium thermocellum. <b>2011</b> , 108, 13752-7   | 147 |

| 1637 | The multiscale coarse-graining method. VII. Free energy decomposition of coarse-grained effective potentials. <b>2011</b> , 134, 224107   | 51 |
|------|---|----|
| 1636 | Ligand-induced modulation of the free-energy landscape of G protein-coupled receptors explored by adaptive biasing techniques. <b>2011</b> , 7, e1002193  | 63 |
| 1635 | Direct observation of the substitution effects on the hydrogen bridge dynamics in selected Schiff basesa comparative molecular dynamics study. <b>2011</b> , 134, 034308                                      | 9  |
| 1634 | Response of water to electric fields at temperatures below the glass transition: a molecular dynamics analysis. <b>2011</b> , 135, 134507   | 11 |
| 1633 | Finding a needle in a haystack: the role of electrostatics in target lipid recognition by PH domains. <b>2012</b> , 8, e1002617   | 32 |
| 1632 | Adhesive Energy of Zinc Oxide and Graphite, Molecular Dynamics and Atomic Force Microscopy Study. <b>2012</b> , 1479, 89-94   |    |
| 1631 | Computational studies on a new cationic peroxidase isoenzyme from artichoke leaves. <b>2012</b> , 3, 60-6   |    |
| 1630 | Natural polarizability and flexibility via explicit valency: the case of water. <b>2012</b> , 136, 084109   | 21 |
| 1629 | Communication: a minimal model for the diffusion-relaxation backbone dynamics of proteins. <b>2012</b> , 136, 191101  | 3  |
| 1628 | Collective degrees of freedom involved in absorption and desorption of surfactant molecules in spherical non-ionic micelles. <b>2012</b> , 137, 164902  | 7  |
| 1627 | Molecular modeling of mechanical stresses on proteins in glassy matrices: formalism. <b>2012</b> , 137, 035103  | 14 |
| 1626 | Molecular Dynamics Simulation of the SmC Phase. <b>2012</b> , 431, 121-128  | 1  |
| 1625 | Direct observation of proteolytic cleavage at the S2 site upon forced unfolding of the Notch negative regulatory region. <b>2012</b> , 109, E2757-65  | 50 |
| 1624 | New insights into the role of the glutamic acid of the E-box motif in group B Streptococcus pilus 2a assembly. <b>2012</b> , 26, 2008-18  | 11 |
| 1623 | Impact of Hydrolysis at High Temperatures on the Apparent Viscosity of Carboxybetaine Viscoelastic Surfactant-Based Acid: Experimental and Molecular Dynamics Simulation Studies. <b>2012</b> , 17, 1119-1130 | 10 |
| 1622 | Molecular dynamics prediction of interfacial strength and validation through atomic force microscopy. <b>2012</b> , 101, 151603   | 12 |
| 1621 | Polarizable molecular dynamics simulations of aqueous dipeptides. <b>2012</b> , 116, 8733-40  | 8  |
| 1620 | Photodynamic efficiency of cationic meso-porphyrins at lipid bilayers: insights from molecular dynamics simulations. <b>2012</b> , 116, 14618-27  | 29 |

| 1619 | Local Fluctuations and Conformational Transitions in Proteins. <b>2012</b> , 8, 4775-85  | 31     |
|------|--|--------|
| 1618 | GROMOS 53A6GLYC, an Improved GROMOS Force Field for Hexopyranose-Based Carbohydrates. <b>2012</b> , 8, 4681-90                               | 93     |
| 1617 | Phase transitions in coarse-grained lipid bilayers containing cholesterol by molecular dynamics simulations. <b>2012</b> , 103, 2125-33      | 47     |
| 1616 | Simulation of multiphase systems utilizing independent force fields to control intraphase and interphase behavior. <b>2012</b> , 33, 1458-66 | 21     |
| 1615 | Atomic structures and energies of grain boundaries in Mg2SiO4 forsterite from atomistic modeling. <b>2012</b> , 39, 749-760                  | 18     |
| 1614 | Development of a tuned interfacial force field parameter set for the simulation of protein adsorption to silica glass. <b>2012</b> , 7, 56   | 16     |
| 1613 | Practically Efficient and Robust Free Energy Calculations: Double-Integration Orthogonal Space Tempering. <b>2012</b> , 8, 810-23            | 70     |
| 1612 | Response of the electric conductivity of double-stranded DNA on moderate mechanical stretching stresses. <b>2012</b> , 85,                   | 19     |
| 1611 | Screening for the Location of RNA using the Chloride Ion Distribution in Simulations of Virus Capsids. <b>2012</b> , 8, 2474-83              | 19     |
| 1610 | Structural and functional characterization of the kindlin-1 pleckstrin homology domain. <b>2012</b> , 287, 43246-61                          | 27     |
| 1609 | Exploring the mineralization of hydrophobins at a liquid interface. <b>2012</b> , 8, 11343   | 10     |
| 1608 | Molecular Dynamics Study of a MARTINI Coarse-Grained Polystyrene Brush in Good Solvent: Structure and Dynamics. <b>2012</b> , 45, 563-571    | 28     |
| 1607 | Water Structure and Hydrogen Bonding at Goethite/Water Interfaces: Implications for Proton Affinities. <b>2012</b> , 116, 4714-4724          | 49     |
| 1606 | Thermodynamic transferability of coarse-grained potentials for polymer-additive systems. <b>2012</b> , 14, 11896-903                         | 24     |
| 1605 | Three-dimensional structure of human 閏efensin 28 via homology modelling and molecular dynamics. <b>2012</b> , 38, 90-101                     | 4      |
|      | Gynanics. 2012, 30, 70 101   |        |
| 1604 | Computer Simulation of the Nonlinear Ontical Properties of Language Blodgett Films of a  | 5      |
| 1604 | Computer Simulation of the Nonlinear Optical Properties of Langmuir <b>B</b> lodgett Films of a  | 5<br>7 |

| 1601 | Molecular dynamics study of water diffusivity at low concentrations in non-swollen and swollen polyurethanes. <b>2012</b> , 53, 3253-3260   | 7   |
|------|---|-----|
| 1600 | Binding preferences, surface attachment, diffusivity, and orientation of a family 1 carbohydrate-binding module on cellulose. <b>2012</b> , 287, 20603-12   | 67  |
| 1599 | Insights on P-Glycoprotein's Efflux Mechanism Obtained by Molecular Dynamics Simulations. <b>2012</b> , 8, 1853-64  | 79  |
| 1598 | Morin inhibits the early stages of amyloid 静eptide aggregation by altering tertiary and quaternary interactions to produce "off-pathway" structures. <b>2012</b> , 51, 5990-6009  | 56  |
| 1597 | Thermodynamics and kinetics of bubble nucleation: simulation methodology. <b>2012</b> , 137, 074109   | 55  |
| 1596 | Molecular Dynamics Simulations of Phosphatidylcholine Membranes: A Comparative Force Field Study. <b>2012</b> , 8, 4593-609   | 154 |
| 1595 | Characterization of a potent antimicrobial lipopeptide via coarse-grained molecular dynamics. <b>2012</b> , 1818, 212-8   | 38  |
| 1594 | Interaction of wild type, G68R and L125M isoforms of the arylamine-N-acetyltransferase from Mycobacterium tuberculosis with isoniazid: a computational study on a new possible mechanism of resistance. <b>2012</b> , 18, 4013-24 | 18  |
| 1593 | Competitive binding of cations to duplex DNA revealed through molecular dynamics simulations. <b>2012</b> , 116, 12946-54   | 77  |
| 1592 | Molecular dynamic simulation studies on the effect of one residue chain staggering on the structure and stability of heterotrimeric collagen-like peptides with interruption. <b>2012</b> , 97, 847-63                            | 9   |
| 1591 | Hydration of calcium oxide surface predicted by reactive force field molecular dynamics. <b>2012</b> , 28, 4187-97  | 139 |
| 1590 | Atomistic simulations of micellization of sodium hexyl, heptyl, octyl, and nonyl sulfates. <b>2012</b> , 116, 2430-7  | 68  |
| 1589 | All-atom stability and oligomerization simulations of polyglutamine nanotubes with and without the 17-amino-acid N-terminal fragment of the Huntingtin protein. <b>2012</b> , 116, 12168-79                                       | 11  |
| 1588 | Insight into the structural deformations of beta-cyclodextrin caused by alcohol cosolvents and guest molecules. <b>2012</b> , 116, 3880-9   | 31  |
| 1587 | Force field development for actinyl ions via quantum mechanical calculations: an approach to account for many body solvation effects. <b>2012</b> , 116, 10885-97   | 35  |
| 1586 | Exploring the Multidimensional Free Energy Surface of Phosphoester Hydrolysis with Constrained QM/MM Dynamics. <b>2012</b> , 8, 3596-604  | 22  |
| 1585 | A novel dendrimeric peptide with antimicrobial properties: structure-function analysis of SB056. <b>2012</b> , 102, 1039-48   | 36  |
| 1584 | Predicting the effect of ions on the conformation of the H-NS dimerization domain. <b>2012</b> , 103, 89-98   | 12  |

| 1583 | Lipase B from Candida antarctica binds to hydrophobic substrate Water interfaces via hydrophobic anchors surrounding the active site entrance. <b>2012</b> , 84, 48-54                                   | 29 |
|------|--|----|
| 1582 | Charybdotoxin and margatoxin acting on the human voltage-gated potassium channel hKv1.3 and its H399N mutant: an experimental and computational comparison. <b>2012</b> , 116, 5132-40                   | 14 |
| 1581 | Mixing properties of sphingomyelin ceramide bilayers: a simulation study. <b>2012</b> , 116, 4500-9  | 28 |
| 1580 | Monte Carlo simulations of charge transport in organic systems with true off-diagonal disorder. <b>2012</b> , 137, 114901  | 16 |
| 1579 | Ligand migration in myoglobin: a combined study of computer simulation and x-ray crystallography. <b>2012</b> , 136, 165101  | 7  |
| 1578 | Variable Hydrogen Bond Strength in Akaganlte. <b>2012</b> , 116, 2303-2312   | 30 |
| 1577 | Virus capsid dissolution studied by microsecond molecular dynamics simulations. <b>2012</b> , 8, e1002502  | 53 |
| 1576 | "SP-G", a putative new surfactant proteintissue localization and 3D structure. <b>2012</b> , 7, e47789   | 24 |
| 1575 | Exploring binding properties of agonists interacting with a Eppioid receptor. <b>2012</b> , 7, e52633  | 6  |
| 1574 | Exploring the essential collective dynamics of interacting proteins: application to prion protein dimers. <b>2012</b> , 80, 1847-65  | 13 |
| 1573 | Characterization of the homodimerization interface and functional hotspots of the CXCR4 chemokine receptor. <b>2012</b> , 80, 1919-28  | 25 |
| 1572 | Molecular dynamics studies of the STAT3 homodimer:DNA complex: relationships between STAT3 mutations and protein-DNA recognition. <b>2012</b> , 52, 1179-92  | 21 |
| 1571 | Molecular simulation and macroscopic modeling of the diffusion of hydrogen, carbon monoxide and water in heavy n-alkane mixtures. <b>2012</b> , 14, 4133-41  | 15 |
| 1570 | The effect of neutral ion aggregate formation on the electrical conductivity of an ionic liquid and its mixtures with chloroform. <b>2012</b> , 13, 1748-52  | 29 |
| 1569 | Development of a united-atom force field for 1-ethyl-3-methylimidazolium tetracyanoborate ionic liquid. <i>Molecular Physics</i> , <b>2012</b> , 110, 1115-1126  | 26 |
| 1568 | Hybrid QM/MM Molecular Dynamics Study of Benzocaine in a Membrane Environment: How Does a Quantum Mechanical Treatment of Both Anesthetic and Lipids Affect Their Interaction. <b>2012</b> , 8, 2197-203 | 13 |
| 1567 | Functional domain motions in proteins on the ~1-100 ns timescale: comparison of neutron spin-echo spectroscopy of phosphoglycerate kinase with molecular-dynamics simulation. <b>2012</b> , 102, 1108-17 | 36 |
| 1566 | Positioning of antioxidant quercetin and its metabolites in lipid bilayer membranes: implication for their lipid-peroxidation inhibition. <b>2012</b> , 116, 1309-18                                     | 95 |

| 1565 | Effect of size on mechanical behavior of Au pillars by molecular dynamics study. 2012, 55, 1111-1117  | 8  |
|------|---|----|
| 1564 | Ligand-based 3-D pharmacophore generation and molecular docking of mTOR kinase inhibitors. <b>2012</b> , 18, 1611-24  | 18 |
| 1563 | Aberrant structures of Parkinson disease-associated ubiquitin C-terminal hydrolase L1 predicted by molecular dynamics. <b>2012</b> , 535, 163-168                                       | 3  |
| 1562 | Computational and experimental evidence of through-space NMR spectroscopic J coupling of hydrogen atoms. <b>2012</b> , 18, 981-6  | 23 |
| 1561 | Dynamics and mechanism of structural diffusion in linear hydrogen bond. <b>2012</b> , 33, 175-88  | 11 |
| 1560 | Vibrational averaging of the chemical shift in crystalline ⊞-glycine. <b>2012</b> , 33, 1080-9  | 24 |
| 1559 | Small-molecule G-quadruplex interactions: Systematic exploration of conformational space using multiple molecular dynamics. <b>2013</b> , 99, 989-1005                                  | 26 |
| 1558 | Molecular dynamics simulations of isoleucine-release pathway in GAF domain of N-CodY from Bacillus Subtilis. <b>2013</b> , 44, 232-40   | 2  |
| 1557 | A morphometric approach for the accurate solvation thermodynamics of proteins and ligands. <b>2013</b> , 34, 1969-74  | 8  |
| 1556 | Aggregation of Alzheimer's amyloid theptide in biological membranes: a molecular dynamics study. <b>2013</b> , 52, 4971-80  | 43 |
| 1555 | Modeling, docking and dynamics simulations of a non-specific lipid transfer protein from Peganum harmala L. <b>2013</b> , 47, 56-65   | 10 |
| 1554 | Aqueous citrate: a first-principles and force-field molecular dynamics study. <b>2013</b> , 3, 16399  | 18 |
| 1553 | Liquid mixtures involving hydrogenated and fluorinated chains: (p, $\Box T$ , x) surface of (ethanol + 2,2,2-trifluoroethanol), experimental and simulation. <b>2013</b> , 117, 9709-17 | 25 |
| 1552 | Identification of a common binding mode for imaging agents to amyloid fibrils from molecular dynamics simulations. <b>2013</b> , 135, 15114-28  | 38 |
| 1551 | Spectroscopic, docking and molecular dynamics simulation studies on the interaction of two Schiff base complexes with human serum albumin. <b>2013</b> , 141, 166-172                   | 27 |
| 1550 | The Influence of Water on the Solubility of Carbon Dioxide in Imidazolium Based Ionic Liquids. <b>2013</b> , 227, 167-176   | 16 |
| 1549 | Comments on a Continuum-Related Parrinello-Rahman Molecular Dynamics Formulation. <b>2013</b> , 113, 93-112   | 7  |
| 1548 | Thermophysical properties of the ionic liquids [EMIM][B(CN)4] and [HMIM][B(CN)4]. <b>2013</b> , 117, 8512-23  | 32 |

| 1547 | Comparison of force fields on the basis of various model approacheshow to design the best model for the [CnMIM][NTf2] family of ionic liquids. <b>2013</b> , 14, 3368-74             |     | 30  |  |
|------|--|-----|-----|--|
| 1546 | Effect of wall adsorption on the nano-droplet evaporation in a nano-channel: A molecular dynamics investigation. <b>2013</b> , 436, 450-458  |     | 1   |  |
| 1545 | Combined QM/MM investigation on the light-driven electron-induced repair of the (6-4) thymine dimer catalyzed by DNA photolyase. <b>2013</b> , 117, 10071-9                          |     | 23  |  |
| 1544 | MD simulations of loading rate dependence of detwinning deformation in nanocrystalline Ni. <b>2013</b> , 56, 491-497   |     | 4   |  |
| 1543 | Self-assembly of DNA duplex in graphene bilayer. <i>Molecular Physics</i> , <b>2013</b> , 111, 1053-1060   | 1.7 | 2   |  |
| 1542 | Time-resolved force distribution analysis. <b>2013</b> , 6, 5  |     | 39  |  |
| 1541 | Double resolution model for studying TMAO/water effective interactions. 2013, 117, 13268-77  |     | 77  |  |
| 1540 | The role of a sodium ion binding site in the allosteric modulation of the A(2A) adenosine G protein-coupled receptor. <b>2013</b> , 21, 2175-85                                      |     | 98  |  |
| 1539 | Propofol modulates the lipid phase transition and localizes near the headgroup of membranes. <b>2013</b> , 175-176, 84-91  |     | 16  |  |
| 1538 | Investigation into the feasibility of thioditaloside as a novel scaffold for galectin-3-specific inhibitors. <b>2013</b> , 14, 1331-42   |     | 29  |  |
| 1537 | Conformational analysis of the frog skin peptide, plasticin-L1, and its effects on production of proinflammatory cytokines by macrophages. <b>2013</b> , 52, 7231-41                 |     | 20  |  |
| 1536 | Interactions between fengycin and model bilayers quantified by coarse-grained molecular dynamics. <b>2013</b> , 105, 1612-23   |     | 25  |  |
| 1535 | One-dimensional potential of mean force underestimates activation barrier for transport across flexible lipid membranes. <b>2013</b> , 139, 134906                                   |     | 26  |  |
| 1534 | Glyceride lipid formulations: molecular dynamics modeling of phase behavior during dispersion and molecular interactions between drugs and excipients. <b>2013</b> , 30, 3238-53     |     | 29  |  |
| 1533 | Molecular dynamics simulation of SDS and CTAB micellization and prediction of partition equilibria with COSMOmic. <b>2013</b> , 29, 11582-92   |     | 47  |  |
| 1532 | Hydration patterns of graphene-based nanomaterials (GBNMs) play a major role in the stability of a helical protein: a molecular dynamics simulation study. <b>2013</b> , 29, 14230-8 |     | 37  |  |
| 1531 | Structural characterization of NETNES glycopeptide from Trypanosoma cruzi. 2013, 373, 28-34  |     | 2   |  |
| 1530 | Bulk Liquid Water at Ambient Temperature and Pressure from MP2 Theory. <b>2013</b> , 4, 3753-3759  |     | 117 |  |

| 1529 | Solvation structures and dynamics of the magnesium chloride (Mg(2+)-Cl(-)) ion pair in water-ethanol mixtures. <b>2013</b> , 117, 8703-9              | 22 |
|------|---|----|
| 1528 | The role of cross-chain ionic interactions for the stability of collagen model peptides. <b>2013</b> , 105, 1681-8                                    | 26 |
| 1527 | Solvation structure and dynamics of potassium chloride ion pair in dimethyl sulfoxide later mixtures. <b>2013</b> , 188, 5-12                         | 17 |
| 1526 | The role of solvent exclusion in the interaction between D124 and the metal site in SOD1: implications for ALS. <b>2013</b> , 18, 931-8               | 6  |
| 1525 | Embedding A#2 in heterogeneous membranes depends on cholesterol asymmetries. <b>2013</b> , 105, 899-910   | 14 |
| 1524 | Hidden Conformation Events in DNA Base Extrusions: A Generalized Ensemble Path Optimization and Equilibrium Simulation Study. <b>2013</b> , 9,        | 15 |
| 1523 | Structure, molecular dynamics, and stress in a linear polymer. <b>2013</b> , 61, 49-59  | 5  |
| 1522 | Benzene adsorption at the aqueous (0 1 1) ⊞-quartz interface: is surface flexibility important?. <b>2013</b> , 39, 1093-1102                          | 11 |
| 1521 | Studies on sensitivity to tension and gating pathway of MscL by molecular dynamic simulation. <b>2013</b> , 29, 256-266                               | 2  |
| 1520 | Tension moderation and fluctuation spectrum in simulated lipid membranes under an applied electric potential. <b>2013</b> , 139, 164902               | 7  |
| 1519 | Electrostatic frequency shifts in amide I vibrational spectra: direct parameterization against experiment. <b>2013</b> , 138, 134116                  | 73 |
| 1518 | Computer Simulation of Self-Assembling Macromolecules. <b>2013</b> , 93-107   | 3  |
| 1517 | Shear deformations in calcium silicate hydrates. <b>2013</b> , 9, 7333  | 87 |
| 1516 | Permeation of polystyrene nanoparticles across model lipid bilayer membranes. <b>2013</b> , 9, 10265  | 20 |
| 1515 | Interaction of Piscidin-1 with zwitterionic versus anionic membranes: a comparative molecular dynamics study. <b>2013</b> , 31, 1393-403              | 11 |
| 1514 | Computational and experimental study of the effect of PEG in the preparation of damascenone-imprinted xerogels. <b>2013</b> , 29, 2024-32             | 9  |
| 1513 | Ionic specific effects on the structure, mechanics and interfacial softness of a polyelectrolyte brush. <b>2013</b> , 160, 297-309; discussion 311-27 | 17 |
| 1512 | Are polar liquids less simple?. <b>2013</b> , 138, 12A502   | 15 |

| 1511 | Simple Quantitative Tests to Validate Sampling from Thermodynamic Ensembles. <b>2013</b> , 9, 909-26   | 52   |
|------|--|------|
| 1510 | A Candidate Ion-Retaining State in the Inward-Facing Conformation of Sodium/Galactose Symporter: Clues from Atomistic Simulations. <b>2013</b> , 9, 1240-6               | 22   |
| 1509 | Biomolecular Simulations. 2013,  | 17   |
| 1508 | Electrostatics interactions in classical simulations. <b>2013</b> , 924, 243-70  | 6    |
| 1507 | Characterization of the structures and dynamics of phosphoric acid doped benzimidazole mixtures: a molecular dynamics study. <b>2013</b> , 19, 109-18                    | 6    |
| 1506 | Effects of surface curvature and surface characteristics of carbon-based nanomaterials on the adsorption and activity of acetylcholinesterase. <b>2013</b> , 62, 222-232 | 32   |
| 1505 | On the weak dependence of water diffusivity on the degree of hydrophobicity of acetylated hydroxypropyl xylan. <b>2013</b> , 98, 644-9                                   | 5    |
| 1504 | Molecular simulations suggest how a branched antimicrobial peptide perturbs a bacterial membrane and enhances permeability. <b>2013</b> , 1828, 1112-21                  | 42   |
| 1503 | NaCl crystallization in apolar nanometer-sized confinement studied by atomistic simulations. <b>2013</b> , 88, 062312  | 4    |
| 1502 | The structural basis for endotoxin-induced allosteric regulation of the Toll-like receptor 4 (TLR4) innate immune receptor. <b>2013</b> , 288, 36215-25                  | 40   |
| 1501 | Modelling the effect of osmolytes on peptide mechanical unfolding. 2013, 578, 138-143  | 5    |
| 1500 | Signal intensities in LH-LTC CP and INEPT MAS NMR of liquid crystals. <b>2013</b> , 230, 165-75  | 63   |
| 1499 | Characteristic NMR spectra of proton transfer in protonated water clusters. 2013, 420, 50-61   | 14   |
| 1498 | Defining the membrane-associated state of the PTEN tumor suppressor protein. <b>2013</b> , 104, 613-21   | 35   |
| 1497 | Prediction of micelle/water and liposome/water partition coefficients based on molecular dynamics simulations, COSMO-RS, and COSMOmic. <b>2013</b> , 29, 3527-37         | 62   |
| 1496 | GROMACS 4.5: a high-throughput and highly parallel open source molecular simulation toolkit. <b>2013</b> , 29, 845-54  | 4786 |
| 1495 | MagiC: Software Package for Multiscale Modeling. <b>2013</b> , 9, 1512-20  | 43   |
| 1494 | Dimers of human 毗efensins and their interactions with the POPG membrane. <b>2013</b> , 39, 849-859   | 3    |

| 1493 | Structural changes in supercooled Al2O3-Y2O3 liquids. 2013, 15, 8589-605   | 18 |
|------|--|----|
| 1492 | Length-dependent stability of ∃-helical peptide upon adsorption to single-walled carbon nanotube. <b>2013</b> , 99, 357-69   | 12 |
| 1491 | The Structure of Silica Surfaces Exposed to Atomic Oxygen. <b>2013</b> , 117, 9311-9321  | 22 |
| 1490 | Molecular mechanism of misfolding and aggregation of A <b>#</b> 13-23). <b>2013</b> , 117, 6175-86   | 39 |
| 1489 | Molecular Dynamics Simulations of Carbon Dioxide Intercalation in Hydrated Na-Montmorillonite. <b>2013</b> , 117, 11028-11039  | 82 |
| 1488 | Classical molecular dynamics in a nutshell. <b>2013</b> , 924, 127-52  | 9  |
| 1487 | Water vapor diffusion into a nanostructured iron oxyhydroxide. <b>2013</b> , 52, 7107-13   | 10 |
| 1486 | Heat Transfer Calculations for Decomposition of Structure I Methane Hydrates by Molecular Dynamics Simulation. <b>2013</b> , 117, 12172-12182                                | 30 |
| 1485 | Dissimilar stability of proteins in graphene bilayer: a molecular dynamics study. <i>Molecular Physics</i> , <b>2013</b> , 111, 545-552                                      | 5  |
| 1484 | Dynamic Heterogeneity in Random and Gradient Copolymers: A Computational Investigation. <b>2013</b> , 46, 5066-5079  | 26 |
| 1483 | Ab initio prediction of equilibrium boron isotope fractionation between minerals and aqueous fluids at high P and T. <b>2013</b> , 101, 285-301                              | 64 |
| 1482 | Conformational dynamics and membrane interactions of the E. coli outer membrane protein FecA: a molecular dynamics simulation study. <b>2013</b> , 1828, 284-93              | 45 |
| 1481 | Stability and membrane interactions of an autotransport protein: MD simulations of the Hia translocator domain in a complex membrane environment. <b>2013</b> , 1828, 715-23 | 22 |
| 1480 | Lipid peroxidation and water penetration in lipid bilayers: a W-band EPR study. <b>2013</b> , 1828, 510-7  | 14 |
| 1479 | Structure and dynamics of [PF6][P(1,2,2,4)] from molecular dynamics simulations. <b>2013</b> , 117, 15176-83   | 11 |
| 1478 | Conformational fluctuations of UreG, an intrinsically disordered enzyme. <b>2013</b> , 52, 2949-54   | 29 |
| 1477 | A New Maximum Likelihood Approach for Free Energy Profile Construction from Molecular Simulations. <b>2013</b> , 9, 153-164  | 59 |
| 1476 | Toward a Broadly Applicable Force Field for d(6)-Piano Stool Complexes. <b>2013</b> , 9, 2313-23   | 6  |

## (2013-2013)

| 1475 | Toward understanding the outer membrane uptake of small molecules by Pseudomonas aeruginosa. <b>2013</b> , 288, 12042-53   | 48 |
|------|--|----|
| 1474 | Enhancement of Lithium Ion Mobility in Ionic Liquid Electrolytes in Presence of Additives. <b>2013</b> , 117, 25343-25351  | 53 |
| 1473 | Simulating the pyrolysis of polyazides: a mechanistic case study of the [[P(N3)6]- anion. 2013, 52, 1747-54  | 3  |
| 1472 | Bridging the gap between theory and experiment to derive a detailed understanding of hammerhead ribozyme catalysis. <b>2013</b> , 120, 25-91                                     | 8  |
| 1471 | Communication: Benzene dimerthe free energy landscape. <b>2013</b> , 139, 201102   | 17 |
| 1470 | Understanding the molecular determinants driving the immunological specificity of the protective pilus 2a backbone protein of group B streptococcus. <b>2013</b> , 9, e1003115   | 34 |
| 1469 | Engineering a more thermostable blue light photo receptor Bacillus subtilis YtvA LOV domain by a computer aided rational design method. <b>2013</b> , 9, e1003129                | 22 |
| 1468 | Antimicrobial peptides design by evolutionary multiobjective optimization. <b>2013</b> , 9, e1003212   | 50 |
| 1467 | Hierarchical Macromolecular Structures: 60 Years after the Staudinger Nobel Prize II. 2013,  | 8  |
| 1466 | Study of lattice thermal conductivity of alpha-zirconium by molecular dynamics simulation. <b>2013</b> , 22, 076601  | 8  |
| 1465 | Unusual sequence effects on nucleotide excision repair of arylamine lesions: DNA bending/distortion as a primary recognition factor. <b>2013</b> , 41, 869-80                    | 38 |
| 1464 | Temperature dependence of the crystal-liquid interfacial free energy and the endpoint of the melting line. <b>2013</b> , 139, 224703   | 24 |
| 1463 | Fitting coarse-grained distribution functions through an iterative force-matching method. <b>2013</b> , 139, 121906  | 62 |
| 1462 | (Ala)(4)-X-(Ala)4 as a model system for the optimization of the <b>1</b> and <b>2</b> amino acid side-chain dihedral empirical force field parameters. <b>2013</b> , 34, 593-603 | 4  |
| 1461 | Combination of COSMOmic and molecular dynamics simulations for the calculation of membrane-water partition coefficients. <b>2013</b> , 34, 1332-40                               | 46 |
| 1460 | Assessing the Stabilization of P-Glycoprotein's Nucleotide-Binding Domains by the Linker, Using Molecular Dynamics. <b>2013</b> , 32, 529-40                                     | 15 |
| 1459 | Insight into TPMT(*)23 mutation mis-folding using molecular dynamics simulation and protein structure analysis. <b>2013</b> , 31, 1066-76  | 2  |
| 1458 | The 2.5 lbtructure of the enterococcus conjugation protein TraM resembles VirB8 type IV secretion proteins. <b>2013</b> , 288, 2018-28   | 47 |

| 1457 | Determining the phase diagram of water from direct coexistence simulations: the phase diagram of the TIP4P/2005 model revisited. <b>2013</b> , 139, 154505  | 48 |
|------|---|----|
| 1456 | High-Performance Modeling of CO2 Sequestration by Coupling Reservoir Simulation and Molecular Dynamics. <b>2013</b> ,   | 2  |
| 1455 | Ion concentration-dependent ion conduction mechanism of a voltage-sensitive potassium channel. <b>2013</b> , 8, e56342  | 12 |
| 1454 | Molecular dynamics simulations of water/mucus partition coefficients for feeding stimulants in fish and the implications for olfaction. <b>2013</b> , 8, e72271   | 5  |
| 1453 | Theoretical Investigation of the D83V Mutation within the Myocyte-Specific Enhancer Factor-2 Beta and Its Role in Cancer. <b>2013</b> , 2013, 1-10  | 3  |
| 1452 | New Hexagonal-rhombic Trilayer Ice Structure Confined between Hydrophobic Plates. <b>2014</b> , 27, 15-19   | 12 |
| 1451 | Two polymorphisms facilitate differences in plasticity between two chicken major histocompatibility complex class I proteins. <b>2014</b> , 9, e89657   | 19 |
| 1450 | Functional mechanism of C-terminal tail in the enzymatic role of porcine testicular carbonyl reductase: a combined experiment and molecular dynamics simulation study of the C-terminal tail in the enzymatic role of PTCR. <b>2014</b> , 9, e90712 | Ο  |
| 1449 | Tensile deformation and failure of amyloid and amyloid-like protein fibrils. <b>2014</b> , 25, 105703   | 32 |
| 1448 | Phospholamban C-terminal residues are critical determinants of the structure and function of the calcium ATPase regulatory complex. <b>2014</b> , 289, 25855-66   | 11 |
| 1447 | Structural Characterization of the Drug Translocation Path of MRP1/ABCC1. <b>2014</b> , 54, 1382-1393   | 5  |
| 1446 | A critical residue selectively recruits nucleotides for t7 RNA polymerase transcription fidelity control. <b>2014</b> , 107, 2130-40  | 20 |
| 1445 | Dynamic characterization and substrate binding of cis-2,3-dihydrobiphenyl-2,3-diol dehydrogenase-an enzyme used in bioremediation. <b>2014</b> , 20, 2531   | 5  |
| 1444 | An allosteric signaling pathway of human 3-phosphoglycerate kinase from force distribution analysis. <b>2014</b> , 10, e1003444   | 16 |
| 1443 | A flexible volumetric comparison of protein cavities can reveal patterns in ligand binding specificity. <b>2014</b> ,   | 3  |
| 1442 | Variational Bayesian clustering on protein cavity conformations for detecting influential amino acids. <b>2014</b> ,  | 2  |
| 1441 | Accelerating electrostatic pair methods on graphical processing units to study molecules in supercritical carbon dioxide. <b>2014</b> , 169, 343-57   | 2  |
| 1440 | Small interfering ribonucleic acid induces liquid-to-ripple phase transformation in a phospholipid membrane. <b>2014</b> , 105, 113702  | 5  |

| 1439 | Precursory signatures of protein folding/unfolding: from time series correlation analysis to atomistic mechanisms. <b>2014</b> , 140, 204905  | 3   |
|------|---|-----|
| 1438 | Communication: minimum in the thermal conductivity of supercooled water: a computer simulation study. <b>2014</b> , 140, 161104   | 16  |
| 1437 | Influence of electric fields on the structure and structure transition of water confined in a carbon nanotube. <b>2014</b> , 140, 154508  | 20  |
| 1436 | Analysis of solvation and gelation behavior of methylcellulose using atomistic molecular dynamics simulations. <b>2014</b> , 118, 13992-4008  | 25  |
| 1435 | Molecular dynamics simulation study on the interaction of collagen-like peptides with gelatinase-A (MMP-2). <b>2014</b> , 101, 779-94   | 10  |
| 1434 | Glucose oxidase from Penicillium amagasakiense: characterization of the transition state of its denaturation from molecular dynamics simulations. <b>2014</b> , 82, 2353-63                           | 12  |
| 1433 | Short-range solvation effects on chiroptical properties: a time-dependent density functional theory and ab initio molecular dynamics computational case study on austdiol. <b>2014</b> , 118, 11751-7 | 6   |
| 1432 | Understanding electrofreezing in water simulations. <b>2014</b> , 141, 074501   | 24  |
| 1431 | Multiscale simulations give insight into the hydrogen in and out pathways of [NiFe]-hydrogenases from Aquifex aeolicus and Desulfovibrio fructosovorans. <b>2014</b> , 118, 13800-11                  | 19  |
| 1430 | Peptide dynamics by molecular dynamics simulation and diffusion theory method with improved basis sets. <b>2014</b> , 140, 104910   | 2   |
| 1429 | How distributed charge reduces the melting points of model ionic salts. <b>2014</b> , 140, 104504   | 7   |
| 1428 | Systematic implicit solvent coarse graining of dimyristoylphosphatidylcholine lipids. <b>2014</b> , 35, 1208-18   | 15  |
| 1427 | Widom line and dynamical crossovers as routes to understand supercritical water. <b>2014</b> , 5, 5806  | 86  |
| 1426 | Restriction of HIV-1 by rhesus TRIM5⊞ is governed by alpha helices in the Linker2 region. <b>2014</b> , 88, 8911-23   | 8   |
| 1425 | Effective interaction between small unilamellar vesicles as probed by coarse-grained molecular dynamics simulations. <b>2014</b> , 86, 215-222  | 9   |
| 1424 | Comparing atomistic molecular mechanics force fields for a difficult target: a case study on the Alzheimer's amyloid peptide. <b>2014</b> , 32, 1817-32   | 62  |
| 1423 | Molecular origins of bending rigidity in lipids with isolated and conjugated double bonds: the effect of cholesterol. <b>2014</b> , 178, 18-26  | 24  |
| 1422 | Classical electrostatics for biomolecular simulations. <b>2014</b> , 114, 779-814   | 195 |
|      |   |     |

| 1421 Membrane attachment and structure models of lipid storage droplet protein 1. <b>2014</b> , 1838, 874-81   | 13   |
|--|------|
| Conformational analysis of processivity clamps in solution demonstrates that tertiary structure does not correlate with protein dynamics. <b>2014</b> , 22, 572-581            | 21   |
| 1419 Scaling behaviour for the water transport in nanoconfined geometries. <b>2014</b> , 5, 4565   | 111  |
| How well does cholesteryl hemisuccinate mimic cholesterol in saturated phospholipid bilayers?. <b>2014</b> , 20, 2121  | 33   |
| Homology modeling and virtual screening for antagonists of protease from yellow head virus. <b>2014</b> , 20, 2116   | 2    |
| The gamma-butyrolactone receptors BulR1 and BulR2 of Streptomyces tsukubaensis: tacrolimus (FK506) and butyrolactone synthetases production control. <b>2014</b> , 98, 4919-36 | 28   |
| Steered molecular dynamics identifies critical residues of the Nodamura virus B2 suppressor of RNAi. <b>2014</b> , 20, 2092  | 10   |
| Insights into the conformational perturbations of novel agonists with $\mathfrak B$ -adrenergic receptor using molecular dynamics simulations. <b>2014</b> , 101, 168-82       | 3    |
| 1413 Theoretical considerations and computational tools. <b>2014</b> , 794, 69-93  |      |
| Simulations of monomeric amyloid $\oplus$ eptide (1-40) with varying solution conditions and oxidation state of Met35: implications for aggregation. <b>2014</b> , 545, 44-52  | 28   |
| Studies of (-)-pironetin binding to $\oplus$ -tubulin: conformation, docking, and molecular dynamics. <b>2014</b> , 79, 3752-64  | 18   |
| 1410 g_mmpbsaa GROMACS tool for high-throughput MM-PBSA calculations. <b>2014</b> , 54, 1951-62  | 2069 |
| Study of orientation and penetration of LAH4 into lipid bilayer membranes: pH and composition dependence. <b>2014</b> , 84, 242-52   | 9    |
| In silico identification of novel kinase inhibitors targeting wild-type and T315I mutant ABL1 from FDA-approved drugs. <b>2014</b> , 10, 1524-37                               | 21   |
| Conformational distribution and ⊞-helix to \Bheet transition of human amylin fragment dimer. <b>2014</b> , 15, 122-31  | 55   |
| 1406 G Protein-Coupled Receptors - Modeling and Simulation. <b>2014</b> ,  | 7    |
| Atomistic Simulations of Poly(ethylene oxide) in Water and an Ionic Liquid at Room Temperature. <b>2014</b> , 47, 438-446  | 47   |
| 1404 Different aggregation dynamics of benzene-water mixtures. <b>2014</b> , 16, 21957-63  | 6    |

| 1403 | Quantum mechanics/molecular mechanics modeling of photoelectron spectra: the carbon 1s core-electron binding energies of ethanol-water solutions. <b>2014</b> , 118, 13217-25                                      | 12 |
|------|--|----|
| 1402 | Effect of including torsional parameters for histidine-metal interactions in classical force fields for metalloproteins. <b>2014</b> , 118, 13106-11   | 12 |
| 1401 | Induced ice melting by the snow flea antifreeze protein from molecular dynamics simulations. <b>2014</b> , 118, 13527-34   | 16 |
| 1400 | Infinitely dilute partial molar properties of proteins from computer simulation. <b>2014</b> , 118, 12844-54   | 10 |
| 1399 | Protein modeling and molecular dynamics simulation of the two novel surfactant proteins SP-G and SP-H. <b>2014</b> , 20, 2513  | 13 |
| 1398 | Molecular dynamics simulations of complex mixtures aimed at the preparation of naproxen-imprinted xerogels. <b>2014</b> , 54, 3330-43  | 5  |
| 1397 | Spontaneous dimer states of the Aft21-30) decapeptide. <b>2014</b> , 16, 13069-73  | 7  |
| 1396 | Molecular origin of the self-assembled morphological difference caused by varying the order of charged residues in short peptides. <b>2014</b> , 118, 12501-10   | 21 |
| 1395 | Atomistic molecular-dynamics simulations enable prediction of the arginine permeation pathway through OccD1/OprD from Pseudomonas aeruginosa. <b>2014</b> , 107, 1853-1861   | 20 |
| 1394 | Thermodynamics of antimicrobial lipopeptide binding to membranes: origins of affinity and selectivity. <b>2014</b> , 107, 1862-1872  | 25 |
| 1393 | Mechanistic insights into the allosteric modulation of opioid receptors by sodium ions. <b>2014</b> , 53, 5140-9   | 63 |
| 1392 | Finite element models and molecular dynamic simulations for studying the response of mast cell under mechanical activation. <b>2014</b> , 59, 3562-3572  |    |
| 1391 | Molecular dynamics simulations identify time scale of conformational changes responsible for conformational selection in molecular recognition of HIV-1 transactivation responsive RNA. <b>2014</b> , 136, 15631-7 | 25 |
| 1390 | Design of coordination polymers with 4?-substituted functionalized terpyridyls in the backbone and pendent cyclopentadienyliron moieties. <b>2014</b> , 5, 3453-3465   | 17 |
| 1389 | Molecular mechanism of Na(+), $K(+)$ -ATPase malfunction in mutations characteristic of adrenal hypertension. <b>2014</b> , 53, 746-54   | 21 |
| 1388 | Study of temperature dependence of thermal conductivity in cross-linked epoxies using molecular dynamics simulations with long range interactions. <b>2014</b> , 22, 025013  | 32 |
| 1387 | Molecular dynamics study of the diffusivity of a hydrophobic drug Cucurbitacin B in pseudo-poly(ethylene oxide-b-caprolactone) micelle environments. <b>2014</b> , 30, 7798-803                                    | 9  |
| 1386 | Solubilization in mixed micelles studied by molecular dynamics simulations and COSMOmic. <b>2014</b> , 118, 3593-604   | 24 |

| 1385 | Understanding the role of water during ionic liquid pretreatment of lignocellulose: co-solvent or anti-solvent?. <b>2014</b> , 16, 3830-3840                                 | 110 |
|------|--|-----|
| 1384 | Can xenon in water inhibit ice growth? Molecular dynamics of phase transitions in water-Xe system. <b>2014</b> , 141, 034503   | 12  |
| 1383 | Improving Trichoderma reesei Cel7B thermostability by targeting the weak spots. <b>2014</b> , 54, 2826-33  | 16  |
| 1382 | Dissipative particle dynamics with an effective pair potential from integral equation theory of molecular liquids. <b>2014</b> , 118, 12034-49                               | 7   |
| 1381 | Atomistic mechanisms of huntingtin N-terminal fragment insertion on a phospholipid bilayer revealed by molecular dynamics simulations. <b>2014</b> , 82, 1409-27             | 10  |
| 1380 | Layer-by-Layer Formation of Oligoelectrolyte Multilayers: A Combined Experimental and Computational Study. <b>2014</b> , 12, S14-S21   | 11  |
| 1379 | Direct osmolyte-macromolecule interactions confer entropic stability to folded states. <b>2014</b> , 118, 7327-34  | 81  |
| 1378 | Insight into HIV-1 reverse transcriptase-aptamer interaction from molecular dynamics simulations. <b>2014</b> , 20, 2380   | 11  |
| 1377 | Roadmaps through free energy landscapes calculated using the multi-dimensional vFEP approach. <b>2014</b> , 10, 24-34  | 45  |
| 1376 | Determining Structural and Mechanical Properties from Molecular Dynamics Simulations of Lipid Vesicles. <b>2014</b> , 10, 4160-4168  | 19  |
| 1375 | Extension and validation of the GROMOS 53A6(GLYC) parameter set for glycoproteins. 2014, 35, 2087-95   | 36  |
| 1374 | Influence of metal ions (Zn2+, Cu2+, Ca2+, Mg2+ and Na+) on the water coordinated neutral and zwitterionic L-histidine dimer. <b>2014</b> , 4, 49040-49052                   | 8   |
| 1373 | V-type nerve agents phosphonylate ubiquitin at biologically relevant lysine residues and induce intramolecular cyclization by an isopeptide bond. <b>2014</b> , 406, 5171-85 | 28  |
| 1372 | ZIBgridfree: efficient conformational analysis by partition-of-unity coupling. <b>2014</b> , 52, 781-804   | 4   |
| 1371 | Ermod: fast and versatile computation software for solvation free energy with approximate theory of solutions. <b>2014</b> , 35, 1592-608                                    | 47  |
| 1370 | Copper-transporting P-type ATPases use a unique ion-release pathway. <b>2014</b> , 21, 43-8  | 77  |
| 1369 | In silico screening and study of novel ERK2 inhibitors using 3D QSAR, docking and molecular dynamics. <b>2014</b> , 53, 1-12   | 5   |
| 1368 | Historical contingency and its biophysical basis in glucocorticoid receptor evolution. <b>2014</b> , 512, 203-7  | 101 |

## (2015-2014)

| 1367 | Molecular dynamics study of mixed alkanethiols covering a gold surface at three different arrangements. <b>2014</b> , 600, 79-86                       | 13 |
|------|--|----|
| 1366 | Ferroelectric hexagonal and rhombic monolayer ice phases. <b>2014</b> , 5, 1757-1764   | 79 |
| 1365 | Molecular dynamics simulations of turbostratic dry and hydrated montmorillonite with intercalated carbon dioxide. <b>2014</b> , 118, 7454-68           | 26 |
| 1364 | Quantum molecular dynamics simulations of liquid benzene using orbital optimization. <b>2014</b> , 133, 1  | 2  |
| 1363 | Intrinsic autocorrelation time of picoseconds for thermal noise in water. <b>2014</b> , 118, 8936-41   | 7  |
| 1362 | Looking at human cytosolic sialidase NEU2 structural features with an interdisciplinary approach. <b>2014</b> , 53, 5343-55                            | 3  |
| 1361 | Diffusion Coefficients of Fluorinated Surfactants in Water: Experimental Results and Prediction by Computer Simulation. <b>2014</b> , 59, 3151-3159    | 18 |
| 1360 | Molecular dynamics simulations of lipid membranes with lateral force: rupture and dynamic properties. <b>2014</b> , 1838, 994-1002                     | 27 |
| 1359 | Galectin-3 interactions with glycosphingolipids. <b>2014</b> , 426, 1439-51  | 55 |
| 1358 | Elastic properties and heterogeneous stiffness of the phi29 motor connector channel. <b>2014</b> , 106, 1338-48  | 19 |
| 1357 | Probing the U-shaped conformation of caveolin-1 in a bilayer. <b>2014</b> , 106, 1371-80   | 28 |
| 1356 | Molecular simulation of adsorption of hydrophobin HFBI to the airWater, DPPCWater and decaneWater interfaces. <b>2014</b> , 42, 66-74                  | 11 |
| 1355 | Electric-field-induced phase transition of confined water nanofilms between two graphene sheets. <b>2014</b> , 118, 8922-8                             | 16 |
| 1354 | Free energy of PAMAM dendrimer adsorption onto model biological membranes. <b>2014</b> , 118, 6792-802   | 18 |
| 1353 | Chromophore photoreduction in red fluorescent proteins is responsible for bleaching and phototoxicity. <b>2014</b> , 118, 4527-34                      | 50 |
| 1352 | Rate-dependent behavior of the amorphous phase of spider dragline silk. <b>2014</b> , 106, 2511-8  | 23 |
|      |  |    |
| 1351 | Protein-fluctuation-induced water-pore formation in ion channel voltage-sensor translocation across a lipid bilayer membrane. <b>2015</b> , 92, 052719 | 3  |

| 1349 | The Widom line and dynamical crossover in supercritical water: Popular water models versus experiments. <b>2015</b> , 143, 114502  | 27 |
|------|--|----|
| 1348 | Transition fields in organic materials: from percolation to inverted Marcus regime. A consistent Monte Carlo simulation in disordered PPV. <b>2015</b> , 142, 094503         | 14 |
| 1347 | Pairwise-additive force fields for selected aqueous monovalent ions from adaptive force matching. <b>2015</b> , 143, 194505  | 34 |
| 1346 | Mechanical behavior of a composite interface: Calcium-silicate-hydrates. <b>2015</b> , 118, 034305   | 14 |
| 1345 | Self-sorting heterodimeric coiled coil peptides with defined and tuneable self-assembly properties. <b>2015</b> , 5, 14063   | 35 |
| 1344 | Energetics of Endotoxin Recognition in the Toll-Like Receptor 4 Innate Immune Response. <b>2015</b> , 5, 17997   | 20 |
| 1343 | Solutes at the liquid:liquid phase boundarySolubility and solvent conformational response alter interfacial microsolvation. <b>2015</b> , 142, 104707                        | 15 |
| 1342 | Promoting the Adsorption of Metal Ions on Kaolinite by Defect Sites: A Molecular Dynamics Study. <b>2015</b> , 5, 14377  | 33 |
| 1341 | Insights into the species-specific TLR4 signaling mechanism in response to Rhodobacter sphaeroides lipid A detection. <b>2015</b> , 5, 7657                                  | 34 |
| 1340 | Dynamics of proton exchange in a model phosphonic acid-functionalized polymer. <b>2015</b> , 115, 1161-1174  | 2  |
| 1339 | Processivity, Substrate Positioning, and Binding: The Role of Polar Residues in a Family 18 Glycoside Hydrolase. <b>2015</b> , 54, 7292-306                                  | 15 |
| 1338 | Three-dimensional structure model and predicted ATP interaction rewiring of a deviant RNA ligase 2. <b>2015</b> , 15, 20   | 4  |
| 1337 | Frequent side chain methyl carbon-oxygen hydrogen bonding in proteins revealed by computational and stereochemical analysis of neutron structures. <b>2015</b> , 83, 403-410 | 31 |
| 1336 | The Dependence of Amyloid-∰ynamics on Protein Force Fields and Water Models. <b>2015</b> , 16, 3278-89   | 77 |
| 1335 | Penetration of HIV-1 Tat47-57 into PC/PE Bilayers Assessed by MD Simulation and X-ray Scattering. <b>2015</b> , 5, 473-94  | 9  |
| 1334 | The Nucleotide Capture Region of Alpha Hemolysin: Insights into Nanopore Design for DNA Sequencing from Molecular Dynamics Simulations. <b>2015</b> , 5, 144-153             | 7  |
| 1333 | Identification of the antiepileptic racetam binding site in the synaptic vesicle protein 2A by molecular dynamics and docking simulations. <b>2015</b> , 9, 125              | 22 |
| 1332 | Structural Determinants for the Binding of Morphinan Agonists to the Expioid Receptor. <b>2015</b> , 10, e0135998  | 15 |

## (2015-2015)

| 1331 | Investigate the binding of catechins to trypsin using docking and molecular dynamics simulation. <b>2015</b> , 10, e0125848   | 46 |
|------|---|----|
| 1330 | Molecular Determinants Underlying Binding Specificities of the ABL Kinase Inhibitors: Combining Alanine Scanning of Binding Hot Spots with Network Analysis of Residue Interactions and Coevolution. <b>2015</b> , 10, e0130203 | 29 |
| 1329 | A Jump-from-Cavity Pyrophosphate Ion Release Assisted by a Key Lysine Residue in T7 RNA Polymerase Transcription Elongation. <b>2015</b> , 11, e1004624   | 23 |
| 1328 | Molecular Dynamics Investigation of gluazo, a Photo-Switchable Ligand for the Glutamate Receptor GluK2. <b>2015</b> , 10, e0135399  | 4  |
| 1327 | A molecular dynamics study of model SI clathrate hydrates: the effect of guest size and guest-water interaction on decomposition kinetics. <b>2015</b> , 17, 9509-18  | 19 |
| 1326 | Molecular Dynamics Simulation Analysis of Anti-MUC1 Aptamer and Mucin 1 Peptide Binding. <b>2015</b> , 119, 6571-83   | 34 |
| 1325 | Salting-Out of Methane in the Aqueous Solutions of Urea and Glycine-Betaine. 2015, 119, 10941-53  | 9  |
| 1324 | Molecular Dynamics. 2015,   | 25 |
| 1323 | Extended Variable Methods. <b>2015</b> , 329-401  | 1  |
| 1322 | Cholesterol under oxidative stress-How lipid membranes sense oxidation as cholesterol is being replaced by oxysterols. <b>2015</b> , 84, 30-41  | 45 |
| 1321 | Myelography iodinated contrast media. I. Unraveling the atropisomerism properties in solution. <b>2015</b> , 12, 1939-50  | 5  |
| 1320 | Predicting protein-ligand binding specificity based on ensemble clustering. 2015,   | O  |
| 1319 | Mechanism of Polymer Collapse in Miscible Good Solvents. <b>2015</b> , 119, 15780-8   | 80 |
| 1318 | Conformational Sampling Reveals Amino Acids with a Steric Influence on Specificity. <b>2015</b> , 22, 861-75  | O  |
| 1317 | Force-Field Induced Bias in the Structure of A型1-30: A Comparison of OPLS, AMBER, CHARMM, and GROMOS Force Fields. <b>2015</b> , 55, 2587-95  | 67 |
| 1316 | Conformational flexibility of nucleosomes: A molecular dynamics study. <b>2015</b> , 70, 147-151  |    |
| 1315 | Atomistic MD simulation reveals the mechanism by which CETP penetrates into HDL enabling lipid transfer from HDL to CETP. <b>2015</b> , 56, 98-108  | 20 |
| 1314 | Interaction of collagen like peptides with gold nanosurfaces: a molecular dynamics investigation. <b>2015</b> , 17, 5172-86   | 20 |

| 1313 Capsular polysaccharide conformations in pneumococcal serotypes  | 19F and 19A. <b>2015</b> , 406, 27-33  |
|---|--|
| Hydrogen bonding in a mixture of protic ionic liquids: a molecular dy 17, 8431-40   | namics simulation study. <b>2015</b> , |
| 1311 Identifying key residues for protein allostery through rigid residue s   | can. <b>2015</b> , 119, 1689-700 20    |
| 1310 Influence of antifreeze proteins on the ice/water interface. <b>2015</b> , 11  | 19, 3407-13                            |
| 1309 Single chain structure of a poly(N-isopropylacrylamide) surfactant in  | n water. <b>2015</b> , 119, 3837-45 47 |
| Free-energy calculations reveal the subtle differences in the interac $\pm$ -hemolysin. <b>2015</b> , 11, 810-6                                 | tions of DNA bases with 3              |
| Structure of Mixed Self-Assembled Monolayers on Gold Nanoparticl<br>Arrangements. <b>2015</b> , 119, 3199-3209                                  | es at Three Different 25               |
| Concurrent cooperativity and substrate inhibition in the epoxidation cytochrome P450 3A4 active site mutants inspired by molecular dyn          |  |
| 1305 A structural mechanism for calcium transporter headpiece closure. 2  | <b>2015</b> , 119, 1407-15             |
| Carboxyl-peptide plane stacking is important for stabilization of bur Cel5A. <b>2015</b> , 55, 104-13   | ried E305 of Trichoderma reesei        |
| Molecular Dynamics Characterizations of the Supercritical CO2Medi <b>2015</b> , 54, 2489-2496   | ated Hexane <b>B</b> rine Interface.   |
| A computational study of the effect of matrix structural order on wa<br>miniproteins. <b>2015</b> , 119, 1847-56                                | ater sorption by Trp-cage 8            |
| Atomic-level study of the effects of O4 molecules on the structural trimer:   \$\$sheet stabilization, salt bridge protection, and binding mech |  |
| 1300 Mechanisms of anion conduction by coupled glutamate transporters   | s. <b>2015</b> , 160, 542-53           |
| Simulating the antimicrobial mechanism of human ⊞efensin-3 with dynamics. <b>2015</b> , 33, 2522-9  | coarse-grained molecular               |
| 1298 The energy landscape of adenylate kinase during catalysis. <b>2015</b> , 22,   | , 124-31 102                           |
| 1297 The effects of globotriaosylceramide tail saturation level on bilayer  | phases. <b>2015</b> , 11, 1352-61 18   |
| Phosphorylation of PPAR Affects the Collective Motions of the PPA 1296 10, e0123984   | AR⊡RXR∃-DNA Complex. <b>2015</b> ,     |

| 1295 | Stability and softening of a lipid monolayer in the presence of a pain-killer drug. 2015, 132, 34-44   | 11  |
|------|--|-----|
| 1294 | Mapping the Dynamics Landscape of Conformational Transitions in Enzyme: The Adenylate Kinase Case. <b>2015</b> , 109, 647-60   | 41  |
| 1293 | Dynamical equations for the period vectors in a periodic system under constant external stress. <b>2015</b> , 93, 974-978  | 1   |
| 1292 | Mutual and Self-Diffusivities in Binary Mixtures of [EMIM][B(CN)4] with Dissolved Gases by Using Dynamic Light Scattering and Molecular Dynamics Simulations. <b>2015</b> , 119, 8583-92 | 25  |
| 1291 | In silico Investigation of the PglB Active Site Reveals Transient Catalytic States and Octahedral Metal Ion Coordination. <b>2015</b> , 25, 1183-95                                      | 7   |
| 1290 | Effect of graphene oxide on the conformational transitions of amyloid beta peptide: A molecular dynamics simulation study. <b>2015</b> , 61, 175-85                                      | 52  |
| 1289 | Interaction of the antimicrobial peptide polymyxin B1 with both membranes of E. coli: a molecular dynamics study. <b>2015</b> , 11, e1004180   | 104 |
| 1288 | Oligomer Formation of Toxic and Functional Amyloid Peptides Studied with Atomistic Simulations. <b>2015</b> , 119, 9696-705  | 23  |
| 1287 | Higher-Affinity Agonists of 5-HT1AR Discovered through Tuning the Binding-Site Flexibility. <b>2015</b> , 55, 1616-27  | 10  |
| 1286 | Molecular dynamics simulation of CO2 hydrates: Prediction of three phase coexistence line. <b>2015</b> , 142, 124505   | 61  |
| 1285 | Characterization of the Dielectric Constant in the Trichoderma reesei Cel7B Active Site. <b>2015</b> , 55, 1369-76   | 4   |
| 1284 | Electrochemical Model for Ionic Liquid Electrolytes in Lithium Batteries. <b>2015</b> , 176, 301-310   | 16  |
| 1283 | Molecular mechanisms for the adhesion of chitin and chitosan to montmorillonite clay. <b>2015</b> , 5, 54580-54588   | 14  |
| 1282 | Retardation of Water Reorientation at the Oil/Water Interface. 2015, 119, 16639-16648  | 13  |
| 1281 | Direct Coexistence Methods to Determine the Solubility of Salts in Water from Numerical Simulations. Test Case NaCl. <b>2015</b> , 119, 8389-96  | 32  |
| 1280 | A network of molecular switches controls the activation of the two-component response regulator NtrC. <b>2015</b> , 6, 7283  | 38  |
| 1279 | Model-free estimation of the effective correlation time for C-H bond reorientation in amphiphilic bilayers: (1)H-(13)C solid-state NMR and MD simulations. <b>2015</b> , 142, 044905     | 20  |
| 1278 | Systematic characterization of protein folding pathways using diffusion maps: application to Trp-cage miniprotein. <b>2015</b> , 142, 085101   | 40  |

| 1277 | Prediction of diffusion coefficients of chlorophenols in water by computer simulation. <b>2015</b> , 396, 9-19  | 15 |
|------|---|----|
| 1276 | Solution Properties of Hemicellulose Polysaccharides with Four Common Carbohydrate Force Fields. <b>2015</b> , 11, 1765-74  | 33 |
| 1275 | The structural impact of DNA mismatches. <b>2015</b> , 43, 4309-21  | 80 |
| 1274 | Structural importance of the C-terminal region in pig aldo-keto reductase family 1 member C1 and their effects on enzymatic activity. <b>2015</b> , 15, 1                   | 7  |
| 1273 | Molecular dynamics of the asymmetric dimers of EGFR: simulations on the active and inactive conformations of the kinase domain. <b>2015</b> , 58, 16-29                     | 9  |
| 1272 | Sodium ion binding pocket mutations and adenosine A2A receptor function. <b>2015</b> , 87, 305-13   | 60 |
| 1271 | Ceramide increases free volume voids in DPPC membranes. <b>2015</b> , 5, 44282-44290  | 10 |
| 1270 | Nano-Scale Corrugations in Graphene: A Density Functional Theory Study of Structure, Electronic Properties and Hydrogenation. <b>2015</b> , 119, 7900-7910                  | 28 |
| 1269 | On the urea induced hydrophobic collapse of a water soluble polymer. <b>2015</b> , 17, 8491-8   | 54 |
| 1268 | Exploring volume, compressibility and hydration changes of folded proteins upon compression. <b>2015</b> , 17, 8499-508   | 23 |
| 1267 | Linear basis function approach to efficient alchemical free energy calculations. 2. Inserting and deleting particles with coulombic interactions. <b>2015</b> , 11, 2536-49 | 39 |
| 1266 | Accurate calculation of conformational free energy differences in explicit water: the confinement-solvation free energy approach. <b>2015</b> , 119, 5194-207               | 19 |
| 1265 | Proton dissociation and transfer in hydrated phosphoric acid clusters. <b>2015</b> , 115, 486-501   | 5  |
| 1264 | In silico identification of novel kinase inhibitors by targeting B-Raf(v660e) from natural products database. <b>2015</b> , 21, 102   | 3  |
| 1263 | The Bacterial Hydrophobin BslA is a Switchable Ellipsoidal Janus Nanocolloid. <b>2015</b> , 31, 11558-63  | 22 |
| 1262 | Effects of lysine residues on structural characteristics and stability of tau proteins. <b>2015</b> , 466, 486-92   | 12 |
| 1261 | On the Nature of an Extended Stokes Shift in the mPlum Fluorescent Protein. <b>2015</b> , 119, 13052-62   | 24 |
| 1260 | Thermo-responsive behavior of borinic acid polymers: experimental and molecular dynamics studies. <b>2015</b> , 11, 7159-64   | 15 |

| 1259 | Simulation assisted characterization of kaolinitemethanol intercalation complexes synthesized using cost-efficient homogenization method. <b>2015</b> , 357, 626-634   | 22 |
|------|--|----|
| 1258 | A Comparison of Barostats for the Mechanical Characterization of Metal-Organic Frameworks. <b>2015</b> , 11, 5583-97   | 58 |
| 1257 | Arbitrary order permanent Cartesian multipolar electrostatic interactions. <b>2015</b> , 142, 034117   | 17 |
| 1256 | Exploring LacI-DNA dynamics by multiscale simulations using the SIRAH force field. <b>2015</b> , 11, 5012-23   | 18 |
| 1255 | Influence of the size and charge of gold nanoclusters on complexation with siRNA: a molecular dynamics simulation study. <b>2015</b> , 17, 30307-17  | 12 |
| 1254 | The impact of interchain hydrogen bonding on thairpin stability is readily predicted by molecular dynamics simulation. <b>2015</b> , 104, 703-6  | 2  |
| 1253 | Direct Correlation of Cell Toxicity to Conformational Ensembles of Genetic A₩ariants. <b>2015</b> , 6, 1990-6  | 15 |
| 1252 | The molecular mechanism of Zinc acquisition by the neisserial outer-membrane transporter ZnuD. <b>2015</b> , 6, 7996   | 44 |
| 1251 | Thermodynamics of Micelle Formation and Membrane Fusion Modulate Antimicrobial Lipopeptide Activity. <b>2015</b> , 109, 750-9  | 25 |
| 1250 | An Analysis of Biomolecular Force Fields for Simulations of Polyglutamine in Solution. <b>2015</b> , 109, 1009-18  | 35 |
| 1249 | Folding and binding energy of a calmodulin-binding cell antiproliferative peptide. <b>2015</b> , 61, 281-9   |    |
| 1248 | The effect of amino substituents on the interactions of quinazolone derivatives with c-KIT G-quadruplex: insight from molecular dynamics simulation study for rational design of ligands. <b>2015</b> , 5, 76642-76650 | 4  |
| 1247 | Exploring the structure and conformational landscape of human leptin. A molecular dynamics approach. <b>2015</b> , 385, 90-101   | 3  |
| 1246 | Calculating the Fugacity of Pure, Low Volatile Liquids via Molecular Simulation with Application to Acetanilide, Acetaminophen, and Phenacetin. <b>2015</b> , 54, 9027-9037  | 20 |
| 1245 | Melting Behavior of a Model Molecular Crystalline GeI4. <b>2015</b> , 84, 064601   | 8  |
| 1244 | Mutational analysis of the Notch2 negative regulatory region identifies key structural elements for mechanical stability. <b>2015</b> , 5, 625-33  | 2  |
| 1243 | Thin Water Films at Multifaceted Hematite Particle Surfaces. <b>2015</b> , 31, 13127-37  | 21 |
| 1242 | Anti-solvent crystallization of a ternary Lennardlones mixture performed by molecular dynamics. <b>2015</b> , 209, 1-5   | 3  |

| 1241 | Effects of thermodynamic inhibitors on the dissociation of methane hydrate: a molecular dynamics study. <b>2015</b> , 17, 32347-57  | 40 |
|------|---|----|
| 1240 | A Stochastic Algorithm for the Isobaric-Isothermal Ensemble with Ewald Summations for All Long<br>Range Forces. <b>2015</b> , 11, 5624-37   | 48 |
| 1239 | Amino acid modified xanthone derivatives: novel, highly promising membrane-active antimicrobials for multidrug-resistant Gram-positive bacterial infections. <b>2015</b> , 58, 739-52 | 84 |
| 1238 | Enhancement of Internal Motions of Lysozyme through Interaction with Gold Nanoclusters and its Optical Imaging. <b>2015</b> , 119, 653-664  | 15 |
| 1237 | Structural properties of Y2O3Al2O3 liquids and glasses: An overview. <b>2015</b> , 407, 228-234   | 7  |
| 1236 | Thermodynamics of the self-assembly of non-ionic chromonic molecules using atomistic simulations. The case of TP6EO2M in aqueous solution. <b>2015</b> , 11, 680-91                   | 24 |
| 1235 | Molecular dynamics simulations of negatively charged DPPC/DPPI lipid bilayers at two levels of resolution. <b>2015</b> , 1058, 61-66  | 12 |
| 1234 | Experimental determination and computational interpretation of biophysical properties of lipid bilayers enriched by cholesteryl hemisuccinate. <b>2015</b> , 1848, 422-32             | 38 |
| 1233 | The effect of structural parameters and positive charge distance on the interaction free energy of antimicrobial peptides with membrane surface. <b>2015</b> , 33, 502-12             | 1  |
| 1232 | MOLECULAR DYNAMIC SIMULATION OF V176G MUTATION ASSOCIATED WITH GERSTMANNETRESSLERECHEINKER AT ELEVATED TEMPERATURE. <b>2016</b> , 78,   |    |
| 1231 | Molecular Dynamics Simulation Study of the Selectivity of a Silica Polymer for Ibuprofen. <b>2016</b> , 17,   | 5  |
| 1230 | A Theoretical Study of the Hydration of Methane, from the Aqueous Solution to the sI<br>Hydrate-Liquid Water-Gas Coexistence. <b>2016</b> , 17,                                       | 8  |
| 1229 | The Role of Cholesterol in Driving IAPP-Membrane Interactions. <b>2016</b> , 111, 140-51  | 58 |
| 1228 | Engineered human angiogenin mutations in the placental ribonuclease inhibitor complex for anticancer therapy: Insights from enhanced sampling simulations. <b>2016</b> , 25, 1451-60  | 10 |
| 1227 | Configuration, Anion-Specific Effects, Diffusion, and Impact on Counterions for Adsorption of Salt Anions at the Interfaces of Clay Minerals. <b>2016</b> , 120, 14621-14630          | 20 |
| 1226 | Quantitative assessment of kinase selectivity based the water-ring network in protein binding sites using molecular dynamics simulations. <b>2016</b> , 221, 316-322                  | 6  |
| 1225 | Molecular Dynamics Simulation Study of Parallel Telomeric DNA Quadruplexes at Different Ionic Strengths: Evaluation of Water and Ion Models. <b>2016</b> , 120, 7380-91               | 26 |
| 1224 | Simulation of coupled folding and binding of an intrinsically disordered protein in explicit solvent with metadynamics. <b>2016</b> , 68, 114-127                                     | 15 |

| 1223 | Thermostability Mechanism for the Hyperthermophilicity of Extremophile Cellulase TmCel12A: Implied from Molecular Dynamics Simulation. <b>2016</b> , 120, 7346-52                                      | 2  |
|------|--|----|
| 1222 | Improved model of hydrated calcium ion for molecular dynamics simulations using classical biomolecular force fields. <b>2016</b> , 105, 752-63   | 31 |
| 1221 | Unravelling the Structural Changes in ⊞-Helical Peptides on Interaction with Convex, Concave, and Planar Surfaces of Boron-Nitride-Based Nanomaterials. <b>2016</b> , 120, 28246-28260                 | 13 |
| 1220 | Light-induced structural changes in a monomeric bacteriophytochrome. <b>2016</b> , 3, 054701   | 25 |
| 1219 | A map of binding cavity conformations reveals differences in binding specificity. 2016,  |    |
| 1218 | The allosteric switching mechanism in bacteriophage MS2. <b>2016</b> , 145, 035101   | 6  |
| 1217 | Temperature of maximum density and excess thermodynamics of aqueous mixtures of methanol. <b>2016</b> , 144, 184505  | 13 |
| 1216 | Striped gold nanoparticles: New insights from molecular dynamics simulations. <b>2016</b> , 144, 244710  | 10 |
| 1215 | Unveiling the Pathogenic Molecular Mechanisms of the Most Common Variant (p.K329E) in Medium-Chain Acyl-CoA Dehydrogenase Deficiency by in Vitro and in Silico Approaches. <b>2016</b> , 55, 7086-7098 | 3  |
| 1214 | Distinct Roles of Histone H3 and H2A Tails in Nucleosome Stability. <b>2016</b> , 6, 31437   | 47 |
| 1213 | Molecular dynamics at constant Cauchy stress. <b>2016</b> , 144, 184107  | 12 |
| 1212 | Collapse-Swelling Transitions of a Thermoresponsive, Single Poly(N-isopropylacrylamide) Chain in Water. <b>2016</b> , 120, 13184-13192   | 41 |
| 1211 | Anisotropy of self-diffusion in forsterite grain boundaries derived from molecular dynamics simulations. <b>2016</b> , 171, 1  | 4  |
| 1210 | Membrane Anchoring and Ion-Entry Dynamics in P-type ATPase Copper Transport. <b>2016</b> , 111, 2417-2429  | 13 |
| 1209 | Characterization of the Annonaceous acetogenin, annonacinone, a natural product inhibitor of plasminogen activator inhibitor-1. <b>2016</b> , 6, 36462   | 8  |
| 1208 | Genetic Algorithm Managed Peptide Mutant Screening: Optimizing Peptide Ligands for Targeted Receptor Binding. <b>2016</b> , 56, 2378-2387  | 8  |
| 1207 | Rapid Equilibration by algorithmic quenching the ringing mode in molecular dynamics. <b>2016</b> , 1, 2857-2865  | 1  |
| 1206 | A canonical replica exchange molecular dynamics implementation with normal pressure in each replica. <b>2016</b> , 145, 044903   | 4  |

| 1205         | A new intermolecular potential for simulations of methanol: The OPLS/2016 model. <b>2016</b> , 145, 034508   |     | 22 |
|--------------|--|-----|----|
| 1204         | Atomistic Modeling of Thermal Conductivity of Epoxy Nanotube Composites. <b>2016</b> , 68, 1396-1410   |     | 12 |
| 1203         | Influence of Tacticity on Hydrophobicity of Poly(N-isopropylacrylamide): A Single Chain Molecular Dynamics Simulation Study. <b>2016</b> , 120, 3765-76  |     | 40 |
| 1202         | The inhibitory mechanism of a fullerene derivative against amyloid-peptide aggregation: an atomistic simulation study. <b>2016</b> , 18, 12582-91  |     | 53 |
| 1201         | Simulation of Temperature-Dependent Charge Transport in Organic Semiconductors with Various Degrees of Disorder. <b>2016</b> , 12, 3087-96   |     | 25 |
| 1200         | Relative Orientation of POTRA Domains from Cyanobacterial Omp85 Studied by Pulsed EPR Spectroscopy. <b>2016</b> , 110, 2195-206  |     | 15 |
| 1199         | Multilevel non-volatile data storage utilizing common current hysteresis of networked single walled carbon nanotubes. <b>2016</b> , 8, 10273-81  |     | 10 |
| 1198         | Correlation between Surface Tension and the Bulk Dynamics in Salty Atmospheric Aquatic Droplets. <b>2016</b> , 120, 11508-11518  |     | 4  |
| 1197         | Phi29 Connector-DNA Interactions Govern DNA Crunching and Rotation, Supporting the Check-Valve Model. <b>2016</b> , 110, 455-469   |     | 8  |
| 1196         | Structure and thermodynamics of nondipolar molecular liquids and solutions from integral equation theory. <i>Molecular Physics</i> , <b>2016</b> , 114, 2461-2476  | 1.7 | 5  |
| 1195         | Determining the Lipid Tilt Modulus by Simulating Membrane Buckles. <b>2016</b> , 120, 6061-73  |     | 25 |
| 1194         | Interaction of the N-AcA∯13☑3)NH2 segment of the beta amyloid peptide with beta-sheet-blocking peptides: site and edge specificity. <b>2016</b> , 94, 583-592  |     | 5  |
| 1193         | Predicting Octanol/Water Partition Coefficients of Alcohol Ethoxylate Surfactants Using a Combination of Molecular Dynamics and the Conductor-like Screening Model for Realistic Solvents. <b>2016</b> , 55, 4782-4789 |     | 8  |
| 1192         | Long-timescale dynamics of the Drew-Dickerson dodecamer. <b>2016</b> , 44, 4052-66   |     | 68 |
|              | Long-timescate dynamics of the Diew-Dickerson dodecamer. 2016, 44, 4032-00   |     |    |
| 1191         | Insights on the mechanical behavior of keratin fibrils. <b>2016</b> , 89, 477-83   |     | 9  |
| 1191<br>1190 |  |     |    |
|              | Insights on the mechanical behavior of keratin fibrils. <b>2016</b> , 89, 477-83  Developing a Predictive Form of MOSCED for Nonelectrolyte Solids Using Molecular Simulation:   |     | 9  |

| 1187 | Formation of Clathrate Hydrates of Water-Soluble Guest Molecules. 2016, 120, 21512-21521  | 25 |
|------|---|----|
| 1186 | Characterization of kaolinite-cetyltrimethylammonium chloride intercalation complex synthesized through eco-friend kaolinite-urea pre-intercalation complex. <b>2016</b> , 508, 265-273                         | 15 |
| 1185 | The effect of urea and taurine osmolytes on hydrophobic association and solvation of methane and neopentane molecules. <b>2016</b> , 223, 660-671   | 1  |
| 1184 | Near-atomic cryo-EM structure of PRC1 bound to the microtubule. <b>2016</b> , 113, 9430-9   | 50 |
| 1183 | Molecular Dynamics Simulations of Amyloid 即eptide (1-42): Tetramer Formation and Membrane Interactions. <b>2016</b> , 111, 937-49   | 59 |
| 1182 | Modular peptides from the thermoplastic squid sucker ring teeth form amyloid-like cross-∄ supramolecular networks. <b>2016</b> , 46, 41-54  | 19 |
| 1181 | Molecular dynamics simulations of Ca2+Clilon pair in polar mixtures of acetone and water: Solvation and dynamical studies. <b>2016</b> , 662, 306-316   | 4  |
| 1180 | Structural and dynamical aspects of uranyl ions in supercritical water: A molecular dynamics simulation study. <b>2016</b> , 224, 599-606   | 6  |
| 1179 | L30A Mutation of Phospholemman Mimics Effects of Cardiac Glycosides in Isolated Cardiomyocytes. <b>2016</b> , 55, 6196-6204   | 3  |
| 1178 | Molecular Dynamics Simulations Predict the Pathways via Which Pristine Fullerenes Penetrate Bacterial Membranes. <b>2016</b> , 120, 11170-11179   | 40 |
| 1177 | Binary Lennard-Jones mixtures with highly asymmetric interactions of the components. 1. Effect of the energy parameters on phase equilibria and properties of liquid-gas interfaces. <b>2016</b> , 429, 242-253 | 15 |
| 1176 | In silico structural characterization of protein targets for drug development against Trypanosoma cruzi. <b>2016</b> , 22, 244  | 6  |
| 1175 | Effects of interface mutations on the dimerization of alanine glyoxylate aminotransferase and implications in the mistargeting of the pathogenic variants F152I and I244T. <b>2016</b> , 131, 137-148           | 11 |
| 1174 | Tuning self-assembled morphology of the Alf16-22) peptide by substitution of phenylalanine residues. <b>2016</b> , 147, 116-123   | 10 |
| 1173 | Comparison of Different TMAO Force Fields and Their Impact on the Folding Equilibrium of a Hydrophobic Polymer. <b>2016</b> , 120, 8757-67  | 28 |
| 1172 | Reverse Stability of Oxyluciferin Isomers in Aqueous Solutions. <b>2016</b> , 120, 8776-83  | 5  |
| 1171 | Destabilization of the metal site as a hub for the pathogenic mechanism of five ALS-linked mutants of copper, zinc superoxide dismutase. <b>2016</b> , 8, 1141-1150   | 4  |
| 1170 | Predicting the Chemical Potential and Osmotic Pressure of Polysaccharide Solutions by Molecular Simulations. <b>2016</b> , 12, 4375-84  | 33 |

| 1169 | Molecular dynamics studies of a вheet blocking peptide with the full-length amyloid beta peptide of Alzheimer目disease. <b>2016</b> , 94, 833-841   | 4  |
|------|--|----|
| 1168 | Evaluation of Methods for the Calculation of the pKa of Cysteine Residues in Proteins. <b>2016</b> , 12, 4662-73   | 63 |
| 1167 | Lowered pH Leads to Fusion Peptide Release and a Highly Dynamic Intermediate of Influenza Hemagglutinin. <b>2016</b> , 120, 9654-60  | 13 |
| 1166 | Efficient molecular packing of glycerol monostearate in Langmuir monolayers at the air-water interface. <b>2016</b> , 508, 85-92   | 9  |
| 1165 | The Free Energy of Small Solute Permeation through the Escherichia coli Outer Membrane Has a Distinctly Asymmetric Profile. <b>2016</b> , 7, 3446-51   | 34 |
| 1164 | Binding Characteristics of Sphingosine-1-Phosphate to ApoM hints to Assisted Release Mechanism via the ApoM Calyx-Opening. <b>2016</b> , 6, 30655  | 17 |
| 1163 | Allosteric-Activation Mechanism of Bovine Chymosin Revealed by Bias-Exchange Metadynamics and Molecular Dynamics Simulations. <b>2016</b> , 120, 10453-10462                                   | 4  |
| 1162 | Interaction between arginine conformers and Hofmeister halide anions. <b>2016</b> , 1095, 93-103   |    |
| 1161 | Theoretical study of the interactions between the first transmembrane segment of NS2 protein and a POPC lipid bilayer. <b>2016</b> , 217, 1-7  | 5  |
| 1160 | Computational investigation of cold denaturation in the Trp-cage miniprotein. <b>2016</b> , 113, 8991-6  | 39 |
| 1159 | Multiscale simulations on conformational dynamics and membrane interactions of the non-structural 2 (NS2) transmembrane domain. <b>2016</b> , 478, 193-198                                     | 4  |
| 1158 | Comparison of systematic coarse-graining strategies for soluble conjugated polymers. <b>2016</b> , 225, 1441-1461  | 13 |
| 1157 | Exploring the Structural Properties of Positively Charged Peptide Dendrimers. <b>2016</b> , 120, 11323-11330   | 15 |
| 1156 | Direct evidence for sequence-dependent attraction between double-stranded DNA controlled by methylation. <b>2016</b> , 7, 11045  | 51 |
| 1155 | Conformational Ensemble of hIAPP Dimer: Insight into the Molecular Mechanism by which a Green Tea Extract inhibits hIAPP Aggregation. <b>2016</b> , 6, 33076                                   | 62 |
| 1154 | Dynamics of proton transfer in imidazole hydrogen-bond chains. <b>2016</b> , 6, 99391-99403  | 4  |
| 1153 | Full-Length OmpA: Structure, Function, and Membrane Interactions Predicted by Molecular Dynamics Simulations. <b>2016</b> , 111, 1692-1702   | 40 |
| 1152 | Molecular Mechanism behind Solvent Concentration-Dependent Optimal Activity of Thermomyces lanuginosus Lipase in a Biocompatible Ionic Liquid: Interfacial Activation through Arginine Switch. | 11 |

| 1151 | Characterization of Mg Distributions around RNA in Solution. <b>2016</b> , 1, 680-688  | 24 |
|------|--|----|
| 1150 | Nonclassical Crystal Growth as Explanation for the Riddle of Polarity in Centrosymmetric Glycine Crystals. <b>2016</b> , 138, 14756-14763                      | 12 |
| 1149 | Optimized atomistic force fields for aqueous solutions of Magnesium and Calcium Chloride: Analysis, achievements and limitations. <b>2016</b> , 225, 1391-1409 | 7  |
| 1148 | Comparison of iterative inverse coarse-graining methods. <b>2016</b> , 225, 1323-1345  | 22 |
| 1147 | Molecular Dynamics Study of Mg/Li Separation via Biomimetic Graphene-Based Nanopores: The Role of Dehydration in Second Shell. <b>2016</b> , 32, 13778-13786   | 39 |
| 1146 | Adaptive molecular resolution approach in Hamiltonian form: An asymptotic analysis. <b>2016</b> , 94, 043321   | 7  |
| 1145 | The singular behavior of a 毗ype semi-synthetic two branched polypeptide: three-dimensional structure and mode of action. <b>2016</b> , 18, 30998-31011         | 12 |
| 1144 | The line tension of two-dimensional ionic fluids. <b>2016</b> , 144, 134705  | 3  |
| 1143 | Structural basis for the membrane association of ankyrinG via palmitoylation. <b>2016</b> , 6, 23981   | 12 |
| 1142 | Computational investigation of dynamical transitions in Trp-cage miniprotein powders. <b>2016</b> , 6, 25612   | 12 |
| 1141 | Cellulose chain binding free energy drives the processive move of cellulases on the cellulose surface. <b>2016</b> , 113, 1873-80                              | 6  |
| 1140 | Salting-out of methane in the aqueous solutions of urea and sarcosine. <b>2016</b> , 128, 599-612  | 2  |
| 1139 | Effect of monoglycerides and fatty acids on a ceramide bilayer. <b>2016</b> , 18, 17446-60   | 22 |
| 1138 | The first crystal structure of human RNase 6 reveals a novel substrate-binding and cleavage site arrangement. <b>2016</b> , 473, 1523-36                       | 14 |
| 1137 | Parametrization of halogen bonds in the CHARMM general force field: Improved treatment of ligand-protein interactions. <b>2016</b> , 24, 4812-4825             | 95 |
| 1136 | Role of Preferential Ions of Ammonium Ionic Liquid in Destabilization of Collagen. <b>2016</b> , 120, 6515-24  | 18 |
| 1135 | Behavior of P85 and P188 Poloxamer Molecules: Computer Simulations Using United-Atom Force-Field. <b>2016</b> , 120, 8631-41                                   | 14 |
| 1134 | Interfacial water thickness at inorganic nanoconstructs and biomolecules: Size matters. <b>2016</b> , 380, 1735-1740   | 20 |

| 1133 | Comparative Molecular Dynamics Study on Tri-n-butyl Phosphate in Organic and Aqueous Environments and Its Relevance to Nuclear Extraction Processes. <b>2016</b> , 120, 5183-93   | 27   |
|------|---|------|
| 1132 | Jumping Diffusion of Water Intercalated in Layered Double Hydroxides. <b>2016</b> , 120, 12924-12931  | 14   |
| 1131 | High-Performance Modeling of Carbon Dioxide Sequestration by Coupling Reservoir Simulation and Molecular Dynamics. <b>2016</b> , 21, 0853-0863  | 5    |
| 1130 | A highly efficient hybrid method for calculating the hydration free energy of a protein. <b>2016</b> , 37, 712-23   | 6    |
| 1129 | Molecular simulations of the effects of phospholipid and cholesterol peroxidation on lipid membrane properties. <b>2016</b> , 1858, 2191-2198   | 27   |
| 1128 | Structures of a bi-functional Kunitz-type STI family inhibitor of serine and aspartic proteases: Could the aspartic protease inhibition have evolved from a canonical serine protease-binding loop?. <b>2016</b> , 195, 259-271 | 4    |
| 1127 | Understanding the dynamics of monomeric, dimeric, and tetrameric ∃-synuclein structures in water. <b>2016</b> , 6, 666-86   | 10   |
| 1126 | Effect of Polarization on the Mobility of C60: A Kinetic Monte Carlo Study. <b>2016</b> , 12, 812-24  | 22   |
| 1125 | Thermal conductivity via atomistic modeling for epoxy-SWNT composites. <b>2016</b> ,  |      |
| 1124 | Properties of Poloxamer Molecules and Poloxamer Micelles Dissolved in Water and Next to Lipid Bilayers: Results from Computer Simulations. <b>2016</b> , 120, 5823-30   | 38   |
| 1123 | Predictive Sampling of Rare Conformational Events in Aqueous Solution: Designing a Generalized Orthogonal Space Tempering Method. <b>2016</b> , 12, 41-52   | 9    |
| 1122 | Insight into the adsorption profiles of the Saprolegnia monoica chitin synthase MIT domain on POPA and POPC membranes by molecular dynamics simulation studies. <b>2016</b> , 18, 5281-90                                       | 9    |
| 1121 | CHARMM-GUI Input Generator for NAMD, GROMACS, AMBER, OpenMM, and CHARMM/OpenMM Simulations Using the CHARMM36 Additive Force Field. <b>2016</b> , 12, 405-13  | 1303 |
| 1120 | Simulations of flow induced structural transition of the  | 14   |
| 1119 | Different nanostructures caused by competition of intra- and inter-郡heet interactions in hierarchical self-assembly of short peptides. <b>2016</b> , 464, 219-28  | 30   |
| 1118 | Improved Parameterization of Amine-Carboxylate and Amine-Phosphate Interactions for Molecular Dynamics Simulations Using the CHARMM and AMBER Force Fields. <b>2016</b> , 12, 430-43  | 87   |
| 1117 | Phosphonium based ionic liquids-stabilizing or destabilizing agents for collagen?. <b>2016</b> , 6, 4022-4033   | 17   |
| 1116 | Molecular dynamics simulations of K+Illion pair in polar mixtures of acetone and water: Preferential solvation and structural studies. <b>2016</b> , 213, 276-288   | 2    |

| 1115 | Two-dimensional interlocked pentagonal bilayer ice: how do water molecules form a hydrogen bonding network?. <b>2016</b> , 18, 14216-21   | 19 |
|------|---|----|
| 1114 | A Systematic Coarse-Grained Model for Methylcellulose Polymers: Spontaneous Ring Formation at Elevated Temperature. <b>2016</b> , 49, 1490-1503                                       | 43 |
| 1113 | The mechanism of excited state proton dissociation in microhydrated hydroxylamine clusters. <b>2016</b> , 18, 5564-79   | 1  |
| 1112 | A molecular understanding of the phase-behavior of thiophene in the ionic liquid [C4mim]+[BF4] for extraction from petroleum streams. <b>2016</b> , 175, 225-231                      | 14 |
| 1111 | Rapid Computation of Thermodynamic Properties over Multidimensional Nonbonded Parameter Spaces Using Adaptive Multistate Reweighting. <b>2016</b> , 12, 1806-23                       | 10 |
| 1110 | Proposed Mode of Binding and Action of Positive Allosteric Modulators at Opioid Receptors. <b>2016</b> , 11, 1220-9   | 43 |
| 1109 | Atomistic Simulation of Oligoelectrolyte Multilayers Growth. <b>2016</b> , 215-228  | 1  |
| 1108 | The dynamic mechanism of presenilin-1 function: Sensitive gate dynamics and loop unplugging control protein access. <b>2016</b> , 89, 147-56  | 38 |
| 1107 | Synthesis, biological evaluation and molecular modeling of pseudo-peptides based statine as inhibitors for human tissue kallikrein 5. <b>2016</b> , 112, 39-47                        | 9  |
| 1106 | Mechanism of Slow Crystal Growth of Tetrahydrofuran Clathrate Hydrate. <b>2016</b> , 120, 3305-3313   | 25 |
| 1105 | Understanding the Solubility of Acetaminophen in 1-n-Alkyl-3-methylimidazolium-Based Ionic Liquids Using Molecular Simulation. <b>2016</b> , 120, 3360-9                              | 12 |
| 1104 | Cinnamic acid amides from Tribulus terrestris displaying uncompetitive ⊞-glucosidase inhibition. <b>2016</b> , 114, 201-8   | 42 |
| 1103 | Dynamics and mechanisms of interactions between ring-shaped heterohexameric TIP49a/b protein complexes and double-stranded DNA. <b>2016</b> , 10, 47-54                               |    |
| 1102 | Effects of Operating Temperature on the Electrical Performance of a Li-air Battery operated with Ionic Liquid Electrolyte. <b>2016</b> , 194, 317-329                                 | 22 |
| 1101 | Mechanical Properties of Tetrapolyethylene and Tetrapoly(ethylene oxide) Diamond Networks via Molecular Dynamics Simulations. <b>2016</b> , 49, 2375-2386                             | 16 |
| 1100 | Reduction in interfacial tension of waterBil interface by supercritical CO2 in enhanced oil recovery processes studied with molecular dynamics simulation. <b>2016</b> , 111, 171-178 | 51 |
| 1099 | Computational 'microscopy' of cellular membranes. <b>2016</b> , 129, 257-68   | 96 |
| 1098 | Exploration of Interfacial Hydration Networks of Target-Ligand Complexes. <b>2016</b> , 56, 148-58  | 17 |

| 1097 | Computer modelling of the surface tension of the gas-liquid and liquid-liquid interface. <b>2016</b> , 45, 1387-409   | 121 |
|------|---|-----|
|      | Molecular assembly of lethal factor enzyme and pre-pore heptameric protective antigen in early stage of translocation. <b>2016</b> , 22, 7  | 4   |
|      | Influence of aqueous ionic strength upon liquid:liquid interfacial structure and microsolvation. <b>2016</b> , 407, 126-134   | 10  |
|      | Molecular Dynamics Simulations of Sulfobetaine-Type Zwitterionic Surfactant at the Decane/Water Interface. <b>2016</b> , 37, 1480-1485  | 9   |
|      | Fluorinated surfactants in solution: Diffusion coefficients of fluorinated alcohols in water. <b>2016</b> , 407, 322-333  | 6   |
| 1092 | Molecular Dynamics Study of N-Dodecyl-N,N-Dimethyl-3-Ammonio-1-Propanesulfonate Mono-Layer Adsorbed at the Air/Water Interface. <b>2016</b> , 37, 1067-1075                           | 7   |
| 1091 | Accurate Estimation of the Entropy of Rotation-Translation Probability Distributions. <b>2016</b> , 12, 1-8   | 14  |
|      | Molecular dynamics simulations of the free and inhibitor-bound cruzain systems in aqueous solvent: insights on the inhibition mechanism in acidic pH. <b>2016</b> , 34, 1969-78       | 10  |
|      | Stability of the kaolinite-guest molecule intercalation system: A molecular simulation study. <b>2016</b> , 409, 434-438  | 4   |
| 1088 | Hydrogen bonds in Zif268 proteins - a theoretical perspective. <b>2016</b> , 34, 1607-24  | 1   |
|      | Measurement artifacts identified in the UV-vis spectroscopic study of adduct formation within the context of molecular imprinting of naproxen. <b>2016</b> , 153, 661-8               | 9   |
| 1086 | Hydrogen bonding in ethanolwater and trifluoroethanolwater mixtures studied by NMR and molecular dynamics simulation. <b>2016</b> , 217, 3-11   | 32  |
|      | Molecular dynamics simulations for the prediction of the dielectric spectra of alcohols, glycols and monoethanolamine. <b>2016</b> , 42, 370-390                                      | 27  |
| 1084 | Change in specific interactions between lactose repressor protein and DNA induced by ligand binding: molecular dynamics and molecular orbital calculations. <b>2016</b> , 42, 242-256 | 5   |
|      | Molecular dynamics simulations of cellulase homologs in aqueous 1-ethyl-3-methylimidazolium chloride. <b>2017</b> , 35, 1990-2002   | 9   |
|      | Investigations of Takeout proteins' ligand binding and release mechanism using molecular dynamics simulation. <b>2017</b> , 35, 1464-1473   | 3   |
|      | Effects of Lithium and Other Monovalent Ions on Palmitoyl Oleoyl Phosphatidylcholine Bilayer. <b>2017</b> , 33, 1105-1115   | 11  |
| 1080 | Local Mode Analysis: Decoding IR Spectra by Visualizing Molecular Details. <b>2017</b> , 121, 3483-3492   | 6   |

| 1079 | The role of dimer asymmetry and protomer dynamics in enzyme catalysis. <b>2017</b> , 355,   | 113 |
|------|---|-----|
| 1078 | Interfacial Structure Analysis for the Morphology Prediction of Adipic Acid Crystals from Aqueous Solution. <b>2017</b> , 17, 1088-1095   | 5   |
| 1077 | TMAO and urea in the hydration shell of the protein SNase. <b>2017</b> , 19, 6345-6357  | 38  |
| 1076 | Microscopic Structure and Solubility Predictions of Multifunctional Solids in Supercritical Carbon Dioxide: A Molecular Simulation Study. <b>2017</b> , 121, 1660-1674                            | 14  |
| 1075 | Sampling conformational space of intrinsically disordered proteins in explicit solvent: Comparison between well-tempered ensemble approach and solute tempering method. <b>2017</b> , 72, 136-147 | 7   |
| 1074 | Dynamic disorder can explain non-exponential kinetics of fast protein mechanical unfolding. <b>2017</b> , 197, 43-49  | 9   |
| 1073 | Computational Modeling of Hydroxypropyl-Methylcellulose Acetate Succinate (HPMCAS) and Phenytoin Interactions: A Systematic Coarse-Graining Approach. <b>2017</b> , 14, 733-745                   | 17  |
| 1072 | Interaction of aurein 1.2 and its analogue with DPPC lipid bilayer. <b>2017</b> , 43, 127-137   | 7   |
| 1071 | The effect of alkyl chain length on material properties of fatty-acid-functionalized amidoamine-epoxy systems. <b>2017</b> , 89, 1-12   | 12  |
| 1070 | Alpha-tocopherol inhibits pore formation in oxidized bilayers. <b>2017</b> , 19, 5699-5704  | 22  |
| 1069 | Potential of Mean Force Calculations of Solute Permeation Across UT-B and AQP1: A Comparison between Molecular Dynamics and 3D-RISM. <b>2017</b> , 121, 1506-1519                                 | 6   |
| 1068 | Electrical Energy Storage by a Magnesium-Copper-Sulfide Rechargeable Battery. <b>2017</b> , 164, A770-A774  | 7   |
| 1067 | Structural properties of amyloid ∰1-40) dimer explored by replica exchange molecular dynamics simulations. <b>2017</b> , 85, 1024-1045  | 14  |
| 1066 | Nucleotide Selectivity at a Preinsertion Checkpoint of T7 RNA Polymerase Transcription Elongation. <b>2017</b> , 121, 3777-3786   | 9   |
| 1065 | Microscopic Origin of Hysteresis in Water Sorption on Protein Matrices. <b>2017</b> , 8, 1185-1190  | 3   |
| 1064 | A refined polarizable water model for the coarse-grained MARTINI force field with long-range electrostatic interactions. <b>2017</b> , 146, 054501  | 47  |
| 1063 | Heterogeneous dielectric generalized Born model with a van der Waals term provides improved association energetics of membrane-embedded transmembrane helices. <b>2017</b> , 38, 1308-1320        | 8   |
| 1062 | Coarse-Grained Simulation of Rodlike Higher-Order Quadruplex Structures at Different Salt Concentrations. <b>2017</b> , 2, 386-396  | 7   |

| 1061 | Efficient Conformational Search Based on Structural Dissimilarity Sampling: Applications for Reproducing Structural Transitions of Proteins. <b>2017</b> , 13, 1411-1423  | 19 |
|------|---|----|
| 1060 | ∃-Synuclein's Uniquely Long Amphipathic Helix Enhances its Membrane Binding and Remodeling Capacity. <b>2017</b> , 250, 183-193   | 16 |
| 1059 | Elucidation of Binding Mechanism of Photodynamic Therapeutic Agent Toluidine Blue O with Chicken Egg White Lysozyme by Spectroscopic and Molecular Dynamics Studies. <b>2017</b> , 93, 1043-1056  | 9  |
| 1058 | Protein Tunnels: The Case of Urease Accessory Proteins. <b>2017</b> , 13, 2322-2331   | 19 |
| 1057 | Solution behaviour of poly(N-isopropylacrylamide) stereoisomers in water: a molecular dynamics simulation study. <b>2017</b> , 19, 11892-11903  | 15 |
| 1056 | Differential binding and activity of the pore-forming toxin sticholysin II in model membranes containing diverse ceramide-derived lipids. <b>2017</b> , 138, 20-31  | 13 |
| 1055 | Dynamics of structural diffusion in phosphoric acid hydrogen-bond clusters. <b>2017</b> , 7, 21492-21506  | 5  |
| 1054 | Solvation Structure of 1,3-Butanediol in Aqueous Binary Solvents with Acetonitrile, 1,4-Dioxane, and Dimethyl Sulfoxide Studied by IR, NMR, and Molecular Dynamics Simulation. <b>2017</b> , 121, 4864-4872                                       | 5  |
| 1053 | Identification of a conserved 8 aa insert in the PIP5K protein in the Saccharomycetaceae family of fungi and the molecular dynamics simulations and structural analysis to investigate its potential functional role. <b>2017</b> , 85, 1454-1467 | 13 |
| 1052 | Electric fields within clay materials: How to affect the adsorption of metal ions. <b>2017</b> , 501, 54-59   | 35 |
| 1051 | Discrimination of Native-like States of Membrane Proteins with Implicit Membrane-based Scoring Functions. <b>2017</b> , 13, 3049-3059   | 5  |
| 1050 | Cross-protection in Neisseria meningitidis serogroups Y and W polysaccharides: A comparative conformational analysis. <b>2017</b> , 446-447, 40-47  | 13 |
| 1049 | Residues of Alpha Helix H3 Determine Distinctive Features of Transforming Growth Factor <b>B</b> . <b>2017</b> , 121, 5483-5498   | 7  |
| 1048 | Revisiting Partition in Hydrated Bilayer Systems. <b>2017</b> , 13, 2290-2299   | 11 |
| 1047 | Combined effects of headgroup charge and tail unsaturation of lipids on lateral organization and diffusion of lipids in model biomembranes. <b>2017</b> , 26, 048701  | 1  |
| 1046 | Swelling and Tensile Properties of Tetra-Polyethylene glycol via Coarse-Grained Molecular Models. <b>2017</b> , 26, 1600098   | 3  |
| 1045 | Coupling of helix E-F motion with the O-nitrito and 2-nitrovinyl coordination in myoglobin. <b>2017</b> , 221, 10-16  | 3  |
| 1044 | Hydration and self-aggregation of a neutral cosolute from dielectric relaxation spectroscopy and MD simulations: the case of 1,3-dimethylurea. <b>2016</b> , 19, 219-230  | 16 |

| 1043 | Buckling Under Pressure: Curvature-Based Lipid Segregation and Stability Modulation in Cardiolipin-Containing Bilayers. <b>2017</b> , 33, 6937-6946  | 39   |
|------|--|------|
| 1042 | Structural Behavior of the Peptaibol Harzianin HK VI in a DMPC Bilayer: Insights from MD Simulations. <b>2017</b> , 112, 2602-2614   | 5    |
| 1041 | A Spring-Loaded Mechanism Governs the Clamp-like Dynamics of the Skp Chaperone. <b>2017</b> , 25, 1079-1088.e.   | 3 24 |
| 1040 | Monitoring the different micelle species and the slow kinetics of tetraethylammonium perfluorooctane-sulfonate by F NMR spectroscopy. <b>2017</b> , 246, 153-164   | 10   |
| 1039 | Gold-Induced Unfolding of Lysozyme: Toward the Formation of Luminescent Clusters. <b>2017</b> , 121, 13335-133   | 4413 |
| 1038 | Structural dissimilarity sampling with dynamically self-guiding selection. <b>2017</b> , 38, 1921-1929   | 10   |
| 1037 | Inhibition of Alamyloid Growth and Toxicity by Silybins: The Crucial Role of Stereochemistry. <b>2017</b> , 8, 1767-1778   | 56   |
| 1036 | Staphylococcus aureus £oxin in aqueous solution: Behavior in monomeric and multimeric states. <b>2017</b> , 227, 21-28   | 2    |
| 1035 | Study of the cold charge transfer state separation at the TQ1/PC BM interface. <b>2017</b> , 38, 1039-1048   | 2    |
| 1034 | Structural heterogeneity of the Eppioid receptor's conformational ensemble in the apo state. <b>2017</b> , 8, 45761  | 15   |
| 1033 | The molecular behavior of a single 軸myloid inside a dipalmitoylphosphatidylcholine bilayer at three different temperatures: An atomistic simulation study: A聞nteraction with DPPC: Atomistic simulation. <b>2017</b> , 85, 1298-1310 | 6    |
| 1032 | Structural insights into type I and type II of nsp4 porcine reproductive and respiratory syndrome virus (nsp4 PRRSV) by molecular dynamics simulations. <b>2017</b> , 74, 125-134  | 1    |
| 1031 | Structures of closed and open states of a voltage-gated sodium channel. <b>2017</b> , 114, E3051-E3060   | 93   |
| 1030 | Molecular dynamics simulation of effect of glycerol monostearate on amorphous polyethylene in the presence of water. <b>2017</b> , 23, 115   | 11   |
| 1029 | Modelling the Polymer Electrolyte/Li-Metal Interface by Molecular Dynamics simulations. <b>2017</b> , 234, 43-51   | 30   |
| 1028 | Identification of the Crucial Residues in the Early Insertion of Pardaxin into Different Phospholipid<br>Bilayers. <b>2017</b> , 57, 929-941   | 9    |
| 1027 | Cry1A(b)16 toxin from Bacillus thuringiensis: Theoretical refinement of three-dimensional structure and prediction of peptides as molecular markers for detection of genetically modified organisms. <b>2017</b> , 85, 1248-1257     | 2    |
| 1026 | Efficient solvation free energy simulations: impact of soft-core potential and a new adaptive  Bayacing method. <i>Molecular Physics</i> , <b>2017</b> , 115, 1322-1334  | 8    |

| 1025 | A simple guiding principle for the temperature dependence of the solubility of light gases in imidazolium-based ionic liquids derived from molecular simulations. <b>2017</b> , 19, 1770-1780   | 16  |
|------|---|-----|
| 1024 | Disrupting a key hydrophobic pair in the oligomerization interface of the actinoporins impairs their pore-forming activity. <b>2017</b> , 26, 550-565   | 21  |
| 1023 | In silico design and bioevaluation of selective benzotriazepine BRD4 inhibitors with potent antiosteoclastogenic activity. <b>2017</b> , 90, 97-111   | 8   |
| 1022 | Increase in the   heet Character of an Amyloidogenic Peptide upon Adsorption onto Gold and Silver Surfaces. 2017, 18, 526-536   | 9   |
| 1021 | Accurate Three States Model for Amino Acids with Two Chemically Coupled Titrating Sites in Explicit Solvent Atomistic Constant pH Simulations and pK(a) Calculations. <b>2017</b> , 13, 147-160 | 12  |
| 1020 | Influence of sequence and lipid type on membrane perturbation by human and rat amyloid peptide (1-42). <b>2017</b> , 614, 1-13  | 12  |
| 1019 | Computational study of the interplay between intermolecular interactions and CO orientations in type I hydrates. <b>2017</b> , 19, 3384-3393  | 13  |
| 1018 | Simulation of Asphaltene Aggregation through Molecular Dynamics: Insights and Limitations. <b>2017</b> , 31, 1108-1125  | 104 |
| 1017 | Disrupting domain-domain interactions is indispensable for EngA-ribosome interactions. <b>2017</b> , 1865, 289-303  | 5   |
| 1016 | Procedure for Transferable Coarse-Grained Models of Aqueous Polysaccharides. <b>2017</b> , 13, 223-236  | 18  |
| 1015 | TMAO mediates effective attraction between lipid membranes by partitioning unevenly between bulk and lipid domains. <b>2017</b> , 19, 29862-29871   | 13  |
| 1014 | Insights on the Mechanism of Action of INH-C as an Antitubercular Prodrug. <b>2017</b> , 14, 4597-4605  | 10  |
| 1013 | Comparative Assessment of Computational Methods for Free Energy Calculations of Ionic Hydration. <b>2017</b> , 57, 2763-2775  | 16  |
| 1012 | Validation of Trimethylamine-N-oxide (TMAO) Force Fields Based on Thermophysical Properties of Aqueous TMAO Solutions. <b>2017</b> , 121, 10674-10688   | 22  |
| 1011 | Temperature-Dependent Structure and Dynamics of Water Intercalated in Layered Double Hydroxides with Different Hydration States. <b>2017</b> , 121, 23752-23762                                 | 9   |
| 1010 | Massively parallel de novo protein design for targeted therapeutics. <b>2017</b> , 550, 74-79   | 235 |
| 1009 | Quasiharmonic analysis of protein energy landscapes from pressure-temperature molecular dynamics simulations. <b>2017</b> , 147, 125103   | 7   |
| 1008 | Mobility field and mobility temperature dependence in PC61BM: A kinetic Monte-Carlo study. <b>2017</b> , 689, 74-81   | 7   |

| 1007 | Membrane Dynamics of I-Secretase Provides a Molecular Basis for Mamyloid Binding and Processing. <b>2017</b> , 8, 2424-2436   | 34  |
|------|---|-----|
| 1006 | Interaction between 1-phenylethanone, 2-phenyl-2-propanol, and isopropenylbenzene with water molecules: A computational study. <b>2017</b> , 1117, 188-195                                  | 4   |
| 1005 | Methylene Blue Location in (Hydroperoxized) Cardiolipin Monolayer: Implication in Membrane Photodegradation. <b>2017</b> , 121, 8512-8522   | 7   |
| 1004 | Pseudo-peptide amyloid-blocking inhibitors: molecular dynamics and single molecule force spectroscopy study. <b>2017</b> , 1865, 1707-1718  | 10  |
| 1003 | Dynamic Specification of Initial Structures in Parallel Cascade Selection Molecular Dynamics (PaCS-MD) Efficiently Promotes Biologically Relevant Rare Events. <b>2017</b> , 90, 1236-1243  | 6   |
| 1002 | Dynamics at a Peptide-TiO Anatase (101) Interface. <b>2017</b> , 121, 8869-8877   | 3   |
| 1001 | Distinct Electrostatic Interactions Govern the Chiro-Optical Properties and Architectural Arrangement of Peptide Digothiophene Hybrid Materials. <b>2017</b> , 50, 7102-7110                | 11  |
| 1000 | Molecular dynamics simulations of ether- and ester-linked phospholipids. <b>2017</b> , 1859, 2297-2307  | 10  |
| 999  | Computational study on acetophenone in amorphous polyethylene. <b>2017</b> , 23, 274  | 7   |
| 998  | Molecular dynamics simulation study of hydration of uranyl nitrate in supercritical water: Dissecting the effect of uranyl ion concentration from solvent density. <b>2017</b> , 495, 48-58 | 2   |
| 997  | Simulation of Reversible Protein-Protein Binding and Calculation of Binding Free Energies Using Perturbed Distance Restraints. <b>2017</b> , 13, 5697-5708                                  | 20  |
| 996  | Effects of disulfide bridges and backbone connectivity on water sorption by protein matrices. <b>2017</b> , 7, 7957   | 2   |
| 995  | Energetics and mechanism of anion permeation across formate-nitrite transporters. <b>2017</b> , 7, 12027  | 16  |
| 994  | Improving the thermal stability of cellobiohydrolase Cel7A from by directed evolution. <b>2017</b> , 292, 17418-1743  | 037 |
| 993  | An allosteric ligand-binding site in the extracellular cap of K2P channels. <b>2017</b> , 8, 378  | 24  |
| 992  | Simulation Studies on the Lipid Interaction and Conformation of Novel Drug-Delivery Pseudopeptidic Polymers. <b>2017</b> , 121, 9113-9125   |     |
| 991  | MD Simulations of Viruslike Particles with Supra CG Solvation Affordable to Desktop Computers. <b>2017</b> , 13, 5106-5116  | 22  |
| 990  | Agonist-induced dimer dissociation as a macromolecular step in G protein-coupled receptor signaling. <b>2017</b> , 8, 226   | 45  |

| 989 | Beyond sixfold coordinated Si in SiO glass at ultrahigh pressures. <b>2017</b> , 114, 10041-10046  | 61 |
|-----|--|----|
| 988 | On the Calculation of Acyl Chain Order Parameters from Lipid Simulations. <b>2017</b> , 13, 5683-5696  | 49 |
| 987 | Organic and Third Phase in HNO3/TBP/n-Dodecane System: No Reverse Micelles. <b>2017</b> , 35, 251-265  | 19 |
| 986 | A polar SxxS motif drives assembly of the transmembrane domains of Toll-like receptor 4. <b>2017</b> , 1859, 2086-2095   | 8  |
| 985 | Molecular dynamics simulation of the aggregation behavior of N-Dodecyl-N,N-Dimethyl-3-Ammonio-1-Propanesulfonate/sodium dodecyl benzene sulfonate surfactant mixed system at oil/water interface. <b>2017</b> , 531, 73-80 | 13 |
| 984 | A comparison of classical interatomic potentials applied to highly concentrated aqueous lithium chloride solutions. <b>2017</b> , 242, 845-858   | 19 |
| 983 | A Multi-Level Theoretical Study to Disclose the Binding Mechanisms of Gold(III)-Bipyridyl Compounds as Selective Aquaglyceroporin Inhibitors. <b>2017</b> , 23, 13802-13813  | 25 |
| 982 | Structure-function studies of BPP-BrachyNH and synthetic analogues thereof with Angiotensin I-Converting Enzyme. <b>2017</b> , 139, 401-411  | 4  |
| 981 | Mg-Channel-Inspired Nanopores for Mg/Li Separation: The Effect of Coordination on the Ionic Hydration Microstructures. <b>2017</b> , 33, 9201-9210   | 26 |
| 980 | Arginine mutations in antibody complementarity-determining regions display context-dependent affinity/specificity trade-offs. <b>2017</b> , 292, 16638-16652   | 33 |
| 979 | Mapping Putative B-Cell Zika Virus NS1 Epitopes Provides Molecular Basis for Anti-NS1 Antibody Discrimination between Zika and Dengue Viruses. <b>2017</b> , 2, 3913-3920  | 24 |
| 978 | Initiation of prolyl cis-trans isomerisation in the CDR-H3 loop of an antibody in response to antigen binding. <b>2017</b> , 7, 16964  | 8  |
| 977 | Structure-Based Insights into the Dynamics and Function of Two-Domain SlpA from Escherichia coli. <b>2017</b> , 56, 6533-6543  | 2  |
| 976 | Structure-function relationships in ABCG2: insights from molecular dynamics simulations and molecular docking studies. <b>2017</b> , 7, 15534  | 39 |
| 975 | Exploring what prompts ITIC to become a superior acceptor in organic solar cell by combining molecular dynamics simulation with quantum chemistry calculation. <b>2017</b> , 19, 31227-31235                               | 25 |
| 974 | Conditional Reversible Work Coarse-Grained Models of Molecular Liquids with Coulomb<br>Electrostatics - A Proof of Concept Study on Weakly Polar Organic Molecules. <b>2017</b> , 13, 6158-6166                            | 9  |
| 973 | Changing the shape of hair with keratin peptides. <b>2017</b> , 7, 51581-51592   | 27 |
| 972 | A coarse-grained polarizable force field for the ionic liquid 1-butyl-3-methylimidazolium hexafluorophosphate. <b>2017</b> , 29, 504004  | 14 |

| 971 | Squid Suckerin Biomimetic Peptides Form Amyloid-like Crystals with Robust Mechanical Properties. <b>2017</b> , 18, 4240-4248  | 15 |
|-----|---|----|
| 970 | Self-Avoiding Conformational Sampling Based on Histories of Past Conformational Searches. <b>2017</b> , 57, 3070-3078   | 5  |
| 969 | Anti-inflammatory effect of active nanofibrous polymeric membrane bearing nanocontainers of atorvastatin complexes. <b>2017</b> , 12, 2651-2674   | 11 |
| 968 | Magnesium sulfate against oxidative damage of membrane lipids: A theoretical model. <b>2017</b> , 117, e25423   | 8  |
| 967 | In silico analyses of the effects of a point mutation and a pharmacological chaperone on the thermal fluctuation of phenylalanine hydroxylase. <b>2017</b> , 228, 47-54   |    |
| 966 | The tyrosine Y250 in Frizzled 4 defines a conserved motif important for structural integrity of the receptor and recruitment of Disheveled. <b>2017</b> , 38, 85-96   | 13 |
| 965 | Impact of molecular flexibility on the site energy shift of chlorophylls in Photosystem II. <b>2017</b> , 229, 93-98  | 7  |
| 964 | Efficient estimation of binding free energies between peptides and an MHC class II molecule using coarse-grained molecular dynamics simulations with a weighted histogram analysis method. <b>2017</b> , 38, 2007-2019              | 14 |
| 963 | Prediction of self-assemblies of sodium dodecyl sulfate and fragrance additives using coarse-grained force fields. <b>2017</b> , 23, 211  | 2  |
| 962 | Regulation of the Equilibrium between Closed and Open Conformations of Annexin A2 by N-Terminal Phosphorylation and S100A4-Binding. <b>2017</b> , 25, 1195-1207.e5  | 31 |
| 961 | Guestflost systems containing anthraquinone dyes with multiple visible transitions giving positive and negative dichroic order parameters: an assessment of principal molecular axes and computational methods. <b>2017</b> , 1-17  | 1  |
| 960 | The effect of dichlorvos on the structural alteration of serum albumins: a combined spectroscopic and molecular dynamic simulation approach. <b>2017</b> , 148, 1141-1151   | 13 |
| 959 | Compromise in competition between free energy and binding effect of intrinsically disordered protein p53 C-terminal domain. <b>2017</b> , 43, 110-120   | 2  |
| 958 | Solvation structures of sodium halides in dimethyl sulfoxide (DMSO)fhethanol (MeOH) mixtures. <b>2017</b> , 43, 154-168   | 3  |
| 957 | Molecular modeling, dynamics studies and density functional theory approaches to identify potential inhibitors of SIRT4 protein from Homo sapiens: a novel target for the treatment of type 2 diabetes. <b>2017</b> , 35, 3316-3329 | 28 |
| 956 | Dynamic conformational changes in the rhesus TRIM5⊞ dimer dictate the potency of HIV-1 restriction. <b>2017</b> , 500, 161-168  | 7  |
| 955 | Insight into the mechanism of chemical modification of antibacterial agents by antibiotic resistance enzyme O-phosphotransferase-IIIA. <b>2017</b> , 89, 84-97  | 1  |
| 954 | Study of conformational changes in serum albumin by binding of chlorfenvinphos using multispectroscopic techniques and molecular dynamic simulation. <b>2017</b> , 148, 781-791   | 17 |

| 953   | Action-FRET of a Gaseous Protein. 2017, 28, 38-49   | 15                        |
|---|---|---------------------------|
| 952   | Comparison of force fields for Alzheimer's A #2: A case study for intrinsically disordered proteins. <b>2017</b> , 26, 174-185  | 92                        |
| 951   | Highly clean and efficient enzymatic dehairing in green solvents. 2017, 140, 1578-1586  | 6                         |
| 950   | Conformational dynamics of Peb4 exhibit "mother's arms" chain model: a molecular dynamics study. <b>2017</b> , 35, 2186-2196  | 4                         |
| 949   | Designing Fcabs: well-expressed and stable high affinity antigen-binding Fc fragments. <b>2017</b> , 30, 657-671  | 6                         |
| 948   | The role of Zn2+, dimerization and N-glycosylation in the interaction of Auxin-Binding Protein 1 (ABP1) with different auxins. <b>2017</b> , 27, 1109-1119  | 2                         |
| 947   | Predicting Critical Micelle Concentrations with Molecular Dynamics Simulations and COSMOmic. <b>2017</b> , 89, 1288-1296  | 10                        |
| 946   | Molecular Simulation Study on the Interaction of Nanoparticles with Clay Minerals: C60 on Surfaces of Pyrophyllite and Kaolinite. <b>2017</b> , 65, 398-409   | 3                         |
| 945   | Localization and Ordering of Lipids Around Aquaporin-0: Protein and Lipid Mobility Effects. <b>2017</b> , 8, 124  | 17                        |
|   |   |                           |
| 944   | The Structure of Liquid and Amorphous Hafnia. <b>2017</b> , 10,   | 21                        |
| 944   | The Structure of Liquid and Amorphous Hafnia. 2017, 10,  T7 RNA polymerase translocation is facilitated by a helix opening on the fingers domain that may also prevent backtracking. 2017, 45, 7909-7921  | 21<br>17                  |
|   | T7 RNA polymerase translocation is facilitated by a helix opening on the fingers domain that may  |                           |
| 943   | T7 RNA polymerase translocation is facilitated by a helix opening on the fingers domain that may also prevent backtracking. <b>2017</b> , 45, 7909-7921  Tacticity-Dependent Interchain Interactions of Poly(N-Isopropylacrylamide) in Water: Toward the  | 17                        |
| 943   | T7 RNA polymerase translocation is facilitated by a helix opening on the fingers domain that may also prevent backtracking. 2017, 45, 7909-7921  Tacticity-Dependent Interchain Interactions of Poly(N-Isopropylacrylamide) in Water: Toward the Molecular Dynamics Simulation of a Thermoresponsive Microgel. 2017, 3,  Assemblies of amyloid-\$0-36 hexamer and its G33V/L34T mutants by replica-exchange molecular   | 17<br>8                   |
| 943<br>942<br>941   | T7 RNA polymerase translocation is facilitated by a helix opening on the fingers domain that may also prevent backtracking. 2017, 45, 7909-7921  Tacticity-Dependent Interchain Interactions of Poly(N-Isopropylacrylamide) in Water: Toward the Molecular Dynamics Simulation of a Thermoresponsive Microgel. 2017, 3,  Assemblies of amyloid-\$0-36 hexamer and its G33V/L34T mutants by replica-exchange molecular dynamics simulation. 2017, 12, e0188794   | 17<br>8<br>11             |
| 943<br>942<br>941<br>940  | T7 RNA polymerase translocation is facilitated by a helix opening on the fingers domain that may also prevent backtracking. 2017, 45, 7909-7921  Tacticity-Dependent Interchain Interactions of Poly(N-Isopropylacrylamide) in Water: Toward the Molecular Dynamics Simulation of a Thermoresponsive Microgel. 2017, 3,  Assemblies of amyloid-\$0-36 hexamer and its G33V/L34T mutants by replica-exchange molecular dynamics simulation. 2017, 12, e0188794  Sequence dependency of canonical base pair opening in the DNA double helix. 2017, 13, e1005463  Concerted regulation of npc2 binding to endosomal/lysosomal membranes by   | 17<br>8<br>11<br>21       |
| <ul><li>943</li><li>942</li><li>941</li><li>940</li><li>939</li></ul> | T7 RNA polymerase translocation is facilitated by a helix opening on the fingers domain that may also prevent backtracking. 2017, 45, 7909-7921  Tacticity-Dependent Interchain Interactions of Poly(N-Isopropylacrylamide) in Water: Toward the Molecular Dynamics Simulation of a Thermoresponsive Microgel. 2017, 3,  Assemblies of amyloid-\$0-36 hexamer and its G33V/L34T mutants by replica-exchange molecular dynamics simulation. 2017, 12, e0188794  Sequence dependency of canonical base pair opening in the DNA double helix. 2017, 13, e1005463  Concerted regulation of npc2 binding to endosomal/lysosomal membranes by bis(monoacylglycero)phosphate and sphingomyelin. 2017, 13, e1005831  Transferability of Polymer Chain Properties between Coarse-Grained and Atomistic Models of | 17<br>8<br>11<br>21<br>23 |

| 935 | Molecular Mechanism, Dynamics, and Energetics of Protein-Mediated Dinucleotide Flipping in a Mismatched DNA: A Computational Study of the RAD4-DNA Complex. <b>2018</b> , 58, 647-660                           | 2   |
|-----|---|-----|
| 934 | Revisiting imidazolium based ionic liquids: Effect of the conformation bias of the [NTf] anion studied by molecular dynamics simulations. <b>2018</b> , 148, 193828   | 34  |
| 933 | Efficient Osmotic Pressure Calculations Using Coarse-Grained Molecular Simulations. 2018, 14, 1171-1176   | 4   |
| 932 | Solvent-enabled control of reactivity for liquid-phase reactions of biomass-derived compounds. <b>2018</b> , 1, 199-207   | 147 |
| 931 | Prediction of the Crystal Morphology of HMX using a Generalized Interfacial Structure Analysis Model. <b>2018</b> , 18, 2349-2357   | 8   |
| 930 | Water Confined in Nanocapillaries: Two-Dimensional Bilayer Squarelike Ice and Associated Solid[IiquidBolid Transition. <b>2018</b> , 122, 6704-6712   | 21  |
| 929 | Molecular Insights into the Membrane Affinities of Model Hydrophobes. <b>2018</b> , 3, 2498-2507  | 7   |
| 928 | Steered molecular dynamics simulations for uncovering the molecular mechanisms of drug dissociation and for drug screening: A test on the focal adhesion kinase. <b>2018</b> , 39, 1307-1318                    | 16  |
| 927 | Highly Disordered Amyloid-∰Monomer Probed by Single-Molecule FRET and MD Simulation. <b>2018</b> , 114, 870-884   | 59  |
| 926 | ♥N-Methylamino-l-alanine (BMAA) Not Involved in Alzheimer's Disease. <b>2018</b> , 122, 4472-4480   | 10  |
| 925 | Rotational and translational dynamics and their relation to hydrogen bond lifetimes in an ionic liquid by means of NMR relaxation time experiments and molecular dynamics simulation. <b>2018</b> , 148, 193843 | 18  |
| 924 | subunit stabilises sodium channel Nav1.7 against mechanical stress. <b>2018</b> , 596, 2433-2445  | 7   |
| 923 | Evidence that TLR4 Is Not a Receptor for Saturated Fatty Acids but Mediates Lipid-Induced Inflammation by Reprogramming Macrophage Metabolism. <b>2018</b> , 27, 1096-1110.e5                                   | 210 |
| 922 | Programed dynamical ordering in self-organization processes of a nanocube: a molecular dynamics study. <b>2018</b> , 20, 9115-9122  | 5   |
| 921 | Flexible Versus Rigid G-Quadruplex DNA Ligands: Synthesis of Two Series of Bis-indole Derivatives and Comparison of Their Interactions with G-Quadruplex DNA. <b>2018</b> , 24, 7926-7938                       | 11  |
| 920 | On flexible force fields for metal-organic frameworks: Recent developments and future prospects. <b>2018</b> , 8, e1363   | 30  |
| 919 | On the molecular origin of the cooperative coil-to-globule transition of poly(N-isopropylacrylamide) in water. <b>2018</b> , 20, 9997-10010   | 66  |
| 918 | pH-Induced Rotation of Lidless Lipase LipA from Bacillus subtilis at Lipase-Detergent Interface. <b>2018</b> , 122, 4802-4812   | 6   |

| 917 | Processive Degradation of Crystalline Cellulose by a Multimodular Endoglucanase via a Wirewalking Mode. <b>2018</b> , 19, 1686-1696  | 29              |
|-----|--|-----------------|
| 916 | Physical Origin of Thermostabilization by a Quadruple Mutation for the Adenosine A Receptor in the Active State. <b>2018</b> , 122, 4418-4427  | 6               |
| 915 | Single molecule FRET investigation of pressure-driven unfolding of cold shock protein A. <b>2018</b> , 148, 123336   | 2               |
| 914 | How Does the Surface Tension Depend on the Surface Area with Coarse-Grained Models?. <b>2018</b> , 14, 2644-265  | 1 <sub>10</sub> |
| 913 | Force Field Benchmark of Amino Acids: I. Hydration and Diffusion in Different Water Models. <b>2018</b> , 58, 1037-1052  | 56              |
| 912 | A Computational Study of the Ionic Liquid-Induced Destabilization of the Miniprotein Trp-Cage. <b>2018</b> , 122, 5707-5715  | 5               |
| 911 | Structural basis for the interaction of the beta-secretase with copper. <b>2018</b> , 1860, 1105-1113  | 6               |
| 910 | The Molecular Basis of the Sodium Dodecyl Sulfate Effect on Human Ubiquitin Structure: A Molecular Dynamics Simulation Study. <b>2018</b> , 8, 2150  | 19              |
| 909 | Characterization of Interactions between Curcumin and Different Types of Lipid Bilayers by Molecular Dynamics Simulation. <b>2018</b> , 122, 2341-2354   | 27              |
| 908 | Elucidation of the Binding Mode of the Carboxyterminal Region of Peptide YY to the Human Y Receptor. <b>2018</b> , 93, 323-334   | 22              |
| 907 | The influence of like-charge attraction on the structure and dynamics of ionic liquids: NMR chemical shifts, quadrupole coupling constants, rotational correlation times and failure of Stokes-Einstein-Debye. <b>2018</b> , 20, 5617-5625 | 19              |
| 906 | The role of d-allo-isoleucine in the deposition of the anti-Leishmania peptide bombinin H4 as revealed by P solid-state NMR, VCD spectroscopy, and MD simulation. <b>2018</b> , 1866, 789-798  | 18              |
| 905 | Lipids Shape the Electron Acceptor-Binding Site of the Peripheral Membrane Protein Dihydroorotate Dehydrogenase. <b>2018</b> , 25, 309-317.e4  | 13              |
| 904 | Salting-in of neopentane in the aqueous solutions of urea and glycine-betaine. <b>2018</b> , 44, 677-687   | O               |
| 903 | Pressure tensor for electrostatic interaction calculated by fast multipole method with periodic boundary condition. <b>2018</b> , 39, 1192-1199  | 2               |
| 902 | Atomistic-level study of the interactions between hIAPP protofibrils and membranes: Influence of pH and lipid composition. <b>2018</b> , 1860, 1818-1825   | 22              |
| 901 | Destabilizing the AXH Tetramer by Mutations: Mechanisms and Potential Antiaggregation Strategies. <b>2018</b> , 114, 323-330   | 10              |
| 900 | Molecular details of spontaneous insertion and interaction of HCV non-structure 3 protease protein domain with PIP2-containing membrane. <b>2018</b> , 86, 423-433   | 1               |

| 899 | Molecular dynamics simulations of asymmetric heterodimers of HER1/HER2 complexes. 2017, 24, 30  | 1   |
|-----|---|-----|
| 898 | Adsorption of Kinetic Hydrate Inhibitors on Growing Surfaces: A Molecular Dynamics Study. <b>2018</b> , 122, 3396-3406  | 45  |
| 897 | Validation and Comparison of Force Fields for Native Cyclodextrins in Aqueous Solution. 2018, 122, 1608-1620  | 525 |
| 896 | A Novel Microemulsion Phase Transition: Toward the Elucidation of Third-Phase Formation in Spent Nuclear Fuel Reprocessing. <b>2018</b> , 122, 1439-1452                                    | 30  |
| 895 | Spontaneous protein desorption from self-assembled monolayer (SAM)-coated gold nanoparticles. <b>2017</b> , 20, 68-74   | 4   |
| 894 | Identification of essential amino acids for glucose transporter 5 (GLUT5)-mediated fructose transport. <b>2018</b> , 293, 2115-2124   | 7   |
| 893 | Solubility of CO2 in triglycerides using Monte Carlo simulations. <b>2018</b> , 476, 39-47  | 7   |
| 892 | The Mechanism by Which Luteolin Disrupts the Cytoplasmic Membrane of Methicillin-Resistant Staphylococcus aureus. <b>2018</b> , 122, 1427-1438  | 9   |
| 891 | Modulating interactions between ligand-coated nanoparticles and phase-separated lipid bilayers by varying the ligand density and the surface charge. <b>2018</b> , 10, 2481-2491            | 33  |
| 890 | Molecular Dynamics Investigation of the Influence of the Hydrogen Bond Networks in Ethanol/Water Mixtures on Dielectric Spectra. <b>2018</b> , 122, 1505-1515                               | 28  |
| 889 | The Interplay of Methyl-Group Distribution and Hydration Pattern of Isomeric Amphiphilic Osmolytes. <b>2018</b> , 122, 5972-5983  | 9   |
| 888 | In silico assessment of the conduction mechanism of the Ryanodine Receptor 1 reveals previously unknown exit pathways. <b>2018</b> , 8, 6886  | 9   |
| 887 | Analysis of the influence of simulation parameters on biomolecule-linked water networks. <b>2018</b> , 82, 117-128  | 1   |
| 886 | Effect of PDGF-B aptamer on PDGFR#PDGF-B interaction: Molecular dynamics study. <b>2018</b> , 82, 145-156   | 17  |
| 885 | A molecular dynamics investigation of the surface tension of water nanodroplets and a new technique for local pressure determination through density correlation. <b>2018</b> , 148, 144503 | 8   |
| 884 | The effect of alkyl chain length on mechanical properties of fatty-acid-functionalized amidoamine-epoxy systems. <b>2018</b> , 150, 70-76   | 7   |
| 883 | On the Calculation of SAXS Profiles of Folded and Intrinsically Disordered Proteins from Computer Simulations. <b>2018</b> , 430, 2521-2539   | 41  |
| 882 | Influence of additives on thermoresponsive polymers in aqueous media: a case study of poly(N-isopropylacrylamide). <b>2018</b> , 20, 9717-9744  | 29  |

| 881 | Confinement effects and mechanistic aspects for montmorillonite nanopores. <b>2018</b> , 523, 18-26  | 24 |
|-----|--|----|
| 88o | A single NaK channel conformation is not enough for non-selective ion conduction. <b>2018</b> , 9, 717   | 33 |
| 879 | Antithrombin conformational modulation by D-myo-inositol 3,4,5,6-tetrakisphosphate (TMI), a novel scaffold for the development of antithrombotic agents. <b>2018</b> , 36, 4045-4056                                   | 2  |
| 878 | Molecular Dynamics Modeling of Methylene Blue-DOPC Lipid Bilayer Interactions. <b>2018</b> , 34, 4314-4323   | 13 |
| 877 | Does an electronic continuum correction improve effective short-range ion-ion interactions in aqueous solution?. <b>2018</b> , 148, 222816   | 25 |
| 876 | Effects of different force fields on the structural character of ∃ synuclein ⊕airpin peptide (35-56) in aqueous environment. <b>2018</b> , 36, 302-317   | 11 |
| 875 | Atomic insight into designed carbamate-based derivatives as acetylcholine esterase (AChE) inhibitors: a computational study by multiple molecular docking and molecular dynamics simulation. <b>2018</b> , 36, 126-138 | 16 |
| 874 | Molecular dynamics analysis of the structural and dynamic properties of the functionally enhanced hepta-variant of mouse 5-aminolevulinate synthase. <b>2018</b> , 36, 152-165   | 4  |
| 873 | Characterizing the interactions of two lipid modifications with lipid rafts: farnesyl anchors vs. palmitoyl anchors. <b>2018</b> , 47, 19-30   | 3  |
| 872 | A computational study to identify the key residues of peroxisome proliferator-activated receptor gamma in the interactions with its antagonists. <b>2018</b> , 36, 1822-1833   | 4  |
| 871 | Molecular modeling and SPRi investigations of interleukin 6 (IL6) protein and DNA aptamers. <b>2018</b> , 36, 1934-1947  | 8  |
| 870 | Wing 1 of protein HOP2 is as important as helix 3 in DNA binding by MD simulation. <b>2018</b> , 36, 1853-1866   | O  |
| 869 | Evidence of anomalous behavior of intermolecular interactions at low concentration of methanol in ethanol-methanol binary system. <b>2018</b> , 188, 301-310   | 7  |
| 868 | Conformational transitions of uracil transporter UraA from Escherichia coli: a molecular simulation study. <b>2018</b> , 36, 3398-3410   | 1  |
| 867 | An effective way to determine the melting curve. <b>2018</b> , 44, 384-388   |    |
| 866 | Multivalent interacting glycodendrimer to prevent amyloid-peptide fibril formation induced by Cu(II): A multidisciplinary approach. <b>2018</b> , 11, 1204-1226  | 19 |
| 865 | Ion Storage in Nanoconfined Interstices Between Vertically Aligned Nanotubes in Electric Double-Layer Capacitors. <b>2018</b> , 15,  | 2  |
| 864 | The effect of surfactant adsorption on surface wettability and flow resistance in slit nanopore: A molecular dynamics study. <b>2018</b> , 513, 379-388  | 14 |

846

Computer Simulations to Explore Membrane Organization and Transport. 2018, 355-392 863 Differential targeting of membrane lipid domains by caffeic acid and its ester derivatives. 2018, 862 115, 232-245 Effects of force fields on the conformational and dynamic properties of amyloid \$1-40\$ dimer 861 17 explored by replica exchange molecular dynamics simulations. 2018, 86, 279-300 Structural insights of RmXyn10A - A prebiotic-producing GH10 xylanase with a non-conserved 860 12 aglycone binding region. 2018, 1866, 292-306 On the effect of mutations in bovine or camel chymosin on the thermodynamics of binding 859 Ο Ecaseins. 2018, 86, 75-87 Permeation pathways through lateral domains in model membranes of skin lipids. 2018, 20, 2162-2174 858 22 Boron Isotope Fractionation Among Vapor Liquids Bolids Melts: Experiments and Atomistic 857 14 Modeling. **2018**, 33-69 Membrane Biophysics. 2018, 856 Simulation study of intercalation complexes of kaolinite with simple amides as primary 855 13 intercalation reagents. **2018**, 143, 118-125 An assessment of optimal time scale of conformational resampling for parallel cascade selection 854 molecular dynamics. 2018, 44, 206-212 Water phase transitions from the perspective of hydrogen-bond network analysis. 2018, 20, 28308-28318 853 5 Nanoparticles based on lipidyl-tyclodextrins: synthesis, characterization, and experimental and 852 computational biophysical studies for encapsulation of atazanavir. 2018, 42, 20171-20179 851 Ethylene glycol solution-induced DNA conformational transitions. 2018, 27, 113102 2 Heterogeneity governs diameter-dependent toughness and strength in SiC nanowires. 2018, 98, 850 12 The Formation of Hydrophobic Core Regulates the Protein Folding of Villin Elucidated with Parallel 849 Cascade Selection Molecular Dynamics. 2018, 47, 1300-1303 Molecular Mechanism of Depolarization-Dependent Inactivation in W366F Mutant of Kv1.2. 2018, 848 122, 10825-10833 Novel glitazones as PPAR agonists: molecular design, synthesis, glucose uptake activity and 3D 847 9 QSAR studies. 2018, 12, 141 High and low density patches in simulated liquid water. 2018, 149, 204507

22

| 845 | Design of a Novel and Selective IRAK4 Inhibitor Using Topological Water Network Analysis and Molecular Modeling Approaches. <b>2018</b> , 23,   | 5  |
|-----|---|----|
| 844 | Simultaneous and Independent Dual Site-Specific Self-Labeling of Recombinant Antibodies. <b>2018</b> , 29, 3586-3594  | 7  |
| 843 | Mechanistic basis for the evolution of chalcone synthase catalytic cysteine reactivity in land plants. <b>2018</b> , 293, 18601-18612   | 15 |
| 842 | Structure and dynamics of Helicobacter pylori nickel-chaperone HypA: an integrated approach using NMR spectroscopy, functional assays and computational tools. <b>2018</b> , 23, 1309-1330      | 12 |
| 841 | d-Amino Acid Pseudopeptides as Potential Amyloid-Beta Aggregation Inhibitors. 2018, 23,   | 6  |
| 840 | Structures, intermolecular interactions, and chemical hardness of binary water-organic solvents: a molecular dynamics study. <b>2018</b> , 24, 292  | 2  |
| 839 | Dielectric relaxation in acetamide + urea deep eutectics and neat molten urea: Origin of time scales via temperature dependent measurements and computer simulations. <b>2018</b> , 149, 124501 | 26 |
| 838 | Insights into the Folding of Disulfide-Rich Econotoxins. <b>2018</b> , 3, 12330-12340   | 9  |
| 837 | Outward open conformation of a Major Facilitator Superfamily multidrug/H antiporter provides insights into switching mechanism. <b>2018</b> , 9, 4005   | 31 |
| 836 | Enzyme <b>P</b> olyelectrolyte Complexes Boost the Catalytic Performance of Enzymes. <b>2018</b> , 8, 10876-10887   | 18 |
| 835 | Free Energy Landscape for Alpha-Helix to Beta-Sheet Interconversion in Small Amyloid Forming Peptide under Nanoconfinement. <b>2018</b> , 122, 9654-9664  | 10 |
| 834 | Novel Mechanism for Cyclic Dinucleotide Degradation Revealed by Structural Studies of Vibrio Phosphodiesterase V-cGAP3. <b>2018</b> , 430, 5080-5093  | 7  |
| 833 | Modeling ion permeation in wild-type and mutant human ⊕7 nachr ion channels. <b>2018</b> , 17, 1850045  |    |
| 832 | Conformational flexibility of histone variant CENP-A is regulated by histone H4: A mechanism to stabilize soluble Cse4. <b>2018</b> , 293, 20273-20284  | 2  |
| 831 | Molecular Dynamics Simulations for the Co-Adsorption of Binary Electrolytes at the Interface of Montmorillonite and Aqueous Solutions. <b>2018</b> , 82, 1384-1391                              | 16 |
| 830 | Folded Structure and Membrane Affinity of the N-Terminal Domain of the Three Human Isoforms of the Mitochondrial Voltage-Dependent Anion-Selective Channel. <b>2018</b> , 3, 11415-11425        | 5  |
| 829 | On the Applicability of Force Fields To Study the Aggregation of Amyloidogenic Peptides Using Molecular Dynamics Simulations. <b>2018</b> , 14, 6063-6075                                       | 51 |
| 828 | Noncovalent Inhibitors of Mosquito Acetylcholinesterase 1 with Resistance-Breaking Potency. <b>2018</b> , 61, 10545-10557   | 4  |

# (2018-2018)

| 827 | Overcoming Convergence Issues in Free-Energy Calculations of Amide-to-Ester Mutations in the Pin1-WW Domain. <b>2018</b> , 58, 2305-2318  | 2  |
|-----|---|----|
| 826 | Structure of the mechanosensitive OSCA channels. <b>2018</b> , 25, 850-858  | 68 |
| 825 | Biomolecular Simulations of Halogen Bonds with a GROMOS Force Field. <b>2018</b> , 14, 5383-5392  | 14 |
| 824 | A Luminal Loop of Wilson Disease Protein Binds Copper and Is Required for Protein Activity. <b>2018</b> , 115, 1007-1018  | 2  |
| 823 | Computational investigation of the conformation transitions of DNA in modified water models. <b>2018</b> , 271, 175-181   | 8  |
| 822 | Dihydrochalcone molecules destabilize Alzheimer's amyloid-protofibrils through binding to the protofibril cavity. <b>2018</b> , 20, 17208-17217                                   | 27 |
| 821 | Bibliography. 421-446   |    |
| 820 | Structural basis for gating pore current in periodic paralysis. <b>2018</b> , 557, 590-594  | 33 |
| 819 | Molecular dynamics simulation for desulphurization of hydrocarbon fuel using ionic liquids. <b>2018</b> , 264, 490-498  | 9  |
| 818 | The architecture of the OmpC-MlaA complex sheds light on the maintenance of outer membrane lipid asymmetry in. <b>2018</b> , 293, 11325-11340                                     | 34 |
| 817 | On-the-Fly Specifications of Reaction Coordinates in Parallel Cascade Selection Molecular Dynamics Accelerate Conformational Transitions of Proteins. <b>2018</b> , 14, 3332-3341 | 8  |
| 816 | Structural basis of actin monomer re-charging by cyclase-associated protein. <b>2018</b> , 9, 1892  | 37 |
| 815 | Activation of Toll-like receptors nucleates assembly of the MyDDosome signaling hub. 2018, 7,   | 49 |
| 814 | Coupled-perturbed DFTB-QM/MM metadynamics: Application to proton-coupled electron transfer. <b>2018</b> , 149, 072328   | 8  |
| 813 | HIV-1 Env gp41 Transmembrane Domain Dynamics Are Modulated by Lipid, Water, and Ion Interactions. <b>2018</b> , 115, 84-94  | 9  |
| 812 | Dynamics and Thermodynamics of Transthyretin Association from Molecular Dynamics Simulations. <b>2018</b> , 2018, 7480749   | 5  |
| 811 | Specific ion effects for polyelectrolytes in aqueous and non-aqueous media: the importance of the ion solvation behavior. <b>2018</b> , 14, 6243-6255                             | 18 |
| 810 | Force Field Benchmark of Amino Acids. 2. Partition Coefficients between Water and Organic Solvents. <b>2018</b> , 58, 1669-1681   | 28 |

| 809 | Membrane partition of bis-(3-hydroxy-4-pyridinonato) zinc(ii) complexes revealed by molecular dynamics simulations <b>2018</b> , 8, 27081-27090  | 4                |
|-----|--|------------------|
| 808 | GRAIL: GRids of phArmacophore Interaction fieLds. <b>2018</b> , 14, 4958-4970  | 12               |
| 807 | A polarizable MARTINI model for monovalent ions in aqueous solution. <b>2018</b> , 149, 163319   | 17               |
| 806 | Anti-Correlation between the Dynamics of the Active Site Loop and C-Terminal Tail in Relation to the Homodimer Asymmetry of the Mouse Erythroid 5-Aminolevulinate Synthase. <b>2018</b> , 19,                  | 5                |
| 805 | In vitro and in silico studies of naphthoquinones and peptidomimetics toward Plasmodium falciparum plasmepsin V. <b>2018</b> , 152, 159-173  | 5                |
| 804 | Structural basis for endotoxin neutralisation and anti-inflammatory activity of thrombin-derived C-terminal peptides. <b>2018</b> , 9, 2762  | 25               |
| 803 | Complete Coupled Binding-Folding Pathway of the Intrinsically Disordered Transcription Factor Protein Brinker Revealed by Molecular Dynamics Simulations and Markov State Modeling. <b>2018</b> , 57, 4404-442 | 10 <sup>12</sup> |
| 802 | Proactive response to tackle the threat of emerging drugs: Synthesis and toxicity evaluation of new cathinones. <b>2018</b> , 290, 146-156   | 22               |
| 801 | The Inhibitory Effect of Hydroxylated Carbon Nanotubes on the Aggregation of Human Islet Amyloid Polypeptide Revealed by a Combined Computational and Experimental Study. <b>2018</b> , 9, 2741-2752           | 31               |
| 800 | A Nonequilibrium Molecular Dynamics Study of Infrared Perturbed Electron Transfer. <b>2018</b> , 14, 4818-4832   | 1                |
| 799 | Phase Diagrams of TIP4P/2005, SPC/E, and TIP5P Water at High Pressure. 2018, 122, 7718-7725  | 22               |
| 798 | Structural Behavior of Isolated Asphaltene Molecules at the OilWater Interface. 2018, 32, 8259-8267  | 11               |
| 797 | Sequence-dependent DNA condensation as a driving force of DNA phase separation. <b>2018</b> , 46, 9401-9413  | 41               |
| 796 | Machine learning and molecular design of self-assembling -conjugated oligopeptides. <b>2018</b> , 44, 930-945  | 18               |
| 795 | Investigation of Nonlinear Output-Input Microwave Power of DMSO-Ethanol Mixture by Molecular Dynamics Simulation. <b>2018</b> , 8, 7186  | 6                |
| 794 | How Reactive are Druggable Cysteines in Protein Kinases?. <b>2018</b> , 58, 1935-1946  | 27               |
| 793 | Molecular Dynamics Simulations of Human Antimicrobial Peptide LL-37 in Model POPC and POPG Lipid Bilayers. <b>2018</b> , 19,   | 27               |
| 792 | Protein Environment: A Crucial Triggering Factor in Josephin Domain Aggregation: The Role of 2,2,2-Trifluoroethanol. <b>2018</b> , 19,   | 2                |

| 791              | Molecular Simulation Studies of Cyanine-Based Chromonic Mesogens: Spontaneous Symmetry Breaking to Form Chiral Aggregates and the Formation of a Novel Lamellar Structure. <b>2018</b> , 1, 1800088  | 4  |
|------------------|--|----|
| 790              | How Does Friction Coefficient Affect the Conformational Sampling Efficiency of Parallel Cascade Selection Molecular Dynamics?. <b>2018</b> , 47, 1119-1122   |    |
| 789              | Dynamics of DDB2-DDB1 complex under different naturally-occurring mutants in Xeroderma Pigmentosum disease. <b>2018</b> , 1862, 2579-2589  | 5  |
| 788              | Influences of Cation Ratio, Anion Type, and Water Content on Polytypism of Layered Double Hydroxides. <b>2018</b> , 57, 7299-7313  | 13 |
| 787              | Metronidazole within phosphatidylcholine lipid membranes: New insights to improve the design of imidazole derivatives. <b>2018</b> , 129, 204-214  | 9  |
| 786              | Parameterization of the CHARMM All-Atom Force Field for Ether Lipids and Model Linear Ethers. <b>2018</b> , 122, 6744-6754   | 18 |
| 7 <sup>8</sup> 5 | Temperature-Shuffled Structural Dissimilarity Sampling Based on a Root-Mean-Square Deviation. <b>2018</b> , 58, 1397-1405  | 5  |
| 7 <sup>8</sup> 4 | Aggregation Behavior of Model Asphaltenes Revealed from Large-Scale Coarse-Grained Molecular Simulations. <b>2019</b> , 123, 2380-2396   | 16 |
| 783              | Improvement in the Predicted Partitioning of Alcohol and Polyethylene Oxide Groups Between Water and Octanol (logP) in Molecular Dynamics Simulations. <b>2019</b> , 108, 214-222                    | 6  |
| 782              | The SIRAH 2.0 Force Field: Altius, Fortius, Citius. <b>2019</b> , 15, 2719-2733  | 53 |
| 781              | Azadirachtin inhibits amyloid formation, disaggregates pre-formed fibrils and protects pancreatic tells from human islet amyloid polypeptide/amylin-induced cytotoxicity. <b>2019</b> , 476, 889-907 | 13 |
| 78o              | Conformation and Cross-Protection in Group B Streptococcus Serotype III and Serotype 14: A Molecular Modeling Study. <b>2019</b> , 12,   | 9  |
| 779              | A pharmacological master key mechanism that unlocks the selectivity filter gate in K channels. <b>2019</b> , 363, 875-880  | 61 |
| 778              | Molecular Mechanisms of DNA Replication and Repair Machinery: Insights from Microscopic Simulations. <b>2019</b> , 2, 1800191  | 4  |
| 777              | Interaction of salt with ether- and ester-linked phospholipid bilayers. <b>2019</b> , 1861, 907-915  | 1  |
| 776              | Analyses based on statistical thermodynamics for large difference between thermophilic rhodopsin and xanthorhodopsin in terms of thermostability. <b>2019</b> , 150, 055101                          | 5  |
| 775              | Investigation of the interactions between Melittin and the PLGA and PLA polymers: molecular dynamic simulation and binding free energy calculation. <b>2019</b> , 6, 055318                          | 12 |
| 774              | Multi-scale approach for modeling stability, aggregation, and network formation of nanoparticles suspended in aqueous solutions. <b>2019</b> , 11, 3979-3992   | 18 |

| 773             | Characterization Of Blood-Brain Barrier Crossing And Tumor Homing Peptides By Molecular Dynamics Simulations. <b>2019</b> , 14, 10123-10136   | 3  |
|-----------------|---|----|
| 772             | Sequential activation of STIM1 links Ca with luminal domain unfolding. <b>2019</b> , 12,  | 21 |
| 77 <sup>1</sup> | Atomistic simulation of PDADMAC/PSS oligoelectrolyte multilayers: overall comparison of tri- and tetra-layer systems. <b>2019</b> , 15, 9437-9451   | 4  |
| 77°             | Effect of Pore Size on the Ion Electrosorption and Hydrogen/Deuterium Electrosorption Using Sodium Chloride in H2O and D2O. <b>2019</b> , 166, A4158-A4167  | 6  |
| 769             | Dissecting C-Htand N-Hteractions in Two Proteins Using a Combined Experimental and Computational Approach. <b>2019</b> , 9, 20149   | 12 |
| 768             | Caffeine destabilizes preformed Aprotofilaments: insights from all atom molecular dynamics simulations. <b>2019</b> , 21, 22067-22080   | 18 |
| 767             | Rational discovery of antimetastatic agents targeting the intrinsically disordered region of MBD2. <b>2019</b> , 5, eaav9810  | 12 |
| 766             | Structure and phase transition behaviors of water in carbon nanotube under the electric field and high pressure. <b>2019</b> , 6, 1250a1  | 2  |
| 765             | Analysis of two common algorithms to compute self-diffusion coefficients in infinite dilution from molecular dynamics simulations and application to n-alkanes (C1 to C35) in water. <b>2019</b> , 485, 211-219 | 1  |
| 764             | Influence of the T to S mutation at the STMK motif on antibiotic resistance of penicillin binding protein 1A: A comprehensive computational study. <b>2019</b> , 87, 185-191                                    | 2  |
| 763             | The role of intermolecular interactions on the encapsulation of human insulin into the chitosan and cholesterol-grafted chitosan polymers. <b>2019</b> , 208, 345-355   | 10 |
| 762             | Molecular Dynamics Study of Kinetic Hydrate Inhibitors: The Optimal Inhibitor Size and Effect of Guest Species. <b>2019</b> , 123, 1806-1816  | 25 |
| 761             | Effect of Familial Mutations on the Interconversion of $\Box$ -Helix to 的heet Structures in an Amyloid-Forming Peptide: Insight from Umbrella Sampling Simulations. <b>2019</b> , 10, 1347-1354                 | 13 |
| 760             | Lipid Rafts: Buffers of Cell Membrane Physical Properties. <b>2019</b> , 123, 2050-2056   | 18 |
| 759             | An evaluation of in-silico methods for predicting solute partition in multiphase complex fluids [A case study of octanol/water partition coefficient. <b>2019</b> , 197, 150-158                                | 14 |
| 758             | Molecular Self-Assembly Strategy for Encapsulation of an Amphipathic ∃-Helical Antimicrobial Peptide into the Different Polymeric and Copolymeric Nanoparticles. <b>2019</b> , 59, 550-563                      | 15 |
| 757             | Three-phase equilibrium curve shift for methane hydrate in oceanic conditions calculated from Molecular Dynamics simulations. <b>2019</b> , 274, 426-433  | 12 |
| 756             | Characterization of Electrospray Ionization (ESI) Parameters on In-ESI Hydrogen/Deuterium Exchange of Carbohydrate-Metal Ion Adducts. <b>2019</b> , 30, 235-247   | 11 |

#### (2020-2019)

| 755                 | Noncovalent Forces of ( $\stackrel{.}{-}$ )- ${+}$ Lipoic Acid. <b>2019</b> , 35, 980-989   | 2                 |
|---------------------|---|-------------------|
| 754                 | Fatty Acids Compete with Affin Binding to Serum Albumin by Quenching Its Conformational Flexibility. <b>2019</b> , 116, 248-257   | 11                |
| 753                 | Cholesterol Flip-Flop in Heterogeneous Membranes. <b>2019</b> , 15, 2064-2070   | 32                |
| 75 <sup>2</sup>     | Thermally triggered nanorocket from double-walled carbon nanotube in water. <b>2019</b> , 45, 417-424   | 5                 |
| 751                 | Using limiting activity coefficients to efficiently evaluate the ability of fixed-charge force fields to model miscible water plus cosolvent mixtures. <b>2019</b> , 45, 322-335  | 8                 |
| 750                 | Conformational stability and dynamics of the cancer-associated isoform 且33p53脚re modulated by p53 peptides and p53-specific DNA. <b>2019</b> , 33, 4225-4235  | 14                |
| 749                 | Duffy binding-like 1日 adhesin from Plasmodium falciparum recognizes ABH histo-blood group saccharide in a type specific manner. <b>2019</b> , 207, 266-275  |                   |
| 748                 | Predicting Residence Time and Drug Unbinding Pathway through Scaled Molecular Dynamics. <b>2019</b> , 59, 535-549   | 37                |
| 747                 | Thermodynamic Characterization of the Dimerization of an Anionic Perylene Bisimide Dye Using Molecular Simulation. <b>2019</b> , 123, 8027-8036   | 2                 |
|                     |   |                   |
| 746                 | A CPU/MIC Collaborated Parallel Framework for GROMACS on Tianhe-2 Supercomputer. <b>2019</b> , 16, 425-433  | 4                 |
| 746<br>745          | A CPU/MIC Collaborated Parallel Framework for GROMACS on Tianhe-2 Supercomputer. <b>2019</b> , 16, 425-433  Insights into resistance mechanism of hepatitis C virus nonstructural 3/4A protease mutant to boceprevir using umbrella sampling simulation study. <b>2020</b> , 38, 1938-1945  | 2                 |
|                     | Insights into resistance mechanism of hepatitis C virus nonstructural 3/4A protease mutant to   |                   |
| 745                 | Insights into resistance mechanism of hepatitis C virus nonstructural 3/4A protease mutant to boceprevir using umbrella sampling simulation study. <b>2020</b> , 38, 1938-1945  Disease-associated mutations alter the dynamic motion of the N-terminal domain of the human   |                   |
| 745<br>744          | Insights into resistance mechanism of hepatitis C virus nonstructural 3/4A protease mutant to boceprevir using umbrella sampling simulation study. 2020, 38, 1938-1945  Disease-associated mutations alter the dynamic motion of the N-terminal domain of the human cardiac ryanodine receptor. 2020, 38, 1054-1070  Molecular description of the coil-to-globule transition of Poly(N-isopropylacrylamide) in  | 2                 |
| 745<br>744<br>743   | Insights into resistance mechanism of hepatitis C virus nonstructural 3/4A protease mutant to boceprevir using umbrella sampling simulation study. 2020, 38, 1938-1945  Disease-associated mutations alter the dynamic motion of the N-terminal domain of the human cardiac ryanodine receptor. 2020, 38, 1054-1070  Molecular description of the coil-to-globule transition of Poly(N-isopropylacrylamide) in water/ethanol mixture at low alcohol concentration. 2020, 297, 111928  Transferable coarse-grained models for poly(ethylene oxide)/poly(methyl methacrylate) blends.   | 2 2 17            |
| 745<br>744<br>743   | Insights into resistance mechanism of hepatitis C virus nonstructural 3/4A protease mutant to boceprevir using umbrella sampling simulation study. 2020, 38, 1938-1945  Disease-associated mutations alter the dynamic motion of the N-terminal domain of the human cardiac ryanodine receptor. 2020, 38, 1054-1070  Molecular description of the coil-to-globule transition of Poly(N-isopropylacrylamide) in water/ethanol mixture at low alcohol concentration. 2020, 297, 111928  Transferable coarse-grained models for poly(ethylene oxide)/poly(methyl methacrylate) blends. 2020, 172, 109346  Molecular Dynamics Simulations of Polymer-Ionic Liquid (1-Ethyl-3-methylimidazolium  | 2<br>2<br>17      |
| 745 744 743 742 741 | Insights into resistance mechanism of hepatitis C virus nonstructural 3/4A protease mutant to boceprevir using umbrella sampling simulation study. 2020, 38, 1938-1945  Disease-associated mutations alter the dynamic motion of the N-terminal domain of the human cardiac ryanodine receptor. 2020, 38, 1054-1070  Molecular description of the coil-to-globule transition of Poly(N-isopropylacrylamide) in water/ethanol mixture at low alcohol concentration. 2020, 297, 111928  Transferable coarse-grained models for poly(ethylene oxide)/poly(methyl methacrylate) blends. 2020, 172, 109346  Molecular Dynamics Simulations of Polymer-Ionic Liquid (1-Ethyl-3-methylimidazolium Tetracyanoborate) Ternary Electrolyte for Sodium and Potassium Ion Batteries. 2020, 60, 485-499  The investigation of the G-quadruplex aptamer selectivity to Pb ion: a joint molecular dynamics | 2<br>2<br>17<br>5 |

| 737 | Expression of Enterocin-P in HEK Platform: Evaluation of Its Cytotoxic Effects on Cancer Cell Lines and Its Potency to Interact with Cell-Surface Glycosaminoglycan by Molecular Modeling. <b>2020</b> , 26, 1503-1512 | 7  |
|-----|--|----|
| 736 | Polymyxin B Loosens Lipopolysaccharide Bilayer but Stiffens Phospholipid Bilayer. <b>2020</b> , 118, 138-150   | 22 |
| 735 | Properties of Aqueous Trehalose Mixtures: Glass Transition and Hydrogen Bonding. <b>2020</b> , 16, 1249-1262   | 12 |
| 734 | Development of a simple, molecular dynamics-based method to estimate the thickness of electrical double layers. <b>2020</b> , 84, 494-501  | 5  |
| 733 | Computational Peptide Engineering Approach for Selection the Best Engendered Camel Lactoferrin-Derive Peptide with Potency to Interact with DNA. <b>2020</b> , 26, 2203-2212   | 4  |
| 732 | Molecular Dynamics Study of the Human Beta-defensins 2 and 3 Chimeric Peptides with the Cell Membrane Model of Pseudomonas aeruginosa. <b>2020</b> , 26, 2039-2056   | 1  |
| 731 | Molecular Dynamics Simulations of the Hypoxia-Inducible Factor PAS-B Domain Confirm That Internally Bound Water Molecules Function To Stabilize the Protein Core for Ligand Binding. <b>2020</b> , 59, 450-459         | 2  |
| 730 | Release of Carbohydrate-Metal Adducts from Electrospray Droplets: Insight into Glycan Ionization by Electrospray. <b>2020</b> , 124, 479-486   | 10 |
| 729 | Competitive Adsorption of Metal Ions at Smectite/Water Interfaces: Mechanistic Aspects, and Impacts of Co-Ions, Charge Densities, and Charge Locations. <b>2020</b> , 124, 1500-1510                                   | 14 |
| 728 | Comparing the void space and long-range structure of an ionic liquid with a neutral mixture of similar sized molecules. <b>2020</b> , 299, 112121  | 6  |
| 727 | Solvate ionic liquids based on lithium bis(trifluoromethanesulfonyl)imide-glyme systems: coordination in MD simulations with scaled charges. <b>2020</b> , 22, 525-535   | 12 |
| 726 | The Lazy Life of Lipid-Linked Oligosaccharides in All Life Domains. <b>2020</b> , 60, 631-643  | 2  |
| 725 | Electrospun PVA-Dacarbazine nanofibers as a novel nano brain-implant for treatment of glioblastoma: in silico and in vitro characterization. <b>2020</b> , 143, 105183   | 20 |
| 724 | Molecular characterization of the outer membrane of Pseudomonas aeruginosa. <b>2020</b> , 1862, 183151   | 13 |
| 723 | Post-Translational Modifications at the Coarse-Grained Level with the SIRAH Force Field. <b>2020</b> , 60, 964-973   | 3  |
| 722 | The effect of the degree of substitution on the solubility of cellulose acetoacetates in water: A molecular dynamics simulation and density functional theory study. <b>2020</b> , 496, 108134                         | 3  |
| 721 | Simple corrections for the static dielectric constant of liquid mixtures from model force fields. <b>2020</b> , 22, 21741-21749  | 7  |
| 720 | Thermosensitive Hydration of Four Acrylamide-Based Polymers in Coil and Globule Conformations. <b>2020</b> , 124, 9745-9756  | 5  |

## (2020-2020)

| 719 | Small Molecule Inhibitors of DYRK1A Identified by Computational and Experimental Approaches. <b>2020</b> , 21,  | 1  |
|-----|---|----|
| 718 | Pressure control using stochastic cell rescaling. <b>2020</b> , 153, 114107   | 10 |
| 717 | Are all-atom any better than united-atom force fields for the description of liquid properties of alkanes?. <b>2020</b> , 26, 296                                   | 8  |
| 716 | Pulsed Electric Fields Can Create Pores in the Voltage Sensors of Voltage-Gated Ion Channels. <b>2020</b> , 119, 190-205  | 16 |
| 715 | Blockage of Store-Operated Ca Influx by Synta66 is Mediated by Direct Inhibition of the Ca Selective Orai1 Pore. <b>2020</b> , 12,                                  | 10 |
| 714 | Xenon Dynamics in Ionic Liquids: A Combined NMR and MD Simulation Study. <b>2020</b> , 124, 6617-6627   | 8  |
| 713 | DNA-binding mechanisms of human and mouse cGAS: a comparative MD and MM/GBSA study. <b>2020</b> , 22, 26390-26401   | 3  |
| 712 | Protein Dynamics Enables Phosphorylation of Buried Residues in Cdk2/Cyclin-A-Bound p27. <b>2020</b> , 119, 2010-2018  | 7  |
| 711 | Lipid-Chaperone Hypothesis: A Common Molecular Mechanism of Membrane Disruption by Intrinsically Disordered Proteins. <b>2020</b> , 11, 4336-4350                   | 38 |
| 710 | Molecular approach about the effect of water on the electrochemical behaviour of Ag ions in urea-choline chloride-water mixture. <b>2020</b> , 26, 339              | 3  |
| 709 | Molecular Cartography of A1 and A2 Asphaltene Subfractions from Classical Molecular Dynamics Simulations. <b>2020</b> , 34, 13954-13965                             | 6  |
| 708 | Tacticity Effects on the Bulk Modulus of Poly(methyl methacrylate) Explored by Coarse-Grained Simulations. <b>2020</b> , 124, 10811-10821                           | 2  |
| 707 | Refined Force Field for Liquid Sulfolane with Particular Emphasis to Its Transport Characteristics. <b>2020</b> , 5, 28285-28295                                    | 6  |
| 706 | Structural Fluctuations of Aromatic Residues in an Apo-Form Reveal Cryptic Binding Sites: Implications for Fragment-Based Drug Design. <b>2020</b> , 124, 9977-9986 | 5  |
| 705 | Theoretical insights into the effect of size and substitution patterns of azobenzene derivatives on the DNA G-quadruplex. <b>2020</b> , 22, 26944-26954             | 3  |
| 704 | Sampling Performance of Multiple Independent Molecular Dynamics Simulations of an RNA Aptamer. <b>2020</b> , 5, 20187-20201   | 3  |
| 703 | Modulating Apagregation by tyrosol-based ligands: The crucial role of the catechol moiety. <b>2020</b> , 265, 106434  | 15 |
| 702 | . 2020,   | 8  |

| 701 | Prediction of Mycobacterium tuberculosis pyrazinamidase function based on structural stability, physicochemical and geometrical descriptors. <b>2020</b> , 15, e0235643                         |    |
|-----|---|----|
| 700 | Microscopic Pressure Tensor in Cylindrical Geometry: Pressure of Water in a Carbon Nanotube. <b>2020</b> , 16, 5548-5561  | 9  |
| 699 | Molecular level insight into stability, activity, and structure of Laccase in aqueous ionic liquid and organic solvents: An experimental and computational research. <b>2020</b> , 317, 113925  | 3  |
| 698 | Destabilization potential of phenolics on Affibrils: mechanistic insights from molecular dynamics simulation. <b>2020</b> , 22, 19643-19658   | 10 |
| 697 | A novel approach to calculate protein adsorption isotherms by molecular dynamics simulations. <b>2020</b> , 1620, 460940  | 3  |
| 696 | Dueling Backbones: Comparing Peptoid and Peptide Analogues of a Mussel Adhesive Protein. <b>2020</b> , 53, 6767-6779  | 11 |
| 695 | Theoretical spectroscopy of isotopically dilute water and hydrophobicity. <b>2020</b> , 153, 094501   | 3  |
| 694 | Molecular modelling techniques for predicting liquid-liquid interfacial properties of methanol plus alkane (-hexane, -heptane, -octane) mixtures. <b>2020</b> , 22, 27121-27133                 | O  |
| 693 | Unravelling the drugability of MSI2 RNA recognition motif (RRM) protein and the prediction of their effective antileukemia inhibitors from traditional herb concoctions. <b>2020</b> , 1-14     |    |
| 692 | K channel C-type gating involves asymmetric selectivity filter order-disorder transitions. <b>2020</b> , 6,   | 23 |
| 691 | Specific elevated adsorption and stability of cations in the interlayer compared with at the external surface of clay minerals. <b>2020</b> , 198, 105814                                       | 8  |
| 690 | The allosteric activation mechanism of a phospholipase A-like toxin from Bothrops jararacussu venom: a dynamic description. <b>2020</b> , 10, 16252   | 7  |
| 689 | Polyol and sugar osmolytes can shorten protein hydrogen bonds to modulate function. <b>2020</b> , 3, 528  | 9  |
| 688 | A mechanochemical model for the simulation of molecules and molecular crystals under hydrostatic pressure. <b>2020</b> , 153, 134503  | 7  |
| 687 | Understanding how water models affect the anomalous pressure dependence of their diffusion coefficients. <b>2020</b> , 153, 104510  | O  |
| 686 | Discovery of potent inhibitors for SARS-CoV-2's main protease by ligand-based/structure-based virtual screening, MD simulations, and binding energy calculations. <b>2020</b> , 22, 23099-23106 | 18 |
| 685 | Benchmarking the performance of MM/PBSA in virtual screening enrichment using the GPCR-Bench dataset. <b>2020</b> , 34, 1133-1145   | 3  |
| 684 | Adduct of the blistering warfare agent sesquimustard with human serum albumin and its mass spectrometric identification for biomedical verification of exposure. <b>2020</b> , 412, 7723-7737   | 6  |
|     |   |    |

#### (2020-2020)

| 683 | Rigorous Computational Study Reveals What Docking Overlooks: Double Trouble from Membrane Association in Protein Kinase C Modulators. <b>2020</b> , 60, 5624-5633   | 4  |
|-----|---|----|
| 682 | Measles Virus Hemagglutinin Protein Establishes a Specific Interaction With the Extreme N-Terminal Region of Human Signaling Lymphocytic Activation Molecule to Enhance Infection. <b>2020</b> , 11, 1830   | 2  |
| 681 | Diffusivities in Binary Mixtures of [AMIM][NTf2] Ionic Liquids with the Dissolved Gases H2, He, N2, CO, CO2, or Kr Close to Infinite Dilution. <b>2020</b> , 65, 4116-4129  | 7  |
| 680 | Cryo-EM structure of human Cx31.3/GJC3 connexin hemichannel. <b>2020</b> , 6, eaba4996  | 19 |
| 679 | Practice of Simulation and Life Cycle Assessment in Tribology-A Review. <b>2020</b> , 13,   | 7  |
| 678 | Low-Frequency Spectra of 1-Methyl-3-octylimidazolium Tetrafluoroborate Mixtures with Methanol, Acetonitrile, and Dimethyl Sulfoxide: A Combined Study of Femtosecond Raman-Induced Kerr Effect Spectroscopy and Molecular Dynamics Simulations. <b>2020</b> , 124, 7857-7871    | 7  |
| 677 | Putative SARS-CoV-2 M Inhibitors from an In-House Library of Natural and Nature-Inspired Products: A Virtual Screening and Molecular Docking Study. <b>2020</b> , 25,   | 21 |
| 676 | Probing relaxation models by means of Fast Field-Cycling relaxometry, NMR spectroscopy and molecular dynamics simulations: Detailed insight into the translational and rotational dynamics of a protic ionic liquid. <b>2020</b> , 319, 114207                                  | 8  |
| 675 | Supercomputer-Based Ensemble Docking Drug Discovery Pipeline with Application to Covid-19. <b>2020</b> , 60, 5832-5852  | 71 |
| 674 | Intrinsic water layering next to soft, solid, hydrophobic, and hydrophilic substrates. <b>2020</b> , 153, 224702  | 1  |
| 673 | Bottom-up derived flexible water model with dipole and quadrupole moments for coarse-grained molecular simulations. <b>2020</b> , 22, 27394-27412   | 2  |
| 672 | Lubricated friction around nanodefects. <b>2020</b> , 6, eaaz3673   | 13 |
| 671 | Comparative Study of the Biphasic Behavior of Cyanex301 and Its Two Analogs by Molecular Dynamics Simulations. <b>2020</b> , 3, 1900242   | Ο  |
| 670 | Structural investigations of molecular solutes within nanostructured ionic liquids. <b>2020</b> , 22, 11593-11608   | 2  |
| 669 | Exploring the Reaction Mechanism of HIV Reverse Transcriptase with a Nucleotide Substrate. <b>2020</b> , 124, 4270-4283   | 5  |
| 668 | Structural basis for divergent and convergent evolution of catalytic machineries in plant aromatic amino acid decarboxylase proteins. <b>2020</b> , 117, 10806-10817  | 15 |
| 667 | Binary Mixtures of Aromatic Compounds (n-Propylbenzene, 1,3,5-Trimethylbenzene, and 1,2,4-Trimethylbenzene) with 2,2,4,6,6-Pentamethylheptane: Densities, Viscosities, Speeds of Sound, Bulk Moduli, Surface Tensions, and Flash Points at 0.1 MPa. <b>2020</b> , 65, 2625-2641 | 10 |
| 666 | Molecular-weight dependence of simulated glass transition temperature for isolated poly(ethylene oxide) chain. <b>2020</b> , 46, 727-735  | 4  |

| 665 | Flexibility of intrinsically disordered degrons in AUX/IAA proteins reinforces auxin co-receptor assemblies. <b>2020</b> , 11, 2277  | 18  |
|-----|--|-----|
| 664 | Serine 298 Phosphorylation in Linker 2 of UHRF1 Regulates Ligand-Binding Property of Its Tandem Tudor Domain. <b>2020</b> , 432, 4061-4075   | 3   |
| 663 | Origin of Unusual Acidity and Li Diffusivity in a Series of Water-in-Salt Electrolytes. <b>2020</b> , 124, 5284-5291   | 14  |
| 662 | Atomic scale investigation of the volume phase transition in concentrated PNIPAM microgels. <b>2020</b> , 152, 204904  | 5   |
| 661 | Molecular dynamics study of functionally relevant interdomain and active site interactions in the autotransporter esterase EstA from Pseudomonas aeruginosa. <b>2020</b> , 46, 743-756 |     |
| 660 | A synthetic ion channel with anisotropic ligand response. <b>2020</b> , 11, 2924   | 19  |
| 659 | 1D hypo-crystals: A novel concept for the crystallization of stereo-irregular polymers. <b>2020</b> , 40, 26-37  | 6   |
| 658 | Tracking Ca ATPase intermediates in real time by x-ray solution scattering. <b>2020</b> , 6, eaaz0981  | 21  |
| 657 | Interaction between Myricetin Aggregates and Lipase under Simplified Intestinal Conditions. <b>2020</b> , 9,   | 1   |
| 656 | Protein docking and steered molecular dynamics suggest alternative phospholamban-binding sites on the SERCA calcium transporter. <b>2020</b> , 295, 11262-11274                        | 7   |
| 655 | Theoretical studies on 1,4-dihydropyridine derivatives as P-glycoprotein allosteric inhibitors: insights on symmetry and stereochemistry. <b>2021</b> , 39, 4752-4763                  | 4   |
| 654 | Improved Parameterization of Protein-DNA Interactions for Molecular Dynamics Simulations of PCNA Diffusion on DNA. <b>2020</b> , 16, 4006-4013   | 12  |
| 653 | Dimerization of A椰0 inside dipalmitoylphosphatidylcholine bilayer and its effect on bilayer integrity: Atomistic simulation at three temperatures. <b>2020</b> , 88, 1540-1552         | 3   |
| 652 | Developing a Fully Glycosylated Full-Length SARS-CoV-2 Spike Protein Model in a Viral Membrane. <b>2020</b> , 124, 7128-7137   | 131 |
| 651 | References. <b>2020</b> , 297-315  |     |
| 650 | Invasion of Pb2+ into montmorillonite-illite clay and the response of interlayer K+ and water. <b>2020</b> , 194, 105693   | 8   |
| 649 | S92 phosphorylation induces structural changes in the N-terminus domain of human mitochondrial calcium uniporter. <b>2020</b> , 10, 9131   | 5   |
| 648 | The Atypical Protein Kinase C Small Molecule Inhibitor Estat, and Its Effects on Invasion Through Decreases in PKC-Protein Expression. <b>2020</b> , 10, 209                           | 3   |

| 647 | Molecular Dynamics Simulations in Statistical Physics: Theory and Applications. 2020,   | 5  |
|-----|---|----|
| 646 | High-content imaging and structure-based predictions reveal functional differences between Niemann-Pick C1 variants. <b>2020</b> , 21, 386-397  | 5  |
| 645 | Computational analysis of amino acids[adhesion to the graphene surface. 2020, 74, 1   | 1  |
| 644 | Electrostatic Interactions Govern Extreme Nascent Protein Ejection Times from Ribosomes and Can<br>Delay Ribosome Recycling. <b>2020</b> , 142, 6103-6110                               | 15 |
| 643 | Probing the Accuracy of Explicit Solvent Constant pH Molecular Dynamics Simulations for Peptides. <b>2020</b> , 16, 2561-2569   | 3  |
| 642 | Coarse-graining of polyisoprene melts using inverse Monte Carlo and local density potentials. <b>2020</b> , 152, 124902   | 14 |
| 641 | Molecular mechanism of the skin permeation enhancing effect of ethanol: a molecular dynamics study <b>2020</b> , 10, 12234-12248  | 13 |
| 640 | Common cancer mutations R175H and R273H drive the p53 DNA-binding domain towards aggregation-prone conformations. <b>2020</b> , 22, 9225-9232   | 7  |
| 639 | Development and Characterization of the Shortest Anti-Adhesion Peptide Analogue of B49Mod1. <b>2020</b> , 25,   | 2  |
| 638 | Self-assembly of small molecules at hydrophobic interfaces using group effect. <b>2020</b> , 12, 5452-5463  | 16 |
| 637 | Symmetry-breaking transitions in the early steps of protein self-assembly. 2020, 49, 175-191  | 19 |
| 636 | Structure and Dynamics of a Thermostable Alcohol Dehydrogenase from the Antarctic Psychrophile sp. TAE123. <b>2020</b> , 5, 14523-14534   | 5  |
| 635 | Capsular GXM Conformation and Epitope Presentation: A Molecular Modelling Study. 2020, 25,  | 7  |
| 634 | Insights into the mechanism of inhibition of phospholipase A2 by resveratrol: An extensive molecular dynamics simulation and binding free energy calculation. <b>2020</b> , 100, 107649 | 4  |
| 633 | Development and application of coarse-grained MARTINI model of skin lipid ceramide [AP]. <b>2020</b> , 26, 182  | 1  |
| 632 | Acquired Functional Capsid Structures in Metazoan Totivirus-like dsRNA Virus. <b>2020</b> , 28, 888-896.e3  | 4  |
| 631 | Calcium-Lipid Interactions Observed with Isotope-Edited Infrared Spectroscopy. <b>2020</b> , 118, 2694-2702   | 5  |
| 630 | Studying O pathways in [NiFe]- and [NiFeSe]-hydrogenases. <b>2020</b> , 10, 10540   | 2  |

| 629 | Non-conventional force fields for applications in spectroscopy and chemical reaction dynamics. <b>2020</b> , 153, 010901   | 10 |
|-----|--|----|
| 628 | Theoretical insights on helix repacking as the origin of P-glycoprotein promiscuity. <b>2020</b> , 10, 9823  | 9  |
| 627 | Insights into the Emerging Networks of Voids in Simulated Supercooled Water. <b>2020</b> , 124, 2180-2190  | 9  |
| 626 | Mixing states of imidazolium-based ionic liquid, [Cmim][TFSI], with cycloethers studied by SANS, IR, and NMR experiments and MD simulations. <b>2020</b> , 22, 5332-5346                             | 1  |
| 625 | Charge-dependent interactions of monomeric and filamentous actin with lipid bilayers. <b>2020</b> , 117, 5861-5872   | 12 |
| 624 | Hexagonal arrangement of phospholipids in bilayer membranes. <b>2020</b> , 29, 030505  | 2  |
| 623 | The self-assembly and microscopic interfacial properties of a supercritical CO2 microemulsion having hydrotropes: Atom-level observation from molecular dynamics simulation. <b>2020</b> , 38, 77-87 | 4  |
| 622 | SAMPL6 host-guest binding affinities and binding poses from spherical-coordinates-biased simulations. <b>2020</b> , 34, 589-600  | 16 |
| 621 | Response Theory for Static and Dynamic Solvation of Ionic and Dipolar Solutes in Water. <b>2020</b> , 180, 721-738   | 2  |
| 620 | New insights on the role of ROS in the mechanisms of sonoporation-mediated gene delivery. <b>2020</b> , 64, 104998   | 7  |
| 619 | Dynamical Model for the Counteracting Effects of Trimethylamine -Oxide on Urea in Aqueous Solutions under Pressure. <b>2020</b> , 124, 1978-1986   | 3  |
| 618 | Novel Sequence Feature of SecA Translocase Protein Unique to the Thermophilic Bacteria: Bioinformatics Analyses to Investigate Their Potential Roles. <b>2019</b> , 8,                               | 2  |
| 617 | Mutual and Thermal Diffusivities as well as Fluid-Phase Equilibria of Mixtures of 1-Hexanol and Carbon Dioxide. <b>2020</b> , 124, 2482-2494   | 18 |
| 616 | Interfacial structure in the liquid-liquid extraction of rare earth elements by phosphoric acid ligands: a molecular dynamics study. <b>2020</b> , 22, 4177-4192                                     | 5  |
| 615 | Performing solvation free energy calculations in LAMMPS using the decoupling approach. <b>2020</b> , 34, 641-646   | 5  |
| 614 | Potential tripeptides against the tyrosine kinase domain of human epidermal growth factor receptor (HER) 2 through computational and kinase assay approaches. <b>2020</b> , 97, 107564               | 3  |
| 613 | Predicting Partition Coefficients of Neutral and Charged Solutes in the Mixed SLES-Fatty Acid Micellar System. <b>2020</b> , 124, 1653-1664  | 2  |
| 612 | Comparing Alchemical Free Energy Estimates to Experimental Values Based on the Ben-Naim Formula: How Much Agreement Can We Expect?. <b>2020</b> , 124, 840-847                                       | 1  |

| 611 | Interaction of camel Lactoferrin derived peptides with DNA: a molecular dynamics study. <b>2020</b> , 21, 60  | 6  |
|-----|---|----|
| 610 | Cryo-Electron Microscopy Structure of the ⊞IIb <b>B</b> -Abciximab Complex. <b>2020</b> , 40, 624-637   | 8  |
| 609 | Molecular Insight into the Interaction between Camptothecin and Acyclic Cucurbit[4]urils as Efficient Nanocontainers in Comparison with Cucurbit[7]uril: Molecular Docking and Molecular Dynamics Simulation. <b>2020</b> , 60, 1791-1803 | 6  |
| 608 | Liquid I iquid Phase Behavior of Solutions of 1,3-Diethylimidazolium Bis((trifluoromethyl)sulfonyl)amide in n-Alkyl Alcohols. <b>2020</b> , 65, 1345-1357   | 3  |
| 607 | Current Status of Carbohydrates Information in the Protein Data Bank. <b>2020</b> , 60, 684-699   | 13 |
| 606 | Phase Separation in Atomistic Simulations of Model Membranes. <b>2020</b> , 142, 2844-2856  | 28 |
| 605 | Evolution of Angiotensin Peptides and Peptidomimetics as Angiotensin II Receptor Type 2 (AT2) Receptor Agonists. <b>2020</b> , 10,  | 7  |
| 604 | Structural and Functional Analysis of Gly212 Mutants Reveals the Importance of Intersubunit Interactions in ASIC1a Channel Function. <b>2020</b> , 7, 58  | 1  |
| 603 | Lennard-Jones Parameters Determined to Reproduce the Solubility of NaCl and KCl in SPC/E, TIP3P, and TIP4P/2005 Water. <b>2020</b> , 16, 2460-2473  | 22 |
| 602 | Unexpected electrochemical behavior of an anolyte redoxmer in flow battery electrolytes: solvating cations help to fight against the thermodynamic@inetic dilemma. 2020, 8, 13470-13479   | 8  |
| 601 | Activation and selectivity of OTUB-1 and OTUB-2 deubiquitinylases. <b>2020</b> , 295, 6972-6982   | 10 |
| 600 | PDADMAC/PSS Oligoelectrolyte Multilayers: Internal Structure and Hydration Properties at Early Growth Stages from Atomistic Simulations. <b>2020</b> , 25,  | 1  |
| 599 | Sodium-salt adduct fullerenes prevent self-association and amyloid Fibril formation: molecular dynamics approach. <b>2020</b> , 18, 335-347   | 1  |
| 598 | Pressure-temperature diagram of wetting and dewetting in a hydrophobic grain boundary and the liquidlike to icelike transition of monolayer water. <b>2020</b> , 101,   | 1  |
| 597 | Structural and molecular insight into the pH-induced low-permeability of the voltage-gated potassium channel Kv1.2 through dewetting of the water cavity. <b>2020</b> , 16, e1007405  | 2  |
| 596 | Temperature and molecular crowding effects on the sensitivity of T30695 aptamer toward Pb2+ ion: a joint molecular dynamics simulation and experimental study. <b>2020</b> , 46, 592-603  | 4  |
| 595 | Molecular dynamics simulations in photosynthesis. <b>2020</b> , 144, 273-295  | 25 |
| 594 | Role of Asp190 in the Phosphorylation of the Antibiotic Kanamycin Catalyzed by the Aminoglycoside Phosphotransferase Enzyme: A Combined QM:QM and MD Study. <b>2020</b> , 124, 3494-3504  | 2  |

| 593 | Novel "ruthenium cyclopentadienyl"-peptide conjugate complexes against human FGFR(+) breast cancer. <b>2020</b> , 49, 5974-5987  | 5  |
|-----|--|----|
| 592 | Phosphorylation-dependent conformational changes of arrestin in the rhodopsin-arrestin complex. <b>2020</b> , 22, 9330-9338  | 1  |
| 591 | Generation of an engineered food-grade Lactococcus lactis strain for production of an antimicrobial peptide: in vitro and in silico evaluation. <b>2020</b> , 20, 19   | 7  |
| 590 | Quantum chemical modeling of molecules under pressure. <b>2021</b> , 121, e26208   | 8  |
| 589 | Investigation of Atrial Natriuretic Peptide as A Competitive Inhibitory Candidate Against Wnt/(Catenin Signalling: A Molecular Dynamics Approach. <b>2021</b> , 27, 353-363                                  |    |
| 588 | Structure, Dynamics, and Interactions of GPI-Anchored Human Glypican-1 with Heparan Sulfates in a Membrane. <b>2021</b> , 31, 593-602  | 1  |
| 587 | In vitro identification of imidazo[1,2-a]pyrazine-based antileishmanial agents and evaluation of L. major casein kinase 1 inhibition. <b>2021</b> , 210, 112956  | 4  |
| 586 | Signaling Mechanism of Phytochromes in Solution. <b>2021</b> , 29, 151-160.e3  | 6  |
| 585 | Structural and dynamical insights into the PH domain of p62 in human TFIIH. <b>2021</b> , 49, 2916-2930  | 3  |
| 584 | Imidazolinium-based Multiblock Amphiphile as Transmembrane Anion Transporter. <b>2021</b> , 16, 147-157  | 6  |
| 583 | Inhibition of Silica Nanoparticle Adhesion to Poly(vinyl alcohol) Surfaces by Ammonia-Mediated Hydration: Implications for Effective Post-Chemical Mechanical Planarization Cleaning. <b>2021</b> , 4, 71-83 | 2  |
| 582 | Modeling Molecules under Pressure with Gaussian Potentials. <b>2021</b> , 17, 583-597  | 5  |
| 581 | Molecular dynamics simulations of aqueous solutions of short chain alcohols. Excess properties and the temperature of maximum density. <b>2021</b> , 528, 112840   | 7  |
| 580 | Molecular dynamics study on TOTO-based ionic liquids with different cations. <b>2021</b> , 529, 112870   |    |
| 579 | Effects of paraffin, fatty acid and long alkyl chain phenol on the solidification of n-hexadecane under harsh subcooling condition: A molecular dynamics simulation study. <b>2021</b> , 285, 119029         | 2  |
| 578 | SAMPL7 TrimerTrip host-guest binding poses and binding affinities from spherical-coordinates-biased simulations. <b>2021</b> , 35, 105-115   | 13 |
| 577 | Elucidation the binding mechanism of -derived isoquinoline alkaloids as Rho-kinase 1 inhibitors by molecular docking and dynamic simulation. <b>2021</b> , 39, 379-394                                       | 3  |
| 576 | Identifying the key residues instrumental in imparting stability to amyloid beta protofibrils - a comparative study using MD simulations of 17-42 residues. <b>2021</b> , 39, 431-456                        | 5  |

| 575 | Molecular Basis of the Anticancer and Antibacterial Properties of CecropinXJ Peptide: An In Silico Study. <b>2021</b> , 22,   | 7 |
|-----|---|---|
| 574 | In silico study of the interactions of Pilocarpus microphyllus imidazolic alkaloids with the main protease (Mpro) of SARS-CoV-2. <b>2021</b> , 47, 74-87  | 4 |
| 573 | Linker residues regulate the activity and stability of hexokinase 2, a promising anticancer target. <b>2021</b> , 296, 100071   | 1 |
| 572 | Identification of Pan-Assay INterference compoundS (PAINS) Using an MD-Based Protocol. <b>2021</b> , 2315, 263-271  | 1 |
| 571 | Evaluation of drug repositioning by molecular docking of pharmaceutical resources available in the Brazilian healthcare system against SARS-CoV-2. <b>2021</b> , 23, 100539                                 | 6 |
| 570 | Molecular dynamics study on the inhibition mechanisms of ReACp53 peptide for p53-R175H mutant aggregation. <b>2021</b> , 23, 23032-23041  | O |
| 569 | Identification and characterisation of putative drug binding sites in human ATP-binding cassette B5 (ABCB5) transporter. <b>2021</b> , 19, 691-704  | 3 |
| 568 | Asymmetric dynamics of dimeric SARS-CoV-2 and SARS-CoV main proteases in an apo form: Molecular dynamics study on fluctuations of active site, catalytic dyad, and hydration water. <b>2021</b> , 1, 100016 | 2 |
| 567 | Polyphenols Weaken Pea Protein Gel by Formation of Large Aggregates with Diminished Noncovalent Interactions. <b>2021</b> , 22, 1001-1014   | 7 |
| 566 | Autism associated SHANK3 missense point mutations impact conformational fluctuations and protein turnover at synapses.  | 2 |
| 565 | Aggregation of the Dipeptide Leu-Gly in Alcohol-Water Binary Solvents Elucidated from the Solvation Structure for Each Moiety. <b>2021</b> , 125, 240-252   | O |
| 564 | Molecular interactions of the 'M and E integral membrane proteins of SARS-CoV-2. <b>2021</b> ,  | 5 |
| 563 | Physico-chemical properties of 4-(methylnitrosamino)-1-(3-pyridyl)-1-butanone (NNK) diazonium ion: a theoretical investigation <b>2021</b> , 11, 26750-26762  |   |
| 562 | Contact Ion Pairs in the Bulk Affect Anion Interactions with Poly(-isopropylacrylamide). <b>2021</b> , 125, 680-688   | 5 |
| 561 | pK Calculations in Membrane Proteins from Molecular Dynamics Simulations. <b>2021</b> , 2315, 185-195   | 1 |
| 560 | USING VORONOI DIAGRAMS TO INTERPRET BULK PROPERTIES OF SOLUTIONS. <b>2021</b> , 62, 58-69   | 2 |
| 559 | NMR and MD simulations reveal the impact of the V23D mutation on the function of yeast oligosaccharyltransferase subunit Ost4. <b>2021</b> , 31, 838-850  | 1 |
| 558 | A method for detection of permeation events in Molecular Dynamics simulations of lipid bilayers.  | 1 |

| 557 | Thermodynamics of DNA Hybridization from Atomistic Simulations. 2021, 125, 771-779   | 4  |
|-----|--|----|
| 556 | Predicting stable binding modes from simulated dimers of the D76N mutant of 2-microglobulin. <b>2021</b> , 19, 5160-5169   | O  |
| 555 | A structural view onto disease-linked mutations in the human neutral amino acid exchanger ASCT1. <b>2021</b> , 19, 5246-5254   | 0  |
| 554 | Electric field-induced gas dissolving in aqueous solutions. <b>2021</b> , 154, 024705  | 10 |
| 553 | A new equation for period vectors of crystals under external stress and temperature in statistical physics: mechanical equilibrium condition and equation of state. <b>2021</b> , 136, 1                                     |    |
| 552 | Albumin Alters the Conformational Ensemble of Amyloid- by Promiscuous Interactions: Implications for Amyloid Inhibition. <b>2020</b> , 7, 629520   | 4  |
| 551 | Assembly of [Ni(Schiff)] Films on an Inert Surface: A Multiscale Computational Study. <b>2021</b> , 125, 2926-2937   | 3  |
| 550 | Investigating crosstalk among PTMs provides novel insight into the structural basis underlying the differential effects of Nt17 PTMs on mutant Httex1 aggregation.   |    |
| 549 | Influence of the Environment on Shaping the Absorption of Monomeric Infrared Fluorescent Proteins. <b>2021</b> , 125, 2231-2240  | O  |
| 548 | On the stability of protein DNA complexes in molecular dynamics simulations using the CUFIX corrections. <b>2021</b> , 78, 461-466   | 4  |
| 547 | A synergetic effect of BARD1 mutations on tumorigenesis. <b>2021</b> , 12, 1243  | 7  |
| 546 | Semi-automated Optimization of the CHARMM36 Lipid Force Field to Include Explicit Treatment of Long-Range Dispersion. <b>2021</b> , 17, 1562-1580  | 6  |
| 545 | Visualization of the mechanosensitive ion channel MscS under membrane tension. <b>2021</b> , 590, 509-514  | 22 |
| 544 | Computational Analysis Reveals a Critical Point Mutation in the -Terminal Region of the Signaling Lymphocytic Activation Molecule Responsible for the Cross-Species Infection with Canine Distemper Virus. <b>2021</b> , 26, | 1  |
| 543 | Quasi-Universal Solubility Behavior of Light Gases in Imidazolium-Based Ionic Liquids with Varying Anions: A Molecular Dynamics Simulation Study. <b>2021</b> , 125, 1647-1659   | 4  |
| 542 | Quantum Simulations of Hydrogen Bonding Effects in Glycerol Carbonate Electrolyte Solutions. <b>2021</b> , 125, 2157-2166  | 4  |
| 541 | Ionic Liquid for PEDOT:PSS Treatment. Ion Binding Free Energy in Water Revealing the Importance of Anion Hydrophobicity. <b>2021</b> , 125, 1916-1923  | 9  |
| 540 | Insights into the Solubility of Poly(vinylphenothiazine) in Carbonate-Based Battery Electrolytes. <b>2021</b> , 13, 12442-12453  | 8  |

| 539 | High Li-ion conductivity in tetragonal LGPO: A comparative first-principles study against known LISICON and LGPS phases. <b>2021</b> , 5,  | 2  |
|-----|--|----|
| 538 | Enhancing the loading and swelling capacity of cellulose crystal through difunctional and multifunctional epoxy crosslinkers and the effects on the elasticity and plasticity: A computational study. <b>2021</b> , 1228, 129436 |    |
| 537 | Determining the hydration free energies of selected small molecules with MP2 and local MP2 through adaptive force matching. <b>2021</b> , 154, 104113  | 2  |
| 536 | Mixing of Surfactin, an Anionic Biosurfactant, with Alkylbenzene Sulfonate, a Chemically Synthesized Anionic Surfactant, at the n-Decane/Water Interface. <b>2021</b> , 24, 445-457  | 3  |
| 535 | Interfacial Polarization and Ionic Structure at the Ionic Liquid-Metal Interface Studied by Vibrational Spectroscopy and Molecular Dynamics Simulations. <b>2021</b> , 125, 2741-2753  | 5  |
| 534 | Interface water-induced hydrophobic carbon chain unfolding in water. <b>2021</b> , 73, 055602  | 2  |
| 533 | Two-dimensional simulated tempering for the isobaric bothermal ensemble with fast on-the-fly weight determination. <i>Molecular Physics</i> , e1904156   |    |
| 532 | Structures and spectroscopic properties of low-energy candidate structures for toluene-(H2O)n (n=1🛮 0) clusters. <b>2021</b> , 326, 115213   |    |
| 531 | Structure, Dynamics, Receptor Binding, and Antibody Binding of the Fully Glycosylated Full-Length SARS-CoV-2 Spike Protein in a Viral Membrane. <b>2021</b> , 17, 2479-2487  | 26 |
| 530 | A potential interaction between the SARS-CoV-2 spike protein and nicotinic acetylcholine receptors. <b>2021</b> , 120, 983-993   | 18 |
| 529 | Moving toward generalizable NZ-1 labeling for 3D structure determination with optimized epitope-tag insertion. <b>2021</b> , 77, 645-662   | 7  |
| 528 | Conformational Plasticity-Rigidity Axis of the Coagulation Factor VII Zymogen Elucidated by Atomistic Simulations of the N-Terminally Truncated Factor VIIa Protease Domain. <b>2021</b> , 11,                                   | 1  |
| 527 | Interaction of Peptides Containing CRAC Motifs with Lipids in Membranes of Various Composition. <b>2021</b> , 15, 120-129  |    |
| 526 | Multilevel summation for periodic electrostatics using B-splines. <b>2021</b> , 154, 144105  | O  |
| 525 | Molecular Dynamics Studies of Therapeutic Liquid Mixtures and Their Binding to Mycobacteria. <b>2021</b> , 12, 626735  | 2  |
| 524 | Antimicrobial Bombinin-like Peptide 3 Selectively Recognizes and Inserts into Bacterial Biomimetic Bilayers in Multiple Steps. <b>2021</b> , 64, 5185-5197   | 3  |
| 523 | Molecular interactions of the M and E integral membrane proteins of SARS-CoV-2. <b>2021</b> ,  | 3  |
| 522 | Asymmetric CorA Gating Mechanism as Observed by Molecular Dynamics Simulations. <b>2021</b> , 61, 2407-2417  | 1  |

| 521 | Glycan-Induced Protein Dynamics in Human Norovirus P Dimers Depend on Virus Strain and Deamidation Status. <b>2021</b> , 26,   | 3  |
|-----|--|----|
| 520 | Diffusivities in Binary Mixtures of n-Hexane or 1-Hexanol with Dissolved CH4, Ne, Kr, R143a, SF6, or R236fa Close to Infinite Dilution. <b>2021</b> , 66, 2218-2232  | 2  |
| 519 | Balance Between Contact and Solvent-Separated Ion Pairs in Mixtures of the Protic Ionic Liquid [EtNH][MeSO] with Water Controlled by Water Content and Temperature. <b>2021</b> , 125, 4476-4488   | 3  |
| 518 | Modeled 3D-Structures of Proteobacterial Transglycosylases from Glycoside Hydrolase Family 17 Give Insight in Ligand Interactions Explaining Differences in Transglycosylation Products. <b>2021</b> , 11, 4048  | 1  |
| 517 | Viscosity, Interfacial Tension, and Density of Binary-Liquid Mixtures of n-Hexadecane with n-Octacosane, 2,2,4,4,6,8,8-Heptamethylnonane, or 1-Hexadecanol at Temperatures between 298.15 and 573.15 K by Surface Light Scattering and Equilibrium Molecular Dynamics Simulations. | 5  |
| 516 | <b>2021</b> , 66, 2264-2280  Understanding and Characterizing the Drug Sorption to PVC and PE Materials. <b>2021</b> , 13, 18594-18603   | 1  |
| 515 | CHARMM-GUI Polymer Builder for Modeling and Simulation of Synthetic Polymers. <b>2021</b> , 17, 2431-2443  | 12 |
| 514 | Electrical conductivity variations of aqueous NaCl solutions with microwave field: A molecular dynamics study. <b>2021</b> , 545, 111134   | 3  |
| 513 | Structural Basis for Selective Oxidation of Phosphorylated Ethylphenols by Cytochrome P450 Monooxygenase CreJ. <b>2021</b> , 87,   | 1  |
| 512 | Efficient isotropic water desalination in anisotropic lamellar nano-channels formed by layered black phosphorus membrane. <b>2021</b> , 504, 114962  | 6  |
| 511 | Fick Diffusion Coefficient in Binary Mixtures of [HMIM][NTf] and Carbon Dioxide by Dynamic Light Scattering and Molecular Dynamics Simulations. <b>2021</b> , 125, 5100-5113   | 3  |
| 510 | Frizzled BRET sensors based on bioorthogonal labeling of unnatural amino acids reveal WNT-induced dynamics of the cysteine-rich domain.  |    |
| 509 | Fisetin inhibits tau aggregation by interacting with the protein and preventing the formation of <code>btrands</code> . <b>2021</b> , 178, 381-393   | 6  |
| 508 | Dynamic Interactions of Fully Glycosylated SARS-CoV-2 Spike Protein with Various Antibodies. <b>2021</b>   |    |
| 507 | Autism-associated missense point mutations impact conformational fluctuations and protein turnover at synapses. <b>2021</b> , 10,  | 5  |
| 506 | Implementation of the Freely Jointed Chain Model to Assess Kinetics and Thermodynamics of Thermosensitive Coil-Globule Transition by Markov States. <b>2021</b> , 125, 4898-4909   | O  |
| 505 | Force Field Benchmark of Amino Acids. 3. Hydration with Scaled Lennard-Jones Interactions. <b>2021</b> , 61, 3571-3582   | 3  |
| 504 | Molecular dynamics simulations of phospholipid bilayer mechanoporation under different strain states comparison between GROMACS and LAMMPS. <b>2021</b> , 29, 055015   | O  |

| 503 | Developing and Assessing Nonbonded Dummy Models of Magnesium Ion with Different Hydration Free Energy References. <b>2021</b> , 61, 2981-2997   | 2  |
|-----|---|----|
| 502 | Hyperdynamics simulations with ab initio forces. <b>2021</b> , 154, 214112  |    |
| 501 | Destabilization of the Alzheimer's amyloid-protofibrils by THC: A molecular dynamics simulation study. <b>2021</b> , 105, 107889  | 1  |
| 500 | Multipronged Regulatory Functions of Serum Albumin in Early Stages of Amyloid-再ggregation. <b>2021</b> , 12, 2409-2420  | 1  |
| 499 | Residue 6.43 defines receptor function in class F GPCRs. <b>2021</b> , 12, 3919   | 5  |
| 498 | Cryo-EM structure of the photosynthetic RC-LH1-PufX supercomplex at 2.8-Iresolution. 2021, 7,   | 15 |
| 497 | Evaluation of Host Defense Peptide (CaD23)-Antibiotic Interaction and Mechanism of Action: Insights from Experimental and Molecular Dynamics Simulations Studies.   | 1  |
| 496 | Mechanism of Vitamin D Receptor Ligand-Binding Domain Regulation Studied by gREST Simulations. <b>2021</b> , 61, 3625-3637  | Ο  |
| 495 | Molecular Dynamics Simulations of Complexation of Am(III) with a Preorganized Dicationic Ligand in an Ionic Liquid. <b>2021</b> , 125, 8532-8538  | 1  |
| 494 | Rosmarinic Acid Potently Detoxifies Amylin Amyloid and Ameliorates Diabetic Pathology in a Transgenic Rat Model of Type 2 Diabetes. <b>2021</b> , 4, 1322-1337  | 4  |
| 493 | A computational study of the interface interaction between SARS-CoV-2 RBD and ACE2 from human, cat, dog, and ferret. <b>2021</b> ,  | 1  |
| 492 | Performing Molecular Dynamics Simulations and Computing Hydration Free Energies on the B3LYP-D3(BJ) Potential Energy Surface with Adaptive Force Matching: A Benchmark Study with Seven Alcohols and One Amine <b>2021</b> , 1, 14-24 | 3  |
| 491 | Investigating Crosstalk Among PTMs Provides Novel Insight Into the Structural Basis Underlying the Differential Effects of Nt17 PTMs on Mutant Httex1 Aggregation. <b>2021</b> , 8, 686086  | 3  |
| 490 | An Enhanced Scheme for Multiscale Modeling of Thermomechanical Properties of Polymer Bulks. <b>2021</b> , 125, 8612-8626  | O  |
| 489 | Predicting stable binding modes from simulated dimers of the D76N mutant of <b>2</b> -microglobulin.  |    |
| 488 | Rational Design of Nonbonded Point Charge Models for Divalent Metal Cations with Lennard-Jones 12-6 Potential. <b>2021</b> , 61, 4031-4044  | 2  |
| 487 | Effect of the single mutation N9Y on the catalytical properties of xylanase Xyn11A from Cellulomonas uda: a biochemical and molecular dynamic simulation analysis. <b>2021</b> , 85, 1971-1985  | 1  |
| 486 | Differential Reversible and Irreversible Interactions between Benzbromarone and Human Cytochrome P450s 3A4 and 3A5. <b>2021</b> , 100, 224-236  | 4  |

Switching Promotor Recognition of Phage RNA Polymerase in Silico Following Path along Lab Directed Evolution.

| 484             | Modulation of Phospholipid Bilayer Properties by Simvastatin. <b>2021</b> , 125, 8406-8418   | 1  |
|-----------------|--|----|
| 483             | New (Iso)quinolinyl-pyridine-2,6-dicarboxamide G-Quadruplex Stabilizers. A Structure-Activity Relationship Study. <b>2021</b> , 14,  | 2  |
| 482             | The impacts of net charge on the water dispersity of nanoparticles. <b>2021</b> , 117105   |    |
| 481             | Insights into the orientation and hydrogen bond influence on thermophysical and transport properties in choline-based deep eutectic solvents and methanol. <b>2021</b> , 117019                      | 2  |
| 480             | Viscosity and Interfacial Tension of Binary Mixtures of n-Hexadecane with Dissolved Gases Using Surface Light Scattering and Equilibrium Molecular Dynamics Simulations. <b>2021</b> , 66, 3205-3218 | 5  |
| 479             | Molecular Dynamics of PEDOT:PSS Treated with Ionic Liquids. Origin of Anion Dependence Leading to Cation Design Principles. <b>2021</b> , 125, 8601-8611   | 3  |
| 478             | Ionic-Group Dependence of Polyelectrolyte Coacervate Phase Behavior. <b>2021</b> , 54, 7572-7581   | O  |
| 477             | Determining structure and action mechanism of LBF14 by molecular simulation. <b>2021</b> , 1-12  | O  |
| 476             | Normal mode calculation and infrared spectroscopy of proteins in water solution: Relationship between amide I transition dipole strength and secondary structure. <b>2021</b> , 185, 369-376         | 1  |
| 475             | The formation and growth model of a CO2 hydrate layer based on molecular dynamics. e17406  | 1  |
| 474             | On the molecular origins of the ferroelectric splay nematic phase. <b>2021</b> , 12, 4962  | 14 |
| 473             | Iron coordination to pyochelin siderophore influences dynamics of FptA receptor from Pseudomonas aeruginosa: a molecular dynamics simulation study. <b>2021</b> , 34, 1099-1119                      | 1  |
| 472             | Allosteric regulation in CRISPR/Cas1-Cas2 protospacer acquisition mediated by DNA and Cas2. <b>2021</b> , 120, 3126-3137   | 1  |
| 47 <sup>1</sup> | Structure-guided glyco-engineering of ACE2 for improved potency as soluble SARS-CoV-2 decoy receptor.  | 1  |
| 470             | Antimicrobial peptide induced colloidal transformations in bacteria-mimetic vesicles: Combining in silico tools and experimental methods. <b>2021</b> , 596, 352-363                                 | 5  |
| 469             | Ultrafast dynamics and scattering of protic ionic liquids induced by XFEL pulses. <b>2021</b> , 28, 1296-1308  | 1  |
| 468             | Somatic genetic rescue of a germline ribosome assembly defect. <b>2021</b> , 12, 5044  | 10 |

| 467 | Antitumor drugs effect on the stability of double-stranded DNA: steered molecular dynamics analysis. <b>2021</b> , 1-10  |    |
|-----|--|----|
| 466 | Adsorption of cations at the illiteWater interface and its effect on intrinsic potassium ions.   | 1  |
| 465 | Effects of layer-charge distribution on swelling behavior of mixed-layer illite-montmorillonite clays: A molecular dynamics simulation study. <b>2021</b> , 335, 116188            | 7  |
| 464 | Coupling of Adsorption Site and Cation Ratio Regulates the Adsorption of Cs+ and Na+ at the Surface of Clay Mineral. <b>2021</b> , 209, 106121                                     | 4  |
| 463 | Large-Scale Molecular Dynamics Simulations Reveal New Insights Into the Phase Transition Mechanisms in MIL-53(Al). <b>2021</b> , 9, 718920   | 3  |
| 462 | The antidepressant drug vilazodone is an allosteric inhibitor of the serotonin transporter. <b>2021</b> , 12, 5063   | 10 |
| 461 | Molecular Dynamics Modeling of Mechanical Properties of Polymer Nanocomposites Reinforced by C7N6 Nanosheet. <b>2021</b> , 4, 240-254  | 2  |
| 460 | Ion dynamics and selectivity of Nav channels from molecular dynamics simulation. <b>2021</b> , 548, 111245   | 10 |
| 459 | Spike mimicry of thrombopoietin may induce thrombocytopenia in COVID-19.   | O  |
| 458 | Insight into Cross-Amyloid Interactions and Morphologies: Molecular Dynamics Simulations of Model Peptide Fragments of Amyloid-¶A₫6-22) and Islet Amyloid Polypeptide (IAPP20-29). |    |
| 457 | The SARS-CoV-2 spike protein is vulnerable to moderate electric fields. <b>2021</b> , 12, 5407   | 5  |
| 456 | The Influence of Sequence Dependence and External Solvents on DNA Conformation. 2022, 193-217  |    |
| 455 | Conformational Fluctuations in GTP-Bound K-Ras: A Metadynamics Perspective with Harmonic Linear Discriminant Analysis. <b>2021</b> , 61, 5212-5222                                 | 6  |
| 454 | 1,3-Dimethyl-2-imidazolidinone: an ideal electrolyte solvent for high-performance LiD2 battery with pretreated Li anode. <b>2021</b> ,   | 1  |
| 453 | Stabilization of Haloalkane Dehalogenase Structure by Interfacial Interaction with Ionic Liquids. <b>2021</b> , 11, 1052   | 1  |
| 452 | Rational Design of Nonbonded Point Charge Models for Highly Charged Metal Cations with Lennard-Jones 12-6 Potential. <b>2021</b> , 61, 4613-4629                                   | 1  |
| 451 | Cation isomerism effect on micellization of pyridinium based surface-active ionic liquids. <b>2021</b> , 337, 116353   | 2  |
| 450 | Acrylic Paints: An Atomistic View of Polymer Structure and Effects of Environmental Pollutants. <b>2021</b> , 125, 10854-10865   | 2  |
|     |  |    |

| 449 | How phosphorylation of peptides affects their interaction with 14-3-3 domains. <b>2021</b> ,   | 0  |
|-----|--|----|
| 448 | Coarse-Grained Molecular Simulation of Polymers Supported by the Use of the SAFT-□Mie Equation of State. 2100031   | 2  |
| 447 | Enthalpic and Entropic Contributions to Interleaflet Coupling Drive Domain Registration and Anti-registration in Biological Membrane.  |    |
| 446 | Receptor-wide Determinants of G Protein Coupling Selectivity in Aminergic GPCRs.   |    |
| 445 | Development of coarse-grained force field to investigate sodium-ion transport mechanisms in cyanoborate-based ionic liquid. <b>2021</b> , 338, 116648  | 2  |
| 444 | pH-Dependent Conformations of an Antimicrobial Spider Venom Peptide, Cupiennin 1a, from<br>Unbiased HREMD Simulations. <b>2021</b> , 6, 24166-24175  | O  |
| 443 | Molecular Dynamics Simulations and Experimental Results Provide Insight into Clinical Performance Differences between Sandimmune and Neoral Lipid-Based Formulations. <b>2021</b> , 38, 1531-154 | 17 |
| 442 | Atypical kinetics of cytochrome P450 2J2: Epoxidation of arachidonic acid and reversible inhibition by xenobiotic inhibitors. <b>2021</b> , 164, 105889  | 1  |
| 441 | Boosted activity by engineering the enzyme microenvironment in cascade reaction: A molecular understanding. <b>2021</b> , 6, 163-172   | 3  |
| 440 | Dynamic Interactions of Fully Glycosylated SARS-CoV-2 Spike Protein with Various Antibodies. <b>2021</b> , 17, 6559-6569   | 2  |
| 439 | Structure and ion-release mechanism of PIB-4-type ATPases.   |    |
| 438 | How Dry-Wet cycling regulates the adsorption of metal ions and disposal of hazardous metals at smectites interfaces. <b>2021</b> , 562, 150108   | 3  |
| 437 | Classical molecular dynamics simulations of the deformation of metals under uniaxial monotonic loading: A review. <b>2021</b> , 254, 106614  | 2  |
| 436 | Molecular dynamics of fluoromethane type I hydrates. <b>2021</b> , 339, 116720   | 2  |
| 435 | Effects of hydrophobic solute on water normal modes. <b>2021</b> , 550, 111303   | 1  |
| 434 | Insights into the Molecular-Level details of betaine interactions with Laccase under various thermal conditions. <b>2021</b> , 339, 116832   | 1  |
| 433 | High-salinity brine desalination with amine-based temperature swing solvent extraction: A molecular dynamics study. <b>2021</b> , 341, 117359  | 2  |
| 432 | Molecular dynamics simulations support the hypothesis that the brGDGT paleothermometer is based on homeoviscous adaptation. <b>2021</b> , 312, 44-56   | 6  |

| 431 | Design and analysis of interactions in ionic liquids based on procaine and pharmaceutically active anions. <b>2021</b> , 166, 105966  | 2  |
|-----|---|----|
| 430 | Ripple-like instability in the simulated gel phase of finite size phosphocholine bilayers. <b>2021</b> , 1863, 183714   | 1  |
| 429 | Molecular aspects of temperature swing solvent extraction for brine desalination using imidazole-based solvents. <b>2022</b> , 247, 116866  | 4  |
| 428 | Modelling the adsorption of proteins to nanoparticles at the solid-liquid interface. <b>2022</b> , 605, 286-295   | 2  |
| 427 | Comparative Study of Interactions between Human cGAS and Inhibitors: Insights from Molecular Dynamics and MM/PBSA Studies. <b>2021</b> , 22,  | 2  |
| 426 | Identification of multiple substrate binding sites in SLC4 transporters in the outward-facing conformation: Insights into the transport mechanism. <b>2021</b> , 296, 100724            | 2  |
| 425 | The importance of intramolecular hydrogen bonds on the translocation of the small drug piracetam through a lipid bilayer <b>2020</b> , 11, 899-908                                      | 9  |
| 424 | Anisotropic crack propagation and self-healing mechanism of freestanding black phosphorus nanosheets. <b>2021</b> , 32, 165704  | 4  |
| 423 | Structural insights and molecular dynamics into the inhibitory mechanism of a Kunitz-type trypsin inhibitor from L. <b>2021</b> , 36, 480-490   | 3  |
| 422 | NMR-Based Structural Characterization of a Two-Disulfide-Bonded Analogue of the FXIIIa Inhibitor Tridegin: New Insights into Structure-Activity Relationships. <b>2021</b> , 22,        | 1  |
| 421 | Molecular mechanisms of resveratrol and EGCG in the inhibition of A軸ggregation and disruption of A軸rotofibril: similarities and differences. <b>2021</b> , 23, 18843-18854              | 4  |
| 420 | Computational prediction of the supramolecular self-assembling properties of organic molecules: the role of conformational flexibility of amide moieties. <b>2021</b> , 23, 20453-20465 | O  |
| 419 | Wrapping Up Viruses at Multiscale Resolution: Optimizing PACKMOL and SIRAH Execution for Simulating the Zika Virus. <b>2021</b> , 61, 408-422   | 8  |
| 418 | Biological evaluation of new TEM1 targeting recombinant antibodies for radioimmunotherapy: In vitro, in vivo and in silico studies. <b>2021</b> , 158, 233-244                          | 1  |
| 417 | Molecular dynamics with coupling to an external bath. <b>1984</b> , 81, 3684-3690   | 61 |
| 416 | Molecular Dynamics: Techniques and Applications to Proteins.  | 1  |
| 415 | Molecular Mechanics and Dynamics Simulations of Enzymes. <b>2002</b> , 153-198  | 2  |
| 414 | Simple Models of Intermolecular Potential for the Condensed Phases of C60. <b>1993</b> , 535-542  | 1  |

| 413 | Molecular Dynamics for Reactions of Heterogeneous Catalysis. <b>1991</b> , 133-144   | О  |
|-----|--|----|
| 412 | Time Scales of Lipid Dynamics and Molecular Dynamics. <b>1996</b> , 3-29   | 16 |
| 411 | Molecular dynamics simulations as a complement to nuclear magnetic resonance and X-ray diffraction measurements. <b>2007</b> , 400, 89-102   | 8  |
| 410 | Deterministic Methods. <b>1986</b> , 13-55   | 1  |
| 409 | Molecular Dynamics Simulation of Phospholipid Bilayers. <b>2001</b> , 89-107   | 3  |
| 408 | Coarse-grained molecular dynamics provides insight into the interactions of lipids and cholesterol with rhodopsin. <b>2014</b> , 796, 75-94  | 25 |
| 407 | Towards Realistic Model Intermolecular Potentials. <b>1990</b> , 29-54   | 4  |
| 406 | Molecular Dynamics Simulations in the Solid State Sciences. <b>1988</b> , 501-590  | 2  |
| 405 | Magic and Mysteries of Modern Molecular Dynamics Simulations. <b>2002</b> , 121-141  | 1  |
| 404 | Trends in Molecular Dynamics Simulation Technique. <b>1995</b> , 217-253   | 2  |
| 403 | Landau free energies and restricted averages. <b>2017</b> , 273-310  | 1  |
| 402 | Light-induced latent heat reduction of silver nanofluids: A molecular dynamics simulation. <b>2020</b> , 162, 120343   | 4  |
| 401 | Residue-Residue Mutual Work Analysis of Retinal-Opsin Interaction in Rhodopsin: Implications for Protein-Ligand Binding. <b>2020</b> , 16, 1834-1842                               | 3  |
| 400 | Solvation Structures of Tetraethylammonium Bromide and Tetrafluoroborate in Aqueous Binary Solvents with Ethanol, Trifluoroethanol, and Acetonitrile. <b>2020</b> , 124, 5009-5020 | 3  |
| 399 | Dynamics and Infrared Spectrocopy of Monomeric and Dimeric Wild Type and Mutant Insulin. <b>2020</b> , 124, 11882-11894  | 8  |
| 398 | Structural Properties of Inverted Hexagonal Phase: A Hybrid Computational and Experimental Approach. <b>2020</b> , 36, 6668-6680   | 2  |
| 397 | Chapter 2:Molecular Dynamics Computer Simulations of Biological Systems. 39-68   | 1  |
| 396 | Chapter 20:Computer Simulation Studies of Heat Capacity Effects Associated with Hydrophobic Effects. <b>2010</b> , 436-456   | 6  |

## (2020-2020)

| 395 | Accurate MP2-based force fields predict hydration free energies for simple alkanes and alcohols in good agreement with experiments. <b>2020</b> , 153, 244505  | 4  |
|-----|--|----|
| 394 | The basic residues in the Orai1 channel inner pore promote opening of the outer hydrophobic gate. <b>2020</b> , 152,   | 14 |
| 393 | Protein dynamics enables phosphorylation of buried residues in Cdk2/Cyclin A-bound p27.  | О  |
| 392 | K2P channel C-type gating involves asymmetric selectivity filter order-disorder transitions.   | 5  |
| 391 | Developing a Fully-glycosylated Full-length SARS-CoV-2 Spike Protein Model in a Viral Membrane. <b>2020</b> ,  | 4  |
| 390 | Glycan-induced protein dynamics in human norovirus P dimers depend on virus strain and deamidation status.   | 1  |
| 389 | Structure, Dynamics, Receptor Binding, and Antibody Binding of Fully-glycosylated Full-length SARS-CoV-2 Spike Protein in a Viral Membrane.  | 1  |
| 388 | Structural basis for divergent and convergent evolution of catalytic machineries in plant aromatic amino acid decarboxylase proteins.  | 2  |
| 387 | Lipid exchange mechanism of the cholesteryl ester transfer protein clarified by atomistic and coarse-grained simulations. <b>2012</b> , 8, e1002299  | 42 |
| 386 | In silico study on binding specificity of gonadotropins and their receptors: design of a novel and selective peptidomimetic for human follicle stimulating hormone receptor. <b>2013</b> , 8, e64475                   | 5  |
| 385 | Insight into the intermolecular recognition mechanism between Keap1 and IKKtombining homology modelling, protein-protein docking, molecular dynamics simulations and virtual alanine mutation. <b>2013</b> , 8, e75076 | 34 |
| 384 | In silico insights into protein-protein interactions and folding dynamics of the saposin-like domain of Solanum tuberosum aspartic protease. <b>2014</b> , 9, e104315  | 17 |
| 383 | Viscous friction between crystalline and amorphous phase of dragline silk. <b>2014</b> , 9, e104832  | 13 |
| 382 | Secondary Structure of Rat and Human Amylin across Force Fields. <b>2015</b> , 10, e0134091  | 37 |
| 381 | Polar Desolvation and Position 226 of Pancreatic and Neutrophil Elastases Are Crucial to their Affinity for the Kunitz-Type Inhibitors ShPI-1 and ShPI-1/K13L. <b>2015</b> , 10, e0137787                              | 3  |
| 380 | Ion Concentration- and Voltage-Dependent Push and Pull Mechanisms of Potassium Channel Ion Conduction. <b>2016</b> , 11, e0150716  | 5  |
| 379 | Molecular simulations and Markov state modeling reveal the structural diversity and dynamics of a theophylline-binding RNA aptamer in its unbound state. <b>2017</b> , 12, e0176229                                    | 19 |
| 378 | Antimicrobial Peptide K11 Selectively Recognizes Bacterial Biomimetic Membranes and Acts by Twisting Their Bilayers. <b>2020</b> , 14,   | 8  |

| 377 | An Amber Force Field for S-Nitrosoethanethiol That Is Transferable to S-Nitrosocysteine. <b>2010</b> , 31, 2903-2908   | 1  |
|-----|--|----|
| 376 | Molecular simulation of interaction between charged nanoparticles and phase-separated biomembranes containning charged lipids. <b>2019</b> , 68, 028701                                    | 2  |
| 375 | ATP-induced asymmetric pre-protein folding as a driver of protein translocation through the Sec machinery. <b>2019</b> , 8,  | 20 |
| 374 | #1-12 linker isomerization governs acid-sensing ion channel desensitization and recovery. <b>2020</b> , 9,   | 16 |
| 373 | Binding mechanism of the matrix domain of HIV-1 gag on lipid membranes. <b>2020</b> , 9,   | 5  |
| 372 | A sulfur-aromatic gate latch is essential for opening of the Orai1 channel pore. <b>2020</b> , 9,  | 10 |
| 371 | DNA sequence and methylation prescribe the inside-out conformational dynamics and bending energetics of DNA minicircles. <b>2021</b> , 49, 11459-11475                                     | 2  |
| 370 | Supramolecular Complexes of Tetrapeptides Capable of Inducing the Human ⊞-Lactalbumin ∰Domain Conformational Transitions. <b>2021</b> , 66, 840-845  |    |
| 369 | Evaluation of Host Defense Peptide (CaD23)-Antibiotic Interaction and Mechanism of Action: Insights From Experimental and Molecular Dynamics Simulations Studies. <b>2021</b> , 12, 731499 | О  |
| 368 | Synonymous mutations can alter protein dimerization through localized interface misfolding involving self-entanglements.   |    |
| 367 | Designing new antitubercular isoniazid derivatives with improved reactivity and membrane trafficking abilities. <b>2021</b> , 144, 112362  | 5  |
| 366 | Multiple Time Steps Algorithms for the Atomistic Simulations of Complex Molecular Systems. <b>2000</b> , 333-387   |    |
| 365 | ?????????????????????. <b>2000</b> , 68, 129-133   |    |
| 364 | Dynamics Methods. <b>2001</b> ,  |    |
| 363 | Argon and Its Companions. <b>1984</b> , 1-4  |    |
| 362 | References. <b>1986</b> , 509-526  |    |
| 361 | Thermodynamics. <b>1987</b> , 283-337  |    |
| 360 | Simulation of Plastic Crystals. <b>1990</b> , 335-355  |    |

| 359 | Molecular Dynamics Calculations on C60-Based Crystals. 1993, 207-210  |  |
|-----|---|--|
| 358 | Hydrophobic Aggregation of Nonionic Surfactants in Aqueous Solution: An MD Simulation Study. <b>1999</b> , 126-133  |  |
| 357 | Molecular Dynamics Simulations and Comparison of Two New and High Selective Imprinted Xerogels. <b>2016</b> , 339-361                                     |  |
| 356 | Molecular Dynamics Simulation of Membrane Free Energy Profiles Using Accurate Force Field for Ionic Liquids. <b>2017</b> , 265-284                        |  |
| 355 | Functional Implications of Disordered Terminal Regions of Macrotyloma uniflorum Bowman-Birk Inhibitors: A Molecular Dynamics Study.                       |  |
| 354 | Molecular basis for the maintenance of lipid asymmetry in the outer membrane ofEscherichia coli.  |  |
| 353 | ATP-induced asymmetric pre-protein folding: a driver of protein translocation?.   |  |
| 352 | Effects of Force Fields on the Conformational and Dynamic Properties of Amyloid ∰1-40) Dimer Explored by Replica Exchange Molecular Dynamics Simulations. |  |
| 351 | Specific cardiolipin-SecY interactions are required for proton-motive-force stimulation of protein secretion.   |  |
| 350 | Structural basis for endotoxin neutralization and anti-inflammatory activity of thrombin-derived C-terminal peptides.                                     |  |
| 349 | Molecular Dynamics simulation of the E.coli FtsZ dimer.   |  |
| 348 | Molecular Dynamics Simulation of the E.coli FtsZ.   |  |
| 347 | Structural plasticity of CENP-A regulated by H4 influences cellular levels and kinetochore assembly.  |  |
| 346 | Molecular Dynamics Simulations of the FtsZ mutant G105S.  |  |
| 345 | HIV-1 Env gp41 Transmembrane Domain Dynamics are Modulated by Lipid, Water, and Ion Interactions.   |  |
| 344 | Molecular mechanism of depolarization-dependent inactivation in W366F mutant of Kv1.2.  |  |
| 343 | Evidence for phospholipid export from the gram-negative inner membrane: time to rethink the Mla pathway?.   |  |
| 342 | Mechanistic basis for the evolution of chalcone synthase catalytic cysteine reactivity in land plants.  |  |

| 341                             | The SIRAH force field 2.0: Altius, Fortius, Citius.  | 0 |
|---------------------------------|--|---|
| 340                             | The outer membrane proteins OmpA, FhuA, OmpF, EstA, BtuB and OmpX have unique lipopolysaccharide fingerprints.   |   |
| 339                             | Conformational dynamics of active site loops 5, 6 and 7 of enzyme Triosephosphate Isomerase: A molecular dynamics study.   | О |
| 338                             | Membrane dynamics of Notch-bound Desecretase produces two distinct Notch conformations.  |   |
| 337                             | ¶1-12 linker isomerization governs Acid-sensing ion channel desensitization and recovery.  |   |
| 336                             | Dynamical rearrangement of human epidermal growth factor receptor 2 upon antibody binding: effects on the dimerization.  |   |
| 335                             | Structural and molecular insight into the pH-induced low-permeability of the voltage-gated potassium channel Kv1.2 through dewetting of the water cavity.  |   |
| 334                             | Interaction between myricetin aggregates and lipase under simplified intestinal conditions.  |   |
| 333                             | Suppression of Electrical and Water Tree by Additive Molecules: A Computational Insight. 2020, 12-21   |   |
|                                 |  |   |
| 332                             | Pulsed electric fields create pores in the voltage sensors of voltage-gated ion channels.  | 1 |
| 332                             | Pulsed electric fields create pores in the voltage sensors of voltage-gated ion channels.  Interaction of camel Lactoferrin derived peptides with DNA: a molecular dynamics study.   | 1 |
|                                 |  | 1 |
| 331                             | Interaction of camel Lactoferrin derived peptides with DNA: a molecular dynamics study.  | 1 |
| 331                             | Interaction of camel Lactoferrin derived peptides with DNA: a molecular dynamics study.  An RNA dynamic ensemble at atomic resolution.   | 1 |
| 331<br>330<br>329               | Interaction of camel Lactoferrin derived peptides with DNA: a molecular dynamics study.  An RNA dynamic ensemble at atomic resolution.  Binding Mechanism of the Matrix Domain of HIV-1 Gag on Lipid Membranes.  | 1 |
| 331<br>330<br>329<br>328        | Interaction of camel Lactoferrin derived peptides with DNA: a molecular dynamics study.  An RNA dynamic ensemble at atomic resolution.  Binding Mechanism of the Matrix Domain of HIV-1 Gag on Lipid Membranes.  Monomeric amyloid peptide (1-42) significantly populates compact fibril-like conformations.   | 1 |
| 331<br>330<br>329<br>328<br>327 | Interaction of camel Lactoferrin derived peptides with DNA: a molecular dynamics study.  An RNA dynamic ensemble at atomic resolution.  Binding Mechanism of the Matrix Domain of HIV-1 Gag on Lipid Membranes.  Monomeric amyloid peptide (1-42) significantly populates compact fibril-like conformations.  Diffusive dynamics of Aspartate-decarboxylase (ADC) liganded with D-serine in aqueous solution.  Molecular Simulations Guidelines for Biological Nanomaterials: From Peptides to Membranes. 2021 | 1 |

| 323 | BLaDE: A Basic Lambda Dynamics Engine for GPU-Accelerated Molecular Dynamics Free Energy Calculations. <b>2021</b> , 17, 6799-6807   | 1 |
|-----|--|---|
| 322 | Enabling Magnesium Anodes by Tuning the Electrode/Electrolyte Interfacial Structure. 2021,   | 3 |
| 321 | Catechol-Containing Compounds are a Broad Class of Protein Aggregation Inhibitors: II. Rosmarinic Acid Potently Detoxifies Amylin Amyloid and Ameliorates Diabetic Pathology in HIP Rats.  | 1 |
| 320 | Development and Testing of Force Field Parameters for Phenylalanine and Tyrosine Derivatives. <b>2020</b> , 7, 608931  | O |
| 319 | Structural basis for voltage-sensor trapping of the cardiac sodium channel by a deathstalker scorpion toxin.   |   |
| 318 | Efficient anisotropic desalination by layer-stacked black phosphorus carbide (⊞-PC) membrane. <b>2022</b> , 522, 115422  | O |
| 317 | Study on simultaneous binding of resveratrol and curcumin to ∄actoglobulin: Multi-spectroscopic, molecular docking and molecular dynamics simulation approaches. <b>2022</b> , 124, 107331 | 1 |
| 316 | Molecular Dynamics Methods in Simulations of Macromolecules. <b>2020</b> , 189-280   |   |
| 315 | Effects of Water Molecules on Metal Complexes of Hydroxyoxime and Carboxylic Acid Extractants. <b>2020</b> , 27, 25-38   | 1 |
| 314 | Improved Parameterization of Protein ${f D}$ NA Interactions for Molecular Dynamics Simulations of PCNA Diffusion on DNA.  |   |
| 313 | Maturation of siRNA by strand separation: Steered molecular dynamics study. 2021, 1-11   | 1 |
| 312 | Molecular Dynamics Simulation Approaches to K Channels. <b>2007</b> , 545-567  |   |
| 311 | Moving toward generalizable NZ-1 labeling for 3D structure determination with optimized epitope tag insertion.   |   |
| 310 | Assessment of Structural Units Deletions in the Archaeal Oligosaccharyltransferase AglB.   |   |
| 309 | Allosteric regulation in CRISPR/Cas1-Cas2 protospacer acquisition mediated by DNA in association with Cas2.  |   |
| 308 | Towards a predictive model for polymer solubility using the noncovalent interaction index: polyethylene as a case study. <b>2021</b> , 23, 25374-25387                                     | O |
| 307 | Structural and dynamic insights into MnCa cluster-depleted Photosystem II. 2021,   | 1 |
| 306 | PcoB is a defense outer membrane protein that facilitates cellular uptake of copper.   |   |

| 305 | Structure, dynamics, and function of SrnR, a transcription factor for nickel-dependent gene expression. <b>2021</b> ,   | 1  |
|-----|---|----|
| 304 | Destabilization of the Alzheimer's amyloid-即eptide by a proline-rich  | 1  |
| 303 | Fine-Tuning the Polarizable CL&Pol Force Field for the Deep Eutectic Solvent Ethaline. 2021,  | 1  |
| 302 | The impact of phosphatidylserine exposure on cancer cell membranes on the activity of the anticancer peptide HB43. <b>2021</b> ,  | 3  |
| 301 | Temperature-Dependent Dielectric Relaxation in Ionic Acetamide Deep Eutectics: Partial Viscosity Decoupling and Explanations from the Simulated Single-Particle Reorientation Dynamics and Hydrogen-Bond Fluctuations. <b>2021</b> , 125, 12552-12567 | 2  |
| 300 | Frizzled BRET sensors based on bioorthogonal labeling of unnatural amino acids reveal WNT-induced dynamics of the cysteine-rich domain. <b>2021</b> , 7, eabj7917   | 1  |
| 299 | Theoretical Design and Experimental Study of New Aptamers with the Enhanced Binding Affinity Relying on Colorimetric Assay for Tetracycline Detection. <b>2021</b> , 349, 118196  | 0  |
| 298 | A General Picture of Cucurbit[8]uril Host-Guest Binding. <b>2021</b> ,  | 16 |
| 297 | Revealing Topological Barriers against Knot Untying in Thermal and Mechanical Protein Unfolding by Molecular Dynamics Simulations. <b>2021</b> , 11,  | O  |
| 296 | Destabilization of Affibrils by omega-3 polyunsaturated fatty acids: a molecular dynamics study. <b>2021</b> , 1-18   | 4  |
| 295 | A Random Batch Ewald Method for Charged Particles in the Isothermal-Isobaric Ensemble.  |    |
| 294 | Evaluation of all-atom force fields in viral capsid simulations and properties <b>2021</b> , 12, 216-220  |    |
| 293 | New insight into the structural changes of apoferritin pores in the process of doxorubicin loading at an acidic pH: Molecular dynamics simulations <b>2021</b> , 141, 105158  | O  |
| 292 | Interactions between polymyxin B and various bacterial membrane mimics: A molecular dynamics study <b>2021</b> , 211, 112288  | О  |
| 291 | Electrostatic interactions contribute to the control of intramolecular thiol-disulfide isomerization in a protein. <b>2021</b> , 23, 26366-26375  | O  |
| 290 | The Role of Triazole and Glucose Moieties in Alkali Metal Cation Complexation by Lower-Rim Tertiary-Amide Calix[4]arene Derivatives <b>2022</b> , 27,   |    |
| 289 | Quantum mechanical, molecular docking, molecular dynamics, ADMET and antiproliferative activity on (Y strain) of chalcone ()-1-(2-hydroxy-3,4,6-trimethoxyphenyl)-3-(3-nitrophenyl)prop-2-en-1-one derived from a natural product <b>2022</b> ,       | 3  |
| 288 | Influence of Long-Range Forces on the Transition States and Dynamics of NaCl Ion-Pair Dissociation in Water <b>2022</b> ,   | 1  |

| 287  | Hypoglycemic and hepatoprotective effects in adult zebrafish () of fisetinidol isolated from : and assays <b>2022</b> , 1-15  | 1 |
|--|---|---|
| 286  | Molecular dynamics and functional characterization of I37R-CFTR lasso mutation provide insights into channel gating activity <b>2022</b> , 25, 103710   | 0 |
| 285  | How to Characterize Amorphous Shapes: The Tale of a Reverse Micelle 2022,   | 1 |
| 284  | Concentration-dependent assembly of Bovine serum albumin molecules in the doxorubicin loading process: Molecular dynamics simulation. <b>2022</b> , 640, 128429   |   |
| 283  | Effect of the degree of hydrogenation on the viscosity, surface tension, and density of the liquid organic hydrogen carrier system based on diphenylmethane. <b>2022</b> , 47, 6111-6130  | 3 |
| 282  | Binding free energies for the SAMPL8 CB8 "Drugs of Abuse" challenge from umbrella sampling combined with Hamiltonian replica exchange <b>2022</b> , 36, 1   | О |
| 281  | Carbohydrate Force Fields: The Role of Small Partial Atomic Charges in Preventing Conformational Collapse <b>2022</b> ,   | 0 |
| 280  | Unravelling the mechanism of glucose binding in a protein-based fluorescence probe: molecular dynamics simulation with a tailor-made charge model <b>2022</b> ,   | О |
| 279  | Switching Promotor Recognition of Phage RNA Polymerase in Silico along Lab Directed Evolution Path <b>2022</b> ,  |   |
|  |   |   |
| 278  | Computational Medicinal Chemistry to Target GPCRs. 2022,  |   |
| 278<br>277                                   | Computational Medicinal Chemistry to Target GPCRs. 2022,  The phase behaviour of cetyltrimethylammonium chloride surfactant aqueous solutions at high concentrations: an all-atom molecular dynamics simulation study 2022,   | 0 |
|  | The phase behaviour of cetyltrimethylammonium chloride surfactant aqueous solutions at high   | 0 |
| 277  | The phase behaviour of cetyltrimethylammonium chloride surfactant aqueous solutions at high concentrations: an all-atom molecular dynamics simulation study 2022,  The use of in silico models for the rationalization of molecularly imprinted polymer synthesis. 2022,  |   |
| <sup>2</sup> 77                              | The phase behaviour of cetyltrimethylammonium chloride surfactant aqueous solutions at high concentrations: an all-atom molecular dynamics simulation study <b>2022</b> ,  The use of in silico models for the rationalization of molecularly imprinted polymer synthesis. <b>2022</b> , 166, 111024  | 0 |
| <sup>277</sup> <sup>276</sup> <sup>275</sup> | The phase behaviour of cetyltrimethylammonium chloride surfactant aqueous solutions at high concentrations: an all-atom molecular dynamics simulation study 2022,  The use of in silico models for the rationalization of molecularly imprinted polymer synthesis. 2022, 166, 111024  Spontaneous Local Membrane Curvature Induced by Transmembrane Proteins 2022,  Genetic and molecular Omp25 analyses from worldwide Brucella canis strains: possible mutational   | 0 |
| 277<br>276<br>275                            | The phase behaviour of cetyltrimethylammonium chloride surfactant aqueous solutions at high concentrations: an all-atom molecular dynamics simulation study 2022,  The use of in silico models for the rationalization of molecularly imprinted polymer synthesis. 2022, 166, 111024  Spontaneous Local Membrane Curvature Induced by Transmembrane Proteins 2022,  Genetic and molecular Omp25 analyses from worldwide Brucella canis strains: possible mutational influences in protein function 2022, 817, 146175  Optimizing Lennard-Jones parameters by coupling single molecule and ensemble target data. 2022  | 0 |
| 277 276 275 274 273                          | The phase behaviour of cetyltrimethylammonium chloride surfactant aqueous solutions at high concentrations: an all-atom molecular dynamics simulation study 2022,  The use of in silico models for the rationalization of molecularly imprinted polymer synthesis. 2022, 166, 111024  Spontaneous Local Membrane Curvature Induced by Transmembrane Proteins 2022,  Genetic and molecular Omp25 analyses from worldwide Brucella canis strains: possible mutational influences in protein function 2022, 817, 146175  Optimizing Lennard-Jones parameters by coupling single molecule and ensemble target data. 2022, 274, 108285  Accelerating the discovery of the beyond rule of five compounds that have high affinities toward | 0 |

| 269 | Structures of human pannexin-1 in nanodiscs reveal gating mediated by dynamic movement of the N terminus and phospholipids <b>2022</b> , 15, eabg6941                                | 6 |
|-----|--|---|
| 268 | Dynamic regulation of O-GlcNAcylation and phosphorylation on STAT3 under hypoxia-induced EMT <b>2022</b> , 110277  | O |
| 267 | Computational investigation of the alkaloids of species as phytopharmaceuticals for the inhibition of sterol 14-demethylase protease of <b>2022</b> , 1-19                           |   |
| 266 | Hard-Cation-Soft-Anion Ionic Liquids for PEDOT:PSS Treatment 2022,   | O |
| 265 | Comparative Molecular Modelling of Capsular Polysaccharide Conformations in Serotypes 1, 2, 1/2 and 14 Identifies Common Epitopes for Antibody Binding <b>2022</b> , 9, 830854       | О |
| 264 | Model Folded Hydrophobic Polymers Reside in Highly Branched Voids <b>2021</b> , 183-189  | 1 |
| 263 | Structural Insights into Self-Assembled Aerosol-OT Aggregates in Aqueous Media Using Atomistic Molecular Dynamics <b>2021</b> , 125, 13789-13803                                     |   |
| 262 | Molecular motion in plastic crystals. <b>1985</b> , 94, 181-199  | 9 |
| 261 | Structure-guided glyco-engineering of ACE2 for improved potency as soluble SARS-CoV-2 decoy receptor <b>2021</b> , 10,   | 2 |
| 260 | Permeation Process of Metal Complexes with Hydroxyoxime and Carboxylic Acid Extractants through Organic-Aqueous Interface. <b>2022</b> , 29, 21-29                                   |   |
| 259 | Molecular simulation of glycerol-derived triether podands for lithium ion solvation 2022,  | О |
| 258 | Controlling Li transport in ionic liquid electrolytes through salt content and anion asymmetry: a mechanistic understanding gained from molecular dynamics simulations <b>2022</b> , | 2 |
| 257 | Effect of ring stiffness and ambient pressure on the dynamical slowdown in ring polymers 2022,   |   |
| 256 | Do antifreeze proteins generally possess the potential to promote ice growth?. 2022,   | 1 |
| 255 | Effect of stoichiometry on crosslinked epoxy resin characteristics: structural heterogeneities, topological defects, properties, free volume and segmental mobility <b>2022</b> ,    | О |
| 254 | A Method for Detection of Water Permeation Events in Molecular Dynamics Simulations of Lipid Bilayers. <b>2022</b> , 52, 1   | 1 |
| 253 | Computational Investigation of Structural Basis for Enhanced Binding of Isoflavone Analogues with Mitochondrial Aldehyde Dehydrogenase <b>2022</b> , 7, 8115-8127                    | 1 |
| 252 | High-Dimensional Parameter Search Method to Determine Force Field Mixing Terms in Molecular Simulations <b>2022</b> , 38, 2840-2851  | 2 |

| 251 | Atomistic Simulation of Lysozyme in Solutions Crowded by Tetraethylene Glycol: Force Field Dependence <b>2022</b> , 27,   |   |
|-----|---|---|
| 250 | The increment of the temperature of maximum density of water by addition of small amounts of tert-butanol: Experimental data and microscopic description revisited <b>2022</b> , 156, 104502    | 0 |
| 249 | Response of Terahertz Protein Vibrations to Ligand Binding: Calmodulin-Peptide Complexes as a Case Study <b>2022</b> ,  |   |
| 248 | Supramolecular Engineering of Alkylated, Fluorinated, and Mixed Amphiphiles <b>2022</b> , e2100914  | 1 |
| 247 | Stress tensor and constant pressure simulation for polarizable Gaussian multipole model <b>2022</b> , 156, 114114   | 0 |
| 246 | Signatures of sluggish dynamics and local structural ordering during ice nucleation <b>2022</b> , 156, 114502   | 1 |
| 245 | Exploring the Effect of Enhanced Sampling on Protein Stability Prediction 2022,   | 1 |
| 244 | Twist-diameter coupling drives DNA twist changes with salt and temperature <b>2022</b> , 8, eabn1384  | 3 |
| 243 | Isolation and In Silico SARS-CoV-2 Main Protease Inhibition Potential of Jusan Coumarin, a New Dicoumarin from <b>2022</b> , 27,  | 2 |
| 242 | Deciphering the mechanisms of HPV E6 mutations in the destabilization of E6/E6AP/p53 complex <b>2022</b> ,  |   |
| 241 | Copper binding leads to increased dynamics in the regulatory N-terminal domain of full-length human copper transporter ATP7B.   |   |
| 240 | Nek1-inhibitor and temozolomide-loaded microfibers as a co-therapy strategy for glioblastoma treatment <b>2022</b> , 617, 121584  |   |
| 239 | Peptide Permeation across a Phosphocholine Membrane: An Atomically Detailed Mechanism Determined through Simulations and Supported by Experimentation <b>2022</b> ,                             | 1 |
| 238 | Alpha-cadinol as a potential ACE-inhibitory volatile compound identified from Phaseolus vulgaris L. through in vitro and in silico analysis <b>2022</b> , 1-15                                  | 1 |
| 237 | The potential of antifungal peptide Sesquin as natural food preservative 2022,  | 2 |
| 236 | Concentration Dependence of Dynamics and Hydrogen Bonding in Aqueous Solutions of Urea, Methyl-substituted Ureas, and Trimethylamine N-Oxide. <b>2022</b> , 119120                              |   |
| 235 | Drug repurposing through virtual screening and in vitro validation identifies tigecycline as a novel putative HCV polymerase inhibitor <b>2022</b> , 570, 9-17                                  |   |
| 234 | Are all-atom any better than united-atom force fields for the description of liquid properties of alkanes? 2. A systematic study considering different chain lengths. <b>2022</b> , 354, 118829 | Ο |

| 233 | Anion Effects on the Mixing States of 1-Methyl-3-octylimidazolium Tetrafluoroborate and Bis(trifluoromethylsulfonyl)amide with Methanol, Acetonitrile, and Dimethyl Sulfoxide on the Meso- and Microscopic Scales <b>2021</b> , 125, 13896-13907 | О |
|-----|--|---|
| 232 | Distinctive Formation of PEG-Lipid Nanopatches onto Solid Polymer Surfaces Interfacing Solvents from Atomistic Simulation <b>2021</b> ,  | Ο |
| 231 | Martini Coarse-Grained Model for Poly(alkylimidazolium) Ionenes and Applications in Aromatic Compound Extraction. <b>2022</b> , 55, 26-34  | 0 |
| 230 | The Role of Key Amino Acids in the Antimicrobial Mechanism of a Bacteriocin Model Revealed by Molecular Simulations. <b>2021</b> ,   | 1 |
| 229 | Specific Ion Solvation and Pairing Effects in Glycerol Carbonate <b>2021</b> , 125, 13635-13643  | 2 |
| 228 | In silico and functional characterisation of an ultra-rare CFTR mutation identifies novel lasso motif interactions regulating channel gating.  |   |
| 227 | Structural basis for the assembly and electron transport mechanisms of the dimeric photosynthetic RCIIH1 supercomplex.   |   |
| 226 | Structure and ion-release mechanism of P-type ATPases <b>2021</b> , 10,  | 2 |
| 225 | A Computational Study of RNA Tetraloop Thermodynamics, Including Misfolded States. 2021,   | 0 |
| 224 | Identification of tripeptides against tyrosine kinase domain of EGFR for lung cancer cell inhibition by in silico and in vitro studies <b>2021</b> ,   | O |
| 223 | Structure-Based Design of an RNase Chimera for Antimicrobial Therapy <b>2021</b> , 23,   | 0 |
| 222 | Rational Design of Nonbonded Point Charge Models for Monovalent Ions with Lennard-Jones 12-6 Potential. <b>2021</b> ,  | 2 |
| 221 | Structural basis for the assembly and quinone transport mechanisms of the dimeric photosynthetic RC-LH1 supercomplex <b>2022</b> , 13, 1977  | 4 |
| 220 | Novel US-CpHMD Protocol to Study the Protonation-Dependent Mechanism of the ATP/ADP Carrier <b>2022</b> ,  | O |
| 219 | Fragmentation Method for Computing Quantum Mechanics and Molecular Mechanics Gradients for Force Matching: Validation with Hydration Free Energy Predictions Using Adaptive Force Matching 2022,   | 1 |
| 218 | Data_Sheet_1.docx. <b>2019</b> ,   |   |
| 217 | Image_1.tif. <b>2019</b> ,   |   |
| 216 | Table_1.pdf. <b>2019</b> ,   |   |

## (2022-2019)

| 215 | Table_2.pdf. <b>2019</b> ,   |   |
|-----|--|---|
| 214 | Video_1.mp4. <b>2019</b> ,   |   |
| 213 | Video_2.mp4. <b>2019</b> ,   |   |
| 212 | Video_3.mp4. <b>2019</b> ,   |   |
| 211 | Video_4.mp4. <b>2019</b> ,   |   |
| 210 | Data_Sheet_1.PDF. <b>2020</b> ,  |   |
| 209 | Data_Sheet_2.xlsx. <b>2020</b> ,   |   |
| 208 | Data_Sheet_1.PDF. <b>2020</b> ,  |   |
| 207 | Data_Sheet_1.PDF. <b>2020</b> ,  |   |
| 206 | Presentation_1.PPTX. <b>2020</b> ,   |   |
| 205 | Tuning Contact Angles of Aqueous Droplets on Hydrophilic and Hydrophobic Surfaces by Surfactants <b>2022</b> ,   | O |
| 204 | Hydrogen bond redistribution effects in mixtures of protic ionic liquids sharing the same cation: non-ideal mixing with large negative mixing enthalpies <b>2022</b> ,           | О |
| 203 | Enthalpic and entropic contributions to interleaflet coupling drive domain registration and antiregistration in biological membrane <b>2022</b> , 105, 044408                    | O |
| 202 | Biophysical insights into OR2T7: Investigation of a potential prognostic marker for glioblastoma <b>2022</b> ,   | O |
| 201 | Effect of Succinonitrile on Ion Transport in PEO-based Lithium-Ion Battery Electrolytes.   | 1 |
| 200 | Simulations of Cross-Amyloid Aggregation of Amyloid-臨nd Islet Amyloid Polypeptide Fragments <b>2022</b> ,  | 1 |
| 199 | Antibiotic-Like Activity of Atomic Layer Boron Nitride for Combating Resistant Bacteria 2022,  | 5 |
| 198 | Toward the Discovery of a Novel Class of Leads for High Altitude Disorders by Virtual Screening and Molecular Dynamics Approaches Targeting Carbonic Anhydrase <b>2022</b> , 23, | 2 |

| 197 | Investigation of the structural and dynamical properties of human uncoupling protein 2 through molecular dynamics simulations <b>2022</b> , 114, 108203                  |   |
|-----|--|---|
| 196 | Investigation of a high-sensitive electrochemical DNA biosensor for determination of Idarubicin and studies of DNA-binding properties. <b>2022</b> , 179, 107546         | 3 |
| 195 | Reverse vaccinology-based prediction of a multi-epitope SARS-CoV-2 vaccine and its tailoring to new coronavirus variants <b>2022</b> , 1-22                              |   |
| 194 | Understanding the different cross-membrane transport kinetics of two charged molecules on DOPG lipid surface with second harmonic generation and MD simulation.          | О |
| 193 | Prediction Of The Impact Of Genetic Variability On Drug Sensitivity For Clinically Relevant EGFR Mutations.  |   |
| 192 | AlphaFold-predicted Protein Structure vs Experimentally Obtained Protein Structure: An Emphasis on the Side Chains. <b>2022</b> , 91,                                    |   |
| 191 | Interaction of Therapeutic d-Peptides with A#2 Monomers, Thermodynamics, and Binding Analysis <b>2022</b> ,  | 3 |
| 190 | Molecular Dynamics Energetics of Polymers in Solution from Supervised Machine Learning.  | 1 |
| 189 | How Peptides Bind to PSD-95/Discs-Large/ZO-1 Domains.  |   |
| 188 | Human serum albumin adsorption on cellulose nanocrystal: A spectroscopy and molecular dynamics simulation research. <b>2022</b> , 597, 153749                            | O |
| 187 | Partial Destabilization of Amyloid-Protofibril by Methionine Photo-oxidation: A Molecular Dynamic Simulation Study.  |   |
| 186 | Drug Interactions with Plasticized PVCs.   |   |
| 185 | Evolutionary association of receptor-wide amino acids with G proteinBoupling selectivity in aminergic GPCRs. <b>2022</b> , 5, e202201439                                 | О |
| 184 | The Influence of Short Motifs on the Anticancer Activity of HB43 Peptide. <b>2022</b> , 14, 1089   | 2 |
| 183 | Modified Poisson <b>B</b> oltzmann theory for polyelectrolytes in monovalent salt solutions with finite-size ions. <b>2022</b> , 156, 214906                             | 1 |
| 182 | Biphasic Behaviors of Nd3+ Bound with Cyanex272, Cyanex301, and Cyanex302: A Molecular Dynamics Simulation Study.  |   |
| 181 | Simulation and theoretical analysis of the origin of the temperature of maximum density of water. <b>2022</b> , 560, 113515  | O |
| 180 | Rational design, molecular docking, dynamic simulation, synthesis, PPAR-I competitive binding and transcription analysis of novel glitazones. <b>2022</b> , 1265, 133354 | O |

| 179 | Refining details of the structural and electronic properties of the CuB site in pMMO enzyme through sequential molecular dynamics/CPKS-EPR calculations.  |   |
|-----|---|---|
| 178 | Impacts of targeting different hydration free energy references in the development of ion potentials.   |   |
| 177 | Inhibition Mechanisms of (⊯Epigallocatechin-3-gallate and Genistein on Amyloid-beta 42 Peptide of Alzheimer Disease via Molecular Simulations. <b>2022</b> , 7, 19665-19675                                 | 1 |
| 176 | Developing Reaction Chemistry Models from Reactive Molecular Dynamics: TATB.  | 1 |
| 175 | Nirmatrelvir Resistant SARS-CoV-2 Variants with High Fitness in Vitro.  | 2 |
| 174 | Exploring TRPC3 Interaction with Cholesterol through Coarse-Grained Molecular Dynamics Simulations. <b>2022</b> , 12, 890   |   |
| 173 | An L-theanine derivative targets against SARS-CoV-2 and its Delta and Omicron variants. 2022, 8, e09660   | O |
| 172 | Controlling the Ion Transport Number in Solvent-in-Salt Solutions. <b>2022</b> , 126, 4572-4583   |   |
| 171 | Optimization of an in Silico Protocol Using Probe Permeabilities to Identify Membrane Pan-Assay Interference Compounds.   | 2 |
| 170 | Computational Insights into the Role of Cholesterol in Inverted Hexagonal Phase Stabilization and Endosomal Drug Release. <b>2022</b> , 38, 7462-7471   | 1 |
| 169 | PcoB is a defense outer membrane protein that facilitates cellular uptake of copper. 2022, 31,  | O |
| 168 | Mechanisms of Listeria monocytogenes disinfection with Benzalkonium chloride: from molecular dynamics to kinetics of time-kill curves.  |   |
| 167 | Structure of SARS-CoV-2 M protein in lipid nanodiscs.   | O |
| 166 | Towards the correct microscopic structure of aqueous CsCl solutions with a comparison of classical interatomic potential models. <b>2022</b> , 361, 119660  | 1 |
| 165 | Deciphering the non-covalent binding patterns of three whey proteins with rosmarinic acid by multi-spectroscopic, molecular docking and molecular dynamics simulation approaches. <b>2022</b> , 132, 107895 | 4 |
| 164 | Tuning Aqueous Self-assembly of Porphyrins by Varying the Number of Cationic Side Chains.   |   |
| 163 | Toward Bottom-Up Understanding of Transport in Concentrated Battery Electrolytes.   | 2 |
| 162 | Molecular Modeling of Ionic Liquids: Force-Field Validation and Thermodynamic Perspective from Large-Scale Fast-Growth Solvation Free Energy Calculations. 2200274  | O |

| 161 | Modeling the Electronic Absorption Spectra of the Indocarbocyanine Cy3. <b>2022</b> , 27, 4062  | 1 |
|-----|---|---|
| 160 | Design, Synthesis, In Silico and In Vitro Studies of New Immunomodulatory Anticancer Nicotinamide Derivatives Targeting VEGFR-2. <b>2022</b> , 27, 4079   | 2 |
| 159 | Potential Autoimmunity Resulting from Molecular Mimicry between SARS-CoV-2 Spike and Human Proteins. <b>2022</b> , 14, 1415   | 2 |
| 158 | A new approach used in docking study for predicting the combination drug efficacy in EML4-ALK target of NSCLC. 1-17   |   |
| 157 | Electric Field Direction-Induced Gas/Water Selectively Entering Nanochannel. 2022, 119852   |   |
| 156 | Chemical and Morphological Structure of Transgenic Switchgrass Organosolv Lignin Extracted by Ethanol, Tetrahydrofuran, and I-Valerolactone Pretreatments. <b>2022</b> , 10, 9041-9052                                | O |
| 155 | On the force field optimisation of \$\$beta\$\$-lactam cores using the force field Toolkit.   |   |
| 154 | Molecular Dynamics in the Light of Non-equilibrium Thermodynamics. <b>2022</b> , 91,  | 1 |
| 153 | Long-range communication between transmembrane- and nucleotide-binding domains does not depend on drug binding to mutant P-glycoprotein.  |   |
| 152 | Evaluation of interaction between Ponceau 4R (P4R) and trypsin using kinetic, spectroscopic, and molecular dynamics simulation methods. <b>2022</b> , 362, 119761   |   |
| 151 | Molecular simulation of methane hydrate growth confined into a silica pore. <b>2022</b> , 362, 119698   |   |
| 150 | Molecular Dynamics Simulation Study of the Far-Infrared Spectrum of a Deep Eutectic Solvent.  | 2 |
| 149 | Human TMPRSS2 non-catalytic ectodomain and SARS-CoV-2 S2' subunit interaction mediated SARS-CoV-2 endocytosis: a model proposal with virtual screening for potential drug molecules to inhibit this interaction. 1-12 |   |
| 148 | An Insulin Receptor-Binding Multifunctional Protein from Tamarindus indica L. Presents a Hypoglycemic Effect in a Diet-Induced Type 2 Diabetes <b>B</b> reclinical Study. <b>2022</b> , 11, 2207                      | Ο |
| 147 | Assessing the effect of a liquid water layer on the adsorption of hydrate anti-agglomerants using molecular simulations.  |   |
| 146 | A Multistage In Silico Study of Natural Potential Inhibitors Targeting SARS-CoV-2 Main Protease. <b>2022</b> , 23, 8407   | 5 |
| 145 | Polymyxins induce lipid scrambling and disrupt the homeostasis of Gram-negative bacteria membrane. <b>2022</b> ,  | 0 |
| 144 | Can a Finite Chain of Hydrogen Cyanide Molecules Model a Crystal?.  | 1 |

| 143 | Binding Models of A#2 Peptide with Membranes Explored by Molecular Simulations.  | 2 |
|-----|--|---|
| 142 | Crystal structure analysis and molecular dynamics simulations of arginase from Thermus thermophilus. 1-11  |   |
| 141 | Modeling of pneumococcal serogroup 10 capsular polysaccharide molecular conformations provides insight into epitopes and observed cross-reactivity. 9,                 | O |
| 140 | Structure of SARS-CoV-2 membrane protein essential for virus assembly. <b>2022</b> , 13,   | 5 |
| 139 | Wine-related flavonols for therapeutic use in Alzheimer∄ disease, an in-silico investigation.  | 1 |
| 138 | The Dynamics of Metal Nanoparticles on a Supporting Interacting Substrate.   |   |
| 137 | Exploring the Dynamics of Shikimate Kinase through Molecular Mechanics. <b>2022</b> , 2, 194-202   |   |
| 136 | Critical Thicknesses of Free-Standing Thin Films of Molten Polymers: A Multiscale Simulation Study.  | 1 |
| 135 | Impact of arginine modified SNARE peptides on interactions with phospholipid bilayers and coiled-coil formation: A molecular dynamics study. <b>2022</b> , 364, 119972 |   |
| 134 | Water-Graphene non-bonded interaction parameters: Development and influence on molecular dynamics simulations. <b>2022</b> , 603, 154477                               | O |
| 133 | Molecular-level solvation and selectivity behavior of Na+, K+, and Li+ within glycerol-derived solvents. <b>2022</b> , 262, 117992                                     | 1 |
| 132 | Molecular modelling of ionic liquids: General guidelines on fixed-charge force fields for balanced descriptions. <b>2022</b> , 2, 100043                               | O |
| 131 | Molecular dynamics simulations to study the role of biphenylalanine in promoting the antibacterial activity of ultrashort peptides. <b>2022</b> , 117, 108282          |   |
| 130 | Superhydrophilicity of ⊞-alumina surfaces results from tight binding of interfacial waters to specific aluminols. <b>2022</b> , 628, 943-954                           |   |
| 129 | Identification of Drug Combination Therapies for SARS-CoV-2: A Molecular Dynamics Simulations Approach. Volume 16, 2995-3013   | 1 |
| 128 | Unveiling molecular details behind improved activity at neutral to alkaline pH of an engineered DyP-type peroxidase. <b>2022</b> , 20, 3899-3910                       | O |
| 127 | Energy landscapes in inorganic chemistry. 2022,  | O |
| 126 | Molecular dynamics simulation of several typical molecular ferroelectrics based on PCC charge model.   | O |

| 125 | Computational study of quinoline-based thiadiazole compounds as potential antileishmanial inhibitors. <b>2022</b> , 46, 17554-17576  | О |
|-----|--|---|
| 124 | Molecular Modeling Studies of Natural Inhibitors of Androgen Signaling in Prostate Cancer. <b>2022</b> , 21, 117693512211185   | 1 |
| 123 | Effect of Layer Charge Density and Cation's Concentration on Sorption Behaviors of Heavy Metal Ions in the Interlayer and Nanopore of Smectite: A Molecular Dynamics Simulation.                         | 0 |
| 122 | Interaction between two polyelectrolytes in monovalent aqueous salt solutions. <b>2022</b> , 24, 21112-21121   | O |
| 121 | Structure and diffusive dynamics of aspartate ∃-decarboxylase (ADC) liganded with d-serine in aqueous solution. <b>2022</b> , 24, 20336-20347  | 1 |
| 120 | Site-specific water dynamics in the first hydration layer of an anti-freeze glyco-protein: a simulation study. <b>2022</b> , 24, 21165-21177   | 1 |
| 119 | QM/MM Simulations for the Broken-Symmetry Catalytic Reaction Mechanism of Human Arginase I. <b>2022</b> , 7, 32536-32548   | 0 |
| 118 | Impact on S. aureus and E. coli membranes of treatment with chlorhexidine and alcohol solutions: insights from molecular simulations and nuclear magnetic resonance.                                     | O |
| 117 | Structural basis of ion uptake in copper-transporting P1B-type ATPases. <b>2022</b> , 13,  | 0 |
| 116 | Characterisation of HOIP RBR E3 ligase conformational dynamics using integrative modelling. <b>2022</b> , 12,  | O |
| 115 | Insights into Allosteric Mechanisms of the Lung-Enriched p53 Mutants V157F and R158L. <b>2022</b> , 23, 10100  | 0 |
| 114 | Hybrid in vitro/in silico analysis of low-affinity proteinprotein interactions that regulate signal transduction by Sema6D.  | 1 |
| 113 | Copper binding leads to increased dynamics in the regulatory N-terminal domain of full-length human copper transporter ATP7B. <b>2022</b> , 18, e1010074   | 0 |
| 112 | Atomistic Insights into A315E Mutation-Enhanced Pathogenicity of TDP-43 Core Fibrils. <b>2022</b> , 13, 2743-2754  | 1 |
| 111 | Identification of promising anti-EBOV inhibitors: de novo drug design, molecular docking and molecular dynamics studies. <b>2022</b> , 9,  | 0 |
| 110 | Melatonin Inhibits hIAPP Oligomerization by Preventing 断heet and Hydrogen Bond Formation of the Amyloidogenic Region Revealed by Replica-Exchange Molecular Dynamics Simulation. <b>2022</b> , 23, 10264 | 1 |
| 109 | Deciphering the QR Code of the CRISPR-Cas9 System: Synergy between Gln768 (Q) and Arg976 (R).  | 0 |
| 108 | Experimental and Theoretical Raman Spectroscopy of Isotopically Pure and Diluted Ice VI.   | 1 |

| 107 | Consistent and Transferable Force Fields for Statistical Copolymer Systems at the Mesoscale.  | O |
|-----|---|---|
| 106 | Influence of force field choice on the conformational landscape of rat and human islet amyloid polypeptide.   | О |
| 105 | Influence of dissolved hydrogen on the viscosity and interfacial tension of the liquid organic hydrogen carrier system based on diphenylmethane by surface light scattering and molecular dynamics simulations. <b>2022</b> , | О |
| 104 | Molecular simulation of the structural and thermodynamic properties of n-alkane/brine interfacial systems with nonionic surfactants. <b>2022</b> , 655, 130301  | O |
| 103 | Molecular modelling of ionic liquids: Physical properties of species with extremely long aliphatic chains from a near-optimal regime. <b>2022</b> , 367, 120492   | O |
| 102 | Structural analysis of cannabinoids against EGFR-TK leads a novel target against EGFR-driven cell lines. <b>2022</b> , 3, 100132  | O |
| 101 | Osmolyte Effect on Enzymatic Stability and Reaction Equilibrium of Formate Dehydrogenase.   | 1 |
| 100 | In Silico Characterization of African Swine Fever Virus Nucleoprotein p10 Interaction with DNA. <b>2022</b> , 14, 2348  | O |
| 99  | Quantum-based machine learning and AI models to generate force field parameters for drug-like small molecules. 9,   | O |
| 98  | A random batch Ewald method for charged particles in the isothermalßobaric ensemble. <b>2022</b> , 157, 144102  | О |
| 97  | G $\!$  | 0 |
| 96  | Insights into Molecular Mechanisms of EGCG and Apigenin on Disrupting Amyloid-Beta Protofibrils Based on Molecular Dynamics Simulations. <b>2022</b> , 126, 8155-8165   | O |
| 95  | Staphylococcus aureusFtsZ and PBP4 bind to the conformationally dynamic N-terminal domain of GpsB.  | 1 |
| 94  | Long-Range Hopping Conductivity in Proteins.  | O |
| 93  | Designing an Epitope-Based Peptide Vaccine Derived from RNA-Dependent RNA Polymerase (RdRp) against Dengue Virus Serotype 2. <b>2022</b> , 10, 1734   | 0 |
| 92  | Structure of SARS-CoV-2 M protein in lipid nanodiscs. 11,   | 1 |
| 91  | Recognition motifs for importin 4 [(L)PPRS(G/P)P] and importin 5 [KP(K/Y)LV] binding, identified by bio-informatic simulation and experimental in vitro validation. <b>2022</b> , 20, 5952-5961                               | 0 |
| 90  | Characterization of kaolinite-3-aminopropyltriethoxysilane intercalation complexes. <b>2023</b> , 231, 106753   | O |

| 89 | Effect of layer charge density and cation concentration on sorption behaviors of heavy metal ions in the interlayer and nanopore of montmorillonite: A molecular dynamics simulation. <b>2023</b> , 657, 130553 | O |
|----|---|---|
| 88 | An immunoinformatic approach employing molecular docking and molecular dynamics simulation for evaluation of l-asparaginase produced by Bacillus velezensis. 1-15   | O |
| 87 | Structure and Transport Properties of Poly(ethylene oxide)-Based Cross-Linked Polymer Electrolytes-A Molecular Dynamics Simulations Study.  | 0 |
| 86 | On the diffusion of ketoprofen and ibuprofen in water: an experimental and theoretical approach. <b>2022</b> , 106955   | O |
| 85 | Conserved Water Networks Identification for Drug Design Using Density Clustering Approaches on Positional and Orientational Data.   | O |
| 84 | Absorption Spectra of Flexible Fluorescent Probes by a Combined Computational Approach: Molecular Dynamics Simulations and Time-Dependent Density Functional Theory.  | O |
| 83 | Electric Field-Controlled Peptide Self-Assembly through Funnel-Shaped Two-Dimensional Nanopores. <b>2022</b> , 14, 51183-51189  | O |
| 82 | Comprehensive in silico screening of flavonoids against SARS-CoV-2 main protease. 1-14  | O |
| 81 | TWN-RENCOD: A novel method for protein binding site comparison. 2023, 21, 425-431   | O |
| 80 | On the not so anomalous water-induced structural transformations of choline chloridellrea (reline) deep eutectic system. <b>2022</b> , 25, 439-454  | O |
| 79 | Molecular-level insights into pH regulation of cation adsorption and exchange at clay particle edges. <b>2023</b> , 232, 106789   | 0 |
| 78 | Lipid bicelles in the study of biomembrane characteristics.   | O |
| 77 | Expanding the therapeutic options for Candida infections using novel inhibitors of secreted aspartyl proteases.   | 0 |
| 76 | Hierarchical Coarse-Grained Strategy for Macromolecular Self-Assembly: Application to Hepatitis B<br>Virus-Like Particles. <b>2022</b> , 23, 14699  | O |
| 75 | Uptake mechanism of iron-phytosiderophore from the soil based on the structure of yellow stripe transporter. <b>2022</b> , 13,  | 0 |
| 74 | Molecular and thermodynamic insights into interfacial interactions between collagen and cellulose investigated by molecular dynamics simulation and umbrella sampling.  | O |
| 73 | Towards a rational design of natural deep eutectic solvents for the extraction of polyphenols from Luma apiculata. <b>2022</b> , 121155   | О |
| 72 | Dynamical interaction analysis of proteins by a random forest-fragment molecular orbital (RF-FMO) method and application to Src tyrosine kinase.  | O |

| 71 | Nirmatrelvir-resistant SARS-CoV-2 variants with high fitness in an infectious cell culture system. <b>2022</b> , 8,   | 3 |
|----|---|---|
| 70 | RNA-guided DNA base damage repair via DNA polymerase-mediated nick translation.   | Ο |
| 69 | Thermally Controlled Exciplex Fluorescence in a Dynamic Homo[2]catenane.  | Ο |
| 68 | Protic Ionic Liquids for Intrinsically Stretchable Conductive Polymers.   | Ο |
| 67 | ADMET prediction, Docking, DM analysis and antibacterial screening of epoxy furan-clerodanes from Croton hypoleucus. <b>2022</b> , 134840   | O |
| 66 | Dynamical nonequilibrium molecular dynamics simulations identify allosteric sites and positions associated with drug resistance in the SARS-CoV-2 main protease.                    | 1 |
| 65 | Full-Length Model of SaCas9-sgRNA-DNA Complex in Cleavage State. <b>2023</b> , 24, 1204   | 0 |
| 64 | Modeling the molecular fingerprint of protein-lipid interactions of MLKL on complex bilayers. 10,   | Ο |
| 63 | SHP-1 tyrosine phosphatase binding to c-Src kinase phosphor-dependent conformations: A comparative structural framework. <b>2023</b> , 18, e0278448                                 | O |
| 62 | Computational Study of the Physical Properties of a High Temperature Molten Salt Mixture of FLiNaK and CeF3. <b>2023</b> , 13, 1085   | 1 |
| 61 | Molecular Modelling of Ionic Liquids: Situations When Charge Scaling Seems Insufficient. 2023, 28, 800  | 0 |
| 60 | Thermodynamic Response Functions and Stokes-Einstein Breakdown in Superheated Water under Gigapascal Pressure.  | Ο |
| 59 | Relaxation dynamics of water in the vicinity of cellulose nanocrystals.   | 0 |
| 58 | Theoretical Study on the Regulating Mechanism of the Transition Between the Open-closed State of hCtBP2: A Combined Molecular Dynamics and Quantum Mechanical Interaction Analysis. | Ο |
| 57 | Molecular Insights into Substrate Binding of the Outer Membrane Enzyme OmpT. 2023, 13, 214  | 0 |
| 56 | A molecular insight into the dehydration of metal-organic framework and its impact on the CO2 capture.  | O |
| 55 | Modulating membrane shape and mechanics of minimal cells by light: area increase, softening and interleaflet coupling of membrane models doped with azobenzene-lipid photoswitches. | 0 |
| 54 | A perspective on the microscopic pressure (stress) tensor: history, current understanding, and future challenges.   | 3 |

| 53 | Hydrophobic Hydration: A Theoretical Investigation of Structure and Dynamics. 2023, 135,   | O |
|----|--|---|
| 52 | Inhibition mechanism of cationic polyacrylamide on montmorillonite surface hydration: A molecular dynamics simulation study. <b>2023</b> , 567, 111792   | O |
| 51 | High-Throughput Prediction of the Impact of Genetic Variability on Drug Sensitivity and Resistance Patterns for Clinically Relevant Epidermal Growth Factor Receptor Mutations from Atomistic Simulations. <b>2023</b> , 63, 321-334 | О |
| 50 | Sequence Tendency for the Interaction between Low-Complexity Intrinsically Disordered Proteins.  | O |
| 49 | Comparison of force fields to study the zinc-finger containing protein NPL4, a target for Antabuse in cancer therapy.  | O |
| 48 | Withanolides of Athenaea velutina with potential inhibitory properties against SARS coronavirus main protease (mpro): molecular modeling studies. 1-9  | O |
| 47 | Polypropylene carbonate-based electrolytes as model for a different approach towards improved ion transport properties for novel electrolytes. <b>2023</b> , 25, 4810-4823   | O |
| 46 | Multidirectional Polarization Impacts on Microwave Heating Efficiency: A Molecular Dynamics Research of Microwave Heating of Common Solvents. <b>2023</b> , 127, 970-979   | O |
| 45 | Effect of Charge State on the Equilibrium and Kinetic Properties of Mechanically Interlocked [5]Rotaxane: A Molecular Dynamics Study. <b>2023</b> , 127, 1254-1263   | O |
| 44 | Molecular dynamics investigation of the asphalteneRaolinite interactions in water, toluene, and waterEoluene mixtures.   | O |
| 43 | Molecular dynamics study of Clipermeation through cystic fibrosis transmembrane conductance regulator (CFTR). <b>2023</b> , 80,  | О |
| 42 | Molecular Dynamics Simulations of Asphaltene Aggregation: Machine-Learning Identification of Representative Molecules, Molecular Polydispersity, and Inhibitor Performance. <b>2023</b> , 8, 4862-4877                               | O |
| 41 | Adsorption of CO32/IHCO3/Ibn the Quartz Surface: Cluster Formation, pH effects, and Mechanistic Aspects.   | О |
| 40 | Aggregation of Asphaltene Subfractions A1 and A2 in Different Solvents from the Perspective of Molecular Dynamics Simulations.   | O |
| 39 | The Effect of Cholesterol in SOPC Lipid Bilayers at Low Temperatures. 2023, 13, 275  | О |
| 38 | Partial Destabilization of Amyloid-Protofibril by Methionine Photo-Oxidation: A Molecular Dynamic Simulation Study. <b>2023</b> , 8, 10148-10159   | O |
| 37 | Structural basis for TRIM72 oligomerization during membrane damage repair. 2023, 14,   | О |
| 36 | Unusual heating effect of the elliptically polarized microwave electric field on sodium chloride solution: A molecular dynamics simulation. <b>2023</b> , 569, 111856  | O |

| 35 | Molecular modelling of ionic liquids: Perfluorinated anionic species with enlarged halogen substitutions. <b>2023</b> , 378, 121599   | О |
|----|---|---|
| 34 | A molecular arm: the molecular bending-unbending mechanism of integrin.   | О |
| 33 | The temperature of maximum density of diluted aqueous solutions of non-polar solutes: A molecular simulation study using TIP4P/2005 water and LJ point solutes. <b>2023</b> , 381, 121815                   | 0 |
| 32 | On the Behavior of the Ethylene Glycol Components of Polydisperse Polyethylene Glycol PEG200. <b>2023</b> , 127, 1178-1196  | О |
| 31 | Thermal site energy fluctuations in photosystem I: new insights from MD/QM/MM calculations. <b>2023</b> , 14, 3117-3131   | O |
| 30 | Conformational changes in the human Cx43/GJA1 gap junction channel visualized using cryo-EM. <b>2023</b> , 14,  | O |
| 29 | Study on molecular mechanisms of CD4 dependency and independency of HIV-1 gp120. <b>2023</b> , 13, 6274-6286  | О |
| 28 | FERM domains recruit ample PI(4,5)P2s to form extensive protein-membrane attachments. <b>2023</b> , 122, 1325-1333  | О |
| 27 | Hierarchical Aggregation in a Complex Fluid-The Role of Isomeric Interconversion. 2023, 127, 2052-2065  | О |
| 26 | In silico prediction of potential inhibitors for SARS-CoV-2 Omicron variant using molecular docking and dynamics simulation-based drug repurposing. <b>2023</b> , 29,                                       | O |
| 25 | Understanding the Reaction Kinetics and Microdynamics between Methylimidazole and Alkyl Thiocyanate for Ionic Liquid Synthesis through Experiments and Theoretical Calculation. <b>2023</b> , 62, 3889-3897 | О |
| 24 | Novel in-frame duplication variant characterization in late infantile metachromatic leukodystrophy using whole-exome sequencing and molecular dynamics simulation. <b>2023</b> , 18, e0282304               | O |
| 23 | Water⊠ motions in x-y and z directions of 2D nanochannels: Entirely different but tightly coupled.  | О |
| 22 | Effect of Glycone Diversity on the Interaction of Triterpenoid Saponins and Lipid Bilayers.   | О |
| 21 | Strongly Solvating Ether Electrolytes for High-Voltage Lithium Metal Batteries. 2023, 15, 13155-13164   | О |
| 20 | Long-range communication between transmembrane- and nucleotide-binding domains does not depend on drug binding to mutant P-glycoprotein. 1-10   | O |
| 19 | Rational Computational Approaches in Drug Discovery: Potential Inhibitors for Allosteric Regulation of Mutant Isocitrate Dehydrogenase-1 Enzyme in Cancers. <b>2023</b> , 28, 2315                          | О |
| 18 | Lipid Bicelles in the Study of Biomembrane Characteristics. <b>2023</b> , 19, 1908-1921   | Ο |

| 17 | Cryo-EM structures of human Cx36/GJD2 neuronal gap junction channel. <b>2023</b> , 14,  | 0 |
|----|---|---|
| 16 | Theoretical Spectroscopy Aided Validation of the Hydration Structure of Trimethylamine N-Oxide (TMAO). <b>2023</b> , 127, 2774-2783                                 | O |
| 15 | Atomistic molecular simulations of A配n conformational ensembles.  | O |
| 14 | Investigation of the Entry Pathway and Molecular Nature of 🏿 Receptor Ligands. 2023, 24, 6367   | O |
| 13 | Energetics and kinetics of membrane permeation of photoresists for bioprinting.   | 0 |
| 12 | A General Picture of Cucurbit[8]uril Host <b>G</b> uest Binding: Recalibrating Bonded Interactions. <b>2023</b> , 28, 3124  | O |
| 11 | Single-molecule fingerprinting of protein-drug interaction using a funneled biological nanopore. <b>2023</b> , 14,  | 0 |
| 10 | Sodium is a negative allosteric regulator of the ghrelin receptor. <b>2023</b> , 42, 112320   | O |
| 9  | G⊞s slow conformational transition upon GTP binding and a novel G⊞s regulator. <b>2023</b> , 26, 106603   | O |
| 8  | Molecular origin of the two-step mechanism of gellan aggregation. <b>2023</b> , 9,  | О |
| 7  | Improving the activity of horseradish peroxidase in betaine-based natural deep eutectic systems.  | O |
| 6  | Enhanced stability of a disaggregated Affibril on removal of ligand inhibits refibrillation: An all atom Molecular Dynamics simulation study. <b>2023</b> , 124481  | O |
| 5  | Study on molecular mechanisms of destabilizing At IB2) protofibrils by licochalcone A and licochalcone B using molecular dynamics simulations. <b>2023</b> , 108500 | 0 |
| 4  | Structure and dynamics of a glucose-based cryoprotectant mixture: a computer simulation study. <b>2023</b> , 142,   | O |
| 3  | Thermodynamic response functions and Stokes-Einstein breakdown in superheated water under gigapascal pressure. <b>2023</b> , 142,                                   | О |
| 2  | The geometry of calix[3]pyrrole and the formation of the calix[3]pyrrole[Fitomplex in solution. <b>2023</b> , 142,  | O |
| 1  | Exploring the structure of halomethanes with xenon: An NMR and MD investigation. 2023, 382, 122011  | 0 |